HAL
open science

Nonequilibrium modeling of solar cells : quantum effects at the nanoscale level

Tahereh Nematiaram

To cite this version:

Tahereh Nematiaram. Nonequilibrium modeling of solar cells : quantum effects at the nanoscale level. Optics [physics.optics]. Université Grenoble Alpes; University of Tabriz (Republique islamique d'Iran), 2017. English. NNT : 2017GREAY056 . tel-01738110

HAL Id: tel-01738110

https://theses.hal.science/tel-01738110v1

Submitted on 20 Mar 2018

HAL is a multi-disciplinary open access archive for the deposit and dissemination of scientific research documents, whether they are published or not. The documents may come from teaching and research institutions in France or abroad, or from public or private research centers.

L'archive ouverte pluridisciplinaire **HAL**, est destinée au dépôt et à la diffusion de documents scientifiques de niveau recherche, publiés ou non, émanant des établissements d'enseignement et de recherche français ou étrangers, des laboratoires publics ou privés.

Communauté UNIVERSITÉ Grenoble Alpes

THÈSE

Pour obtenir le grade de

DOCTEUR DE LA COMMUNAUTE UNIVERSITE GRENOBLE ALPES

Préparée dans le cadre d'une cotutelle *entre la Communauté Université Grenoble Alpes* et *Université de Tabriz*

Spécialité : **PHYSIQUE/NANOPHYSIQUE**

Arrêté ministériel : le 6 janvier 2005 - 7 août 2006

Présentée par

«Tahereh NEMATIARAM»

Thèse dirigée par **«Didier MAYOU»** et **«Asghar ASGARI»**
codirigée par **«Sohrab Ahmadi»**

préparée au sein des
L'Institut Néel, CNRS – Université Grenoble-Alpes dans

L'École Doctorale de Physique de Grenoble et à

L'Institut de Recherche en Physique Appliquée et Astronomie, Université de Tabriz

Modélisation hors-équilibre des cellules solaires: effets quantiques au niveau nanométrique

Thèse soutenue publiquement le **«7 juin 2017»,**
devant le jury composé de :

M. Nicolas Cavassilas
Maître de conférence, Université de Marseille (Rapporteur)
M. Yaser Abdi
Professeur associé, Université de Téhéran (Rapporteur)
M. Hassan Bidadi
Professeur, Université de Tabriz (Examinateur)
M. Saeid Shojaei
Professeur associé, Université de Tabriz (Examinateur)
M. Didier Mayou
Directeur de recherche, Université Grenoble-Alpes (Directeur de thèse)
M. Asghar Asgari
Professeur, Université de Tabriz (Directeur de thèse)
M. Sohrab Ahmadi
Professeur associé, Université de Tabriz (Co-Directeur de thèse)
M. Behrooz Rezaie
Professeur assistant, Université de Tabriz (Président)

Communauté
UNIVERSITÉ Grenoble Alpes

Non-equilibrium Modeling of Solar Cells: Quantum Effects at the Nanoscale Level

Tahereh NEMATIARAM

Supervisors: Didier MAYOU, Asghar ASGARI

Advisor: Sohrab AHMADI

A dissertation submitted in partial fulfillment of the requirements for the degree of Doctor of Philosophy

(Nano-physics) in the University of Grenoble Alpes
and
(Photonics) in the University of Tabriz

June 2017

Abstract

A fundamental global challenge is to develop an inexpensive, stable and scalable technology for efficiently harvesting solar photon energy and converting it into convenient forms. Photovoltaic energy conversion is attracting great attention such that several generations of solar cells have emerged. In a general statement, one can divide the existing types of solar cells into two distinct classes: conventional inorganic photovoltaics (IPVs), such as silicon p-n junctions, and excitonic solar cells (XSCs). The mechanistic distinction of IPVs and XSCs results in fundamental differences in their photovoltaic behavior.

According to the type of materials used in their structure, excitonic solar cells are classified into two categories: dye-sensitized solar cells (DSC) and organic photovoltaics (OPV) developed in single-layer and bi-layer including planar and bulk hetero–junction configurations. Quantum dot solar cells (QDSC) are another type of solar cells that have a similar configurations to DSCs or OPVs.

While understanding the performance of excitonic solar cells has been a central effort of the scientific community for many years, theoretical approaches facilitating the understanding of electron-hole interaction and recombination effects on the cell performance are needed. Necessarily, there should be a unified, quantitative picture of the fundamental processes underlying solar energy conversion, including photon absorption, exciton diffusion, exciton dissociation and charge separation as well as an understanding of their consequences on actual device properties.

Semiclassical theories are inefficient tools to treat quantum phenomena in nano–structured solar cells, and on the other hand, due to the Coulomb attraction between the photo generated carriers, the application of standard Non-Equilibrium Green Function (NEGF) formalism presents some difficulties although some specific methods allow to circumvent this problem. Therefore, in this thesis we develop a new quantum formalism, which is based on quantum scattering theory and on the Lippmann-Schwinger equation, to provide a comprehensive framework for understanding the fundamental processes taking place in the operation of excitonic solar cells.

Especially we focus on aspects which have received little consideration in the past and we address the short–range and long–range electron–hole Coulomb interaction, electron–hole recombination, the existence of extra evacuation channels, electron–phonon coupling and polaronic bands formation.

Of specific interests of the methodology developed in this thesis is that both exciton pair creation and dissociation are treated in the energy domain, and therefore there is access to detailed spectral information, which can be used as a framework to interpret the cell performance.

The basic idea of our methodology is shown through the example of two-level photovoltaic systems. Two-level systems, that are systems with essentially only two energy levels, are important kind of systems and quite effective when dealing with the transport phenomena, and device physics.

Here, the two-level excitonic solar cells are considered in the permanent and transitory regimes of charge injection. The molecular photocells where the energy conversion process takes place in a single molecular donor-acceptor complex attached to electrodes are considered as a representative of XSCs in the permanent regime. As an example for the photovoltaic devices in the transitory regime, we consider the bulk hetero–junction organic photovoltaic cells (BHJ OPVs) which are the most common approach to OPVs and consists of mixed donor and acceptor species that form interpenetrating connective networks. In these systems, the exciton created by the photon absorption in the donor side must reach first the donor–acceptor interface. From this moment only a transitory regime begins where the charges can be separated and injected in their respective leads.

We demonstrate that the charge carrier separation is a complex process that is affected by different parameters, such as the strength of the electron–hole interaction and the non–radiative recombination rate. Furthermore, depending on the cell structure, the electron-hole interaction can normally decrease or abnormally increase the cell efficiency. The proposed model helps to understand the mechanisms of excitonic solar cells, and it can be used to optimize their yield.

Dedication

I dedicate this dissertation to my beloved parents,

for their endless love, encouragement, great support and continued care.

Acknowledgments

I wish to express my sincerest gratitude and appreciation to all people who helped me to make my thesis work a success. This work was defined as a joint-supervision project and I was incredibly fortunate to work with two great scientists. I express my sincere thanks to my supervisors, Prof. Asghar Asgari and Dr. Didier Mayou, for orienting my thesis project and for letting me grow as a research scientist. Their perpetual energy and enthusiasm in research extremely motivated me in my studies and I believe that it was not possible to complete the work at this level without their advices and insightful comments.

It gives me great pleasure to acknowledge Prof. Matthias Ernzerhof for his kind help and advices on my research and related projects. It was an excellent experience for me to stay in his team at the University of Montréal as an intern.

I would also like to thank Prof. Sohrab Ahmadi (University of Tabriz), Dr. Simone Fratini, Dr. Petrutza Anghel-Vasilescu (Institut Néel) and Dr. Yongxi Zhou (University of Montréal) for generously offering their time for fruitful discussions.

I thank my committee members; Dr. Nicolas Cavassilas, Prof. Yaser Abdi, Prof. Hassan Bidadi, Prof. Saeid Shojaei, Prof. Behrooz Rezaie for letting my defense to be an enjoyable moment, and for their comments and suggestions.

I express my sincere thanks to president of University of Tabriz, Prof. Mohammad-Reza Pour-Mohammadi, head of RIAPA, Prof. Asghar Asgari, head of Grenoble École Doctoral de Physique, Prof. Johann Collot and also head of our department (PLUM) at Institut Néel, Dr. Serge Huant and the former head Dr. Alain Ibanez for their support with administrative matters. I also acknowledge the financial support and all the facilities provided by Campus France and Institut Néel.

I thank my fellow office mates in Grenoble, Kevin-Davis Richler and Ghassen Jemai for the stimulating discussions. My time at Tabriz, Grenoble and Montréal was enriched by many people, I thank all of them.

Last but certainly not least, I am deeply grateful to my family, who always believed in me and supported my decisions. The accomplishment of this thesis would not have been possible without their love, support and encouragement.

Publications Related To The Thesis

[**1**] T. N. Aram, M. Ernzerhof, A. Asgari, and D. Mayou, "The impact of long-range electron-hole interaction on the charge separation yield of molecular photocells", **The Journal of Chemical Physics**, 146(3), 034103, 2017.

[**2**] T. N. Aram, P. Anghel-Vasilescu, A. Asgari, M. Ernzerhof, and D. Mayou, "Modeling of molecular photocells: Application to two-level photovoltaic system with electron-hole interaction", **The Journal of Chemical Physics**, 145(12), 124116, 2016.

[**3**] T. N. Aram, A. Asgari and D. Mayou, "Charge separation in organic solar cells: Effects of Coulomb interaction, recombination and hole propagation", **EPL (Europhysics Letters)**, 115(1), 18003, 2016.

[**4**] T. N. Aram, A. Asgari, M. Ernzerhof, P. Quémerais and D. Mayou, "Quantum modeling of two-level photovoltaic systems", **EPJ Photovoltaics**, 8, 85503, 2017.

[**5**] M. Ernzerhof, M. A. Bélanger, D. Mayou and T. N. Aram, "Simple model of a coherent molecular photocell", **The Journal of Chemical Physics**, 144(13), 134102, 2016.

[**6**] T. N. Aram, M. Ernzerhof, A. Asgari and D. Mayou, "Offset energies at molecular photocells and their influence on the charge separation yield", **In preparation**.

[**7**] T. N. Aram, M. Ernzerhof, A. Asgari and D. Mayou, "Charges injection in polaronic bands and exciton dissociation yield", **In preparation**.

[**8**] T. N. Aram, M. Ernzerhof, A. Asgari and D. Mayou, "Performance description of excitonic solar cells based on a new quantum formalism", **In preparation**.

Participation In Conferences & Research Visits

[**1**] T. N. Aram, P. Anghel-Vasilescu, M. Ernzerhof and D. Mayou, "Non equilibrium quantum model for solar cells: a photon scattering point of view", **Theory and Modeling for PV**, October 1-2, 2015, Marseille, France. **(Invited Talk)**

[**2**] T. N. Aram, P. Anghel-Vasilescu, M. Ernzerhof and D. Mayou, "Electron-hole interaction and photovoltaic yield of a two-level system", **Journées Nationales du PhotoVoltaïque (JNPV)**, December 1-4, 2015, Dourdan (Paris), France.

[**3**] T. N. Aram, A. Asgari, M. Ernzerhof and D. Mayou, "Non-equilibrium quantum modeling of nanostructure based photovoltaic cells", **Theory and Modeling for PV**, October 6-7, 2016, Saclay (Paris), France.

[**4**] T. N. Aram, A. Asgari, and D. Mayou, "Quantum modeling of molecular photocells: Effects of electron–hole interaction and recombination", **Nanostructured Solar Cells (NSSC)**, December 22nd, 2016, Tehran, Iran.

[**5**] T. N. Aram, P. Anghel-Vasilescu, A. Asgari, M. Ernzerhof and D. Mayou, "Yield of charge separation in organic solar cells", **RIAPA International Annual Meeting On Low Dimensional Systems**, May 23-24th, 2017, Tabriz, Iran.

[**6**] **Research Visit**. Institut de Recherche et Développement sur l'Énergie Photovoltaïque (IRDEP), Paris, France. May 18th, 2016.

[**7**] **Research Visit**. Département de Chimie, Université de Montréal, Québec, Canada. June & July, 2016.

Contents

1 Introduction **1**

1.1 Historical Background Of Photovoltaic Cells 2

1.2 Basic Theory Of Inorganic Photovoltaics 5

1.3 Excitonic Solar Cells 7

1.3.1 Bulk Hetero–Junction (BHJ) Organic Photovoltaic Cells . . . 11

1.3.1.1 Device Physics 13

1.3.1.2 Light Absorption & Exciton Creation 13

1.3.1.3 Exciton Diffusion & Charge Separation 14

1.3.1.4 Charge Carriers Transport & Collection 16

1.3.2 Dye–Sensitized Solar Cells 16

1.3.2.1 Device Structure 17

1.3.2.2 Basic Operating Principle 18

1.3.2.3 Light Absorption 20

1.3.2.4 Charge Carriers Separation 20

1.3.2.5 Charge Carriers Transport 21

1.3.2.6 Charge Carriers Recombination 21

1.4 Theoretical Models Of Excitonic Solar Cells 22

1.5 Organization Of The Thesis 24

2 Formalism & Numerical Methods **25**

2.1 Scattering Theory 25

2.1.1 The Lippmann–Schwinger Equation 26

2.1.2 Green's Function Method 26

2.1.3 The Born Series 27
2.2 Two–level Photovoltaic Systems 28
2.3 Hilbert Space Of The Electron–Hole Pair 30
2.3.1 The Electron–Hole Pair Hamiltonian 30
2.4 Expression Of Spectral Weight (Density Of States) 32
2.4.1 The Krylov Space 34
2.4.2 The Recursion Method 34
2.4.3 Continued Fraction 37
2.4.4 Spectral Decomposition 39
2.5 Fluxes & Quantum Yield 40
2.5.1 Scattering State 40
2.5.2 Fluxes 44
2.5.2.1 Flux Of Absorbed Photons 45
2.5.2.2 Flux Of Current & Recombination 48
2.5.3 Expression Of The Quantum Yield 52
2.5.3.1 Permanent Regime 52
2.5.3.2 Transitory Regime 53

3 Two–Level Systems With Local Interaction 57
3.1 Mono–Channel Condition 59
3.1.1 Asymmetric Coupling : Bulk Hetero–Junction 59
3.1.1.1 Local Density Of States (LDOS) 60
3.1.1.2 Weight Of Excitonic States & Charge Separation Yield 64
3.1.2 Symmetric Coupling : Molecular Photo-cell 66
3.1.2.1 Local Density Of States (LDOS) 67
3.1.2.2 Charge Separation Yield 69
3.1.3 Message To Take Home 71
3.2 Multi–Channel System 72
3.2.1 Two Identical Energy Continuums 72
3.2.2 Two Different Energy Continuums 73

3.2.3 Message To Take Home 75
3.3 Non–resonant Coupling To The Leads 76
3.3.1 Message To Take Home 81

4 Two-Levels Systems With Non–Local Interaction 83
4.1 Long–Range Electron–Hole Coulomb Interaction 84
4.1.1 Energy Levels Of The Hydrogen Atom & Of The Tight–Binding Chain 84
4.1.2 Asymmetric Coupling: Bulk Hetero–Junction Organic Photovoltaic Cells 86
4.1.2.1 Local Density Of States (LDOS) 87
4.1.2.2 Charge Separation Yield 89
4.1.2.3 Message To Take Home 90
4.1.3 Symmetric Coupling: Molecular Photo-cells 91
4.1.3.1 Local Density Of States (LDOS) 91
4.1.3.2 Weight Of Excitonic States & Charge Separation Yield 93
4.1.3.3 Message To Take Home 96
4.2 Charge Injection In Polaronic Bands & Quantum Yield Of Excitonic Solar Cells 97
4.2.1 Coupling To The Phonon Modes: Theoretical Model In The Small Polaron Limit 97
4.2.1.1 Local Green's Function & Spectrum Of Polaronic Bands 99
4.2.2 The Impact Of Quantized Vibrations On The Charge Separation Yield 105
4.2.2.1 Short–Range Electron–Hole Interaction 105
4.2.3 Long–Range Electron–Hole Interaction 110
4.2.4 Message To Take Home 113

5 Conclusions & Perspectives 115

A Tight–Binding Hamiltonian 118

B Projection Operators **121**

B.1 Projection Operators On The Recursion Chain 122

List of Figures

1-1 Efficiency chart of different photovoltaic technologies. This plot is of the National Renewable Energy Laboratory (NREL) highlighting the progress in photovoltaic power conversion. Source: http://www.nrel.gov/ncpv/. 4

1-2 Basic operation principle of inorganic solar cells. Step (i): Light (photon) absorption by a valence band electron occurs if the photon energy amounts to at least the band gap energy. The excited electron is then in the conduction band of the semiconductor material and free to move, as is the hole in the valence band. Step (ii): because of the electric field at a pn–junction, photo–excited electrons and holes flow in opposite directions close to the junction. Figure adapted from: http://www.science-kick.com. 6

1-3 Different types of excitonic solar cells. a) Single layer OPV b) Planar OPV c) Bulk hetero–junction OPV d) Dye–sensitized solar cell. Figures adapted from [39, 40]. 8

1-4 Flexible, plastic PV cell. Figure adapted from [67]. 11

1-5 Schematic diagram of the photo–current generation mechanism in bulk hetero–junction organic solar cells. (i) Exciton generation arising from the absorption of a photon; (ii) Exciton diffusion to a donor–acceptor interface; (iii) The separation of the charge pair; (iv) Charge transport to the respective electrodes; (v) Charge collection. Left: from a kinetic point of view, right: simplified energy diagram for working principle of OSCs. Figure adapted from [75]. 12

1-6 Schematic depiction of a dye-sensitized solar cell. Figure adapted from [116]. 17

1-7 Schematic representation of the elementary steps involved in a dye-sensitized solar cells based on 7-diethylamine-3′,4′-dihydroxyflavylium dye. The frontier orbital plots of HOMO and LUMO were drawn and calculated by Gaussian 09 software. Figure adapted from [121]. 19

2-1 The two–level model in the permanent (Top panel) and transitory (Bottom panel) regime of illumination. (Top panel) A molecular photo–cell with one HOMO and one LUMO orbitals attached to the electrodes. The red line represents the electron–hole interaction and recombination inside the molecule and the hopping integrals of electron and hole are denoted by C and J. Z is the energy of absorbed photon. U and Γ_R represent respectively the electron–hole interaction and recombination inside the molecule. (Bottom panel) Schematic representation of a donor–acceptor system. Charge evacuation leads are considered as semi–infinite chains. Here, J_1 and J_2 are the coupling energies between two adjacent sites in the electron and hole chains, respectively. Also, C_1 and C_2 represent the first coupling energies between the interface states and charge evacuation chains. 29

2-2 The Hilbert space of the electron–hole pair by considering just one evacuation channel for each charge carrier, with one state at each point (x, y) of the lattice. The coordinates x and y of a given state represent the position of electron and hole in their respective leads. $\varepsilon(x, y)$ is the onsite energy of each site of the square lattice and the hopping integrals (C and J) are along the bonds of the square lattice. 31

2-3 Real and imaginary parts of Green's function $G_{00}(E)$. 33

2-4 A typical recursion chain. The parameters a_n represents the onsite energy of each state, while the parameters b_n are the hopping energies between two adjacent states. $|\Psi_n\rangle$ is the wave function associated to the state n. 35

2-5 Propagation of different order of recursion wave vectors $|\Psi_n\rangle$. 36

2-6 Weight of the scattered wave function $|\Psi_P(z)\rangle$ on different sites (x, y) of the square lattice normalized to its value on the initial site $(\frac{|\langle x,y|\Psi_P(z)\rangle|^2}{|\langle 0,0|\Psi_P(z)\rangle|^2})$ for various absorbed photon energies (z). The cell parameters are $J_1 = J_2 = 0.2$, $C_1 = C_2 = 0.1$ and the energy difference between LUMO and HOMO energy levels (Δ) is equal to 2, therefore the energy continuum (EC) is between 1.2 and 2.8 (All energies are in eV unit). 43

2-7 Flux conservation. Flux of current, recombination and photons are represented on the square lattice. The sum of the two fluxes starting from site (0,0) (violet and green) is equal to the flux of electron–hole pairs injected in the material. The sum of all the violet contributions is equal to the flux of electron injected in its lead. If there are no localized states these two fluxes are equal. The recombination flux is denoted by red arrow. $|0, 0\rangle$ determines either the first excited state or the D–A interface. 45

3-1 The two–level model in the permanent (Left panel) and transitory (Right panel) regime of illumination. (Left panel) A molecular photocell with one HOMO and one LUMO orbitals attached to the electrodes in materials I (right) and II (left). The red line represents the electron–hole interaction (U) and recombination (Γ_R) inside the molecule and the hopping integrals of electron and hole are denoted by C and J. Z is the energy of absorbed photon. (Right panel) Schematic representation of a donor–acceptor system. Charge evacuation channels are considered as semi-infinite chains. Here, J_1 and J_2 are the coupling energies between two adjacent sites in the electron and hole chains, respectively. Also, C_1 and C_2 represent the first coupling energies between the interface states and charge evacuation chains. 58

3-2 Local density of states for electron–hole pair in non–interacting condition. 61

3-3 DOS for electron–hole pair under short–range interaction condition. (a) Fixed–hole case (b) Mobile–hole cases. (c) Variation of the $U_{Critical}$ as a function of C_1 and C_2. 63

3-4 Variation of the $P_{Critical}$ as a function of coupling parameters C_1 and C_2. 65

3-5 Weight of the excitonic peaks (P) as a function of short–range interaction strength (U) for different values of hole coupling parameter (C_2). 65

3-6 Yield (Y) of charge separation as a function of short–range interaction energy U obtained with different first coupling energies to the hole lead. The legend presented in the first panel, is valid for all the other panels. Γ_R is the recombination parameter. The strength of long–range interaction V is assumed to be zero. 67

3-7 Density of States as a function of absorbed photon energy in a mono–channel system under different conditions. (a, b) For different values of interaction energy (U). (c) For different coupling parameters (C_1&C_2). (d) For different interaction energies and recombination parameters (U&Γ_R). 68

3-8 Photovoltaic yield as a function of absorbed photon energy and recombination parameter (Γ_R) for different values of coupling parameter C. 69
3-9 Photovoltaic yield as a function of interaction energy (U) and recombination parameter (Γ_R) in a mono–channel system for different values of coupling parameters (C_1 and C_2). 70
3-10 Photovoltaic yield and LDOS in a multi–channel system with identical energy continuums. (a, c, e) Photovoltaic yield as a function of interaction energy (U) and recombination parameter (Γ_R) for different values of coupling parameters of the hole to material II and material I (C_2 and C_3). (b, d, f) DOS as a function of incident photon energy for different values of interaction energy. The energy continuum range is indicated by coloured band below the DOS plots. 73
3-11 LDOS and yield in a multi–channel system with different energy continuums. (a) LDOS as a function of absorbed photon energy for different values of U. The energy continuums EC_1 (electron in material I and hole in material II) and EC_2 (electron and hole in material I) ranges are shown by colored bands below the plot. Here, $C_2 = C_3 = 0.1eV$. (b) LDOS computed for $C_3 = 0.1eV$, $U = -1eV$ and different values of C_2. (c) LDOS computed for $C_2 = 0.1eV$, $U = -1eV$ and different values of C_3. (d, e, f) Photovoltaic yield in a multi–channel system with different energy continuums as a function of interaction energy (U) and recombination parameter (Γ_R) for different values of coupling parameters of the hole to material II and material I (C_2 and C_3). . . 74
3-12 Local density of states as a function of absorbed photon energy for different values of LUMO–LUMO offset. 77
3-13 Weight of bound state in the electron spectrum as a function of LUMO–LUMO offset. 78

3-14 Local density of states as a function of absorbed photon energy for different values of LUMO–LUMO offset and different strength of interaction energy. 79
3-15 Photovoltaic yield as a function of short–range interaction energy U and recombination parameter Γ_R for different values of LUMO–LUMO offset δ. 81

4-1 The energy levels of Hydrogen atom based on the Bohr model. Each main shell is associated with a value of the principal quantum number n [176]. 85
4-2 Local Density Of States (LDOS) as a function of energy for a one–dimensional tight–binding chain by considering different values of Coulomb interaction energy V. 87
4-3 Density of states for electron–hole pair under long–range Coulomb interaction condition. These figures are obtained for $U = V = -0.4\,eV$ and different hole coupling parameter C_2 as indicated in the figure. . 88
4-4 Yield (Y) of charge separation as a function of U obtained with different first coupling parameters to the hole lead C_2. The legend presented in the first panel, is valid for all the other panels. Γ_R represents the recombination parameter and V is the strength of long–range Coulomb interaction. 89
4-5 The two–level model for a molecular photo-cell with one HOMO and one LUMO orbitals attached to the electrodes. The red line represents the electron–hole interaction and recombination inside the molecule and the hopping integrals of electron and hole are denoted by C and J. 91
4-6 LDOS as a function of the energy of the absorbed photon. The impact of the coupling parameter C and the strength of the electron–hole interaction is illustrated in the various panels. 92

4-7 Weight of the excitonic peaks (P) as a function of U. The various curves are obtained upon variation of the coupling parameter C and the strength of the long–range electron–hole interaction V. 94
4-8 Charge separation yield as a function of short–range interaction energy (U) and recombination parameter (Γ_R). The various plots are obtained upon the variation of the electron–hole interaction and for different strengths of the coupling parameters. The coupling parameters in the panels of left and right columns are $C = 0.1\ eV$ and $C = 0.2\ eV$, respectively. 95
4-9 Schematic depiction of the chain model to describe the electron–vibration coupling which can occur on every single acceptor site when electron arrives at that site. C represents the coupling parameter between interface state and initial acceptor site. The coupling between adjacent sites on the acceptor chain is shown by J. g is the strength of coupling to the phonon chains. 98
4-10 Schematic diagram of the electron–vibration chain model. The electron–vibration couplings occurs on every single site of the acceptor chain when electron arrives at that site. The onsite energy ϵ_0 is the energy of the LUMO orbital of the electron at the interface of the BHJ OPV. J and C are hopping integrals representing the coupling between adjacent electronic sites. The parameters $n\hbar\omega_0$ represent the onsite energy of the nth site of the phonon chain while $g\sqrt{n}$ is the hopping energy. 101
4-11 The phonon Green's function for different values of electron–phonon coupling parameter α. The figures are obtained for $\hbar\omega_0 = J = 1\ eV$. . 102
4-12 The local density of states in the bulk part for different electron–phonon coupling constant α. The figures are obtained for $\hbar\omega_0 = J = 1\ eV$. 104
4-13 Yield as a function of incoming electron energy ε_0, for various values of the electron–phonon coupling constant α. 106

4-14 From top to the bottom: Charge separation yield, local density of states in the bulk part and close to the interface for different injection energies corresponding to the red marked points in the yield plot. The electron–phonon coupling constant is $\alpha = \sqrt{0.4}$. 107

4-15 Continuation of Fig. 4-14. Local density of states close to the interface for different injection energies corresponding to the red marked points in the yield plot for different injection energies. 108

4-16 Yield as a function of incoming electron energy ε_0, for various values of the electron–phonon coupling constant α and electron–hole recombination parameter Γ_R. 110

4-17 Yield as a function of incoming electron energy ε_0, for various values of the electron–phonon coupling constant α and coupling parameter C. 111

4-18 Yield as a function of incoming electron energy ε_0, for various values of the electron–phonon coupling constant α in the presence of long–range electron–hole binding $V = -1\ eV$. 111

4-19 Yield and local density of states in the bulk part and close to the interface for different injection energies. The electron-phonon coupling constant is $\alpha = \sqrt{0.4}$ and the Coulomb interaction energy is $V = -1\ eV$.112

4-20 Yield as a function of incoming electron energy ε_0, in the presence of long–range electron–hole interaction $V = -1\ eV$, for various values of the electron–phonon coupling constant α and electron–hole recombination parameter Γ_R. The legend presented in the first panel is valid for all the other panels. 113

A-1 Finite one–dimensional tight–binding chain of sites $n \in 1, ..., N = 5$. . 120

B-1 A typical recursion chain. The parameters a_n represents the onsite energy of each state, while the parameters b_n are the hopping energies between two adjacent states. $|\Psi_n\rangle$ is the wave–function associated to the state n. 122

Chapter 1

Introduction

Human existence has been dependent upon a need for energy. The world's human population is growing rapidly and hence the demand for energy and different sources of energy is increasing dramatically. People need available, reliable, affordable, clean and inexpensive energy. Ever since the Industrial Revolution, the majority of the world's energy is supplied from fossil fuels including coal, oil, petroleum and natural gas. However, these energy resources are limited and despite their impressive effects on extraordinary advances in technology, they suffer a number of disadvantages including environmental hazards, rising prices, acid rain, effects on human health and non–renewable. Therefore, continued reliance on them may have significant environmental and social consequences.

This situation imposes to the scientists from all over the world to develop alternative energy sources to start up a transition in energy production. Fortunately, much attention has been paid to renewable, sustainable, inexpensive and clean energy sources that can meet the demand of modern developments [1].

Renewable energies including wind power, solar, geothermal, hydroelectric, and biomass provide considerable benefits for our climate and economy and address some of the concerns. Nevertheless, they contribute in a limited part of the energy production [2]. Among them solar energy is an attractive source since it is available, CO_2-free and abundant energy resource on the planet Earth [3, 4]. As reported, in only 6 hours the deserts receive more energy from the sun that is larger than the

energy consumption of the world in one year. Assuming the use of only 1% of the desert areas of the world, the potential for electric energy generation with solar energy should be enough to meet the world's energy demand. The assessments confirm that the world is beginning to take advantages of the solar power [5–7].

1.1 Historical Background Of Photovoltaic Cells

In renewable energy harvesting, among the different technologies to convert solar energy into electricity, photovoltaic (PV) technology also referred to as the solar cell, is one of the most popular approaches as it has a lower price in comparison to others, e.g., the hybrid gas–solar technology. It is expected that the PV technology could make the transition from fossil fuels to renewable energy possible [8].

Photovoltaic devices that transform solar energy into electrical energy have become extensively studied and evolved since their first practical developing in 1950 at Bell Laboratories [9]. The researchers in the Bell Telephone Company developed a silicon–based photovoltaic cell with an efficiency of 6% that opened the way for the first commercializing of the photovoltaics.

From 1950s to the beginning of 1970s, PV research and development was directed basically toward space applications [10]. After the oil crisis in the early 1970s in the Middle East, photovoltaic became seriously considered as an alternative energy source and since then there have been growing attempts to develop PV technology and broaden its applications [11, 12].

The energy conversion efficiency of a solar cell is defined as a ratio of the electric power generated by the solar cell to the incident sunlight energy into the solar cell per time. The success of photovoltaics as a renewable energy technology arguably rests on two important points: the efficiency of solar energy conversion into electricity and the cost per watt of produced power.

Basic properties of the solar cell including the typical range of efficiencies are determined based on the material used in their structure [13]. As shown in Fig. 1-1, through applying various materials and manufacturing methods, different types of

solar cells have been developed. Current photovoltaic technology can be classified by generations as:

- **First generation**: silicon wafer based technology or crystalline silicon (c-Si), which is the 85–90% of the global annual market at present [14]. First generation solar cells are relatively expensive and reach a power–conversion efficiency of 25.6% [15]; this value is reduced in commercial products, and based on Shockley–Queisser limit cannot exceed 33% [16].

- **Second generation**: thin films, currently are present on the 10–15% of the commercial modules. They are subdivided into three groups:
a) Amorphous Silicon (a-Si)
b) Cadmium-Telluride (CdTe)
c) Copper-Indium-Diselenide (CIS) and Copper-Indium-Gallium-Diselenide (CIGS)
Issues of costs and flexibility are partially addressed by second generation solar cells. However, typical commercial thin–film cells have much lower efficiencies of around 10–12%, and their efficiency drops off with prolonged use [17].

- **Third generation**: an emerging technology that uses organic semiconductors. It is the combination of first and second generation of solar cells advantages and potentially is able to overcome the Shockley–Queisser limit. It must increase in efficiency that maintains the cost advantage of the second–generation cells.
Third generation solar cells are also known as excitonic solar cells (XSC) due to their charge generation mechanism based on the formation of an exciton. The power conversion efficiency of XSCs cells has increased from around 1% to over 11% in the past 15 years [18].
Excitonic solar cells offer the possibility of low–cost, light–weight, flexible and portable solar cells [19–21]. At present however, they don't match the efficiency and long–term stability of first and second generation solar cells and research is still needed to realize their full potential.

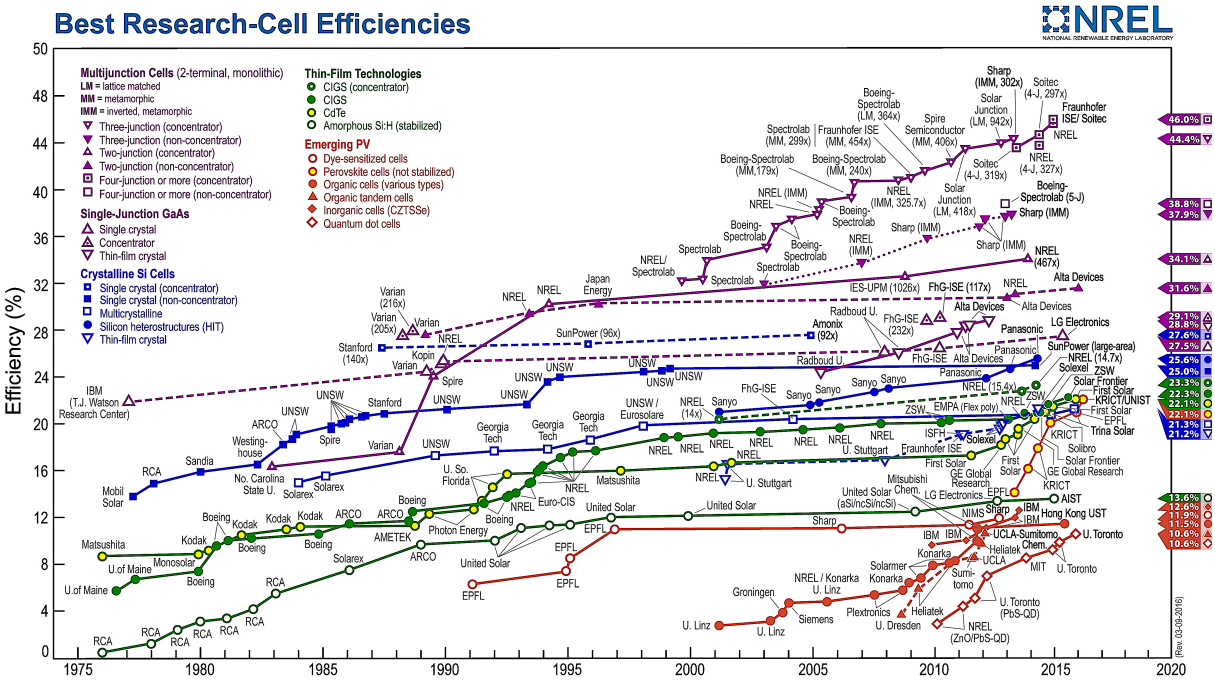

Figure 1-1: Efficiency chart of different photovoltaic technologies. This plot is of the National Renewable Energy Laboratory (NREL) highlighting the progress in photovoltaic power conversion. Source: http://www.nrel.gov/ncpv/.

As pointed above, there are various types of solar cell technologies such that they come in many sizes and shapes with quite different efficiencies. As a general statement, the various types of solar cells can broadly be divided into two distinct families: conventional p–n junctions and excitonic solar cells (XSCs).

In conventional p–n junction solar cells including the first and second generation solar cells, light is absorbed by exciting an electron across a semiconductor band–gap and leads directly to the creation of free electron–hole pairs. Whereas, in the third generation solar cells, also known as excitonic solar cells, light is absorbed by a dye molecule, polymer or quantum dot and creates a tightly bound electron–hole pair (so–called exciton). This occurs for two reasons [22–24]:

(I) as compared to inorganic semiconductors such as Si, organic semiconductors have a much lower dielectric constant. Carbon is an element in second row of the periodic table and its valence electrons are more tightly bound to the nucleus than those of

silicon, its neighbor in the third row. The dielectric constant of crystalline carbon (diamond) is 5.7 while in crystalline silicon is 11.9 [25]. Due to the low dielectric constant of the organic materials, the attractive Coulomb potential well around the incipient electron–hole pair extends over a large volume,

(II) the non–covalent electronic interactions between organic molecules are weak, resulting in a narrow bandwidth; therefore, the electron's wave function is spatially confined, allowing it to be localized in the potential well of its conjugate hole (and vice versa). Therefore, a tightly bound electron–hole pair (a Frenkel exciton) is the usual product of light absorption in organic semiconductors which then dissociates across a hetero–interface to generate charge carriers [26, 27].

This dissertation will focus on understanding the basic operation principle of nano-structured solar cells by considering excitonic solar cells as examples. However, before going into the detailed investigation of XSCs, a short description of conventional inorganic solar cells operation mechanism could be helpful to understand the main differences between emerging and traditional PV cells.

1.2 Basic Theory Of Inorganic Photovoltaics

A solar cell is an optoelectronic device which is designed to convert sunlight into electrical current, i.e., the flow of electrons and holes. In a normal condition, the photo–generated electrons and holes in a semiconductor, move through the lattice without any special order and lead to a net zero electrical current flow. The flow of electrons and holes should be directed in a preferred direction to create a non–zero net electrical current. Generally, in an inorganic solar cell, the preferred direction is selected through forming a p–n junction.

In a p–n junction, the p–type semiconductor includes more positive charges, or holes, while the n–type semiconductor material contains extra negative charges, or electrons. As shown in Fig. 1-2, when p–type and n–type materials are arranged

in contact with each other, electrons diffusion from the n-type material across the junction into the p–type material occurs due to the big difference in electron concentration between n- and p- type semiconductors. A similar process happens for the holes diffusion into the n–type material.

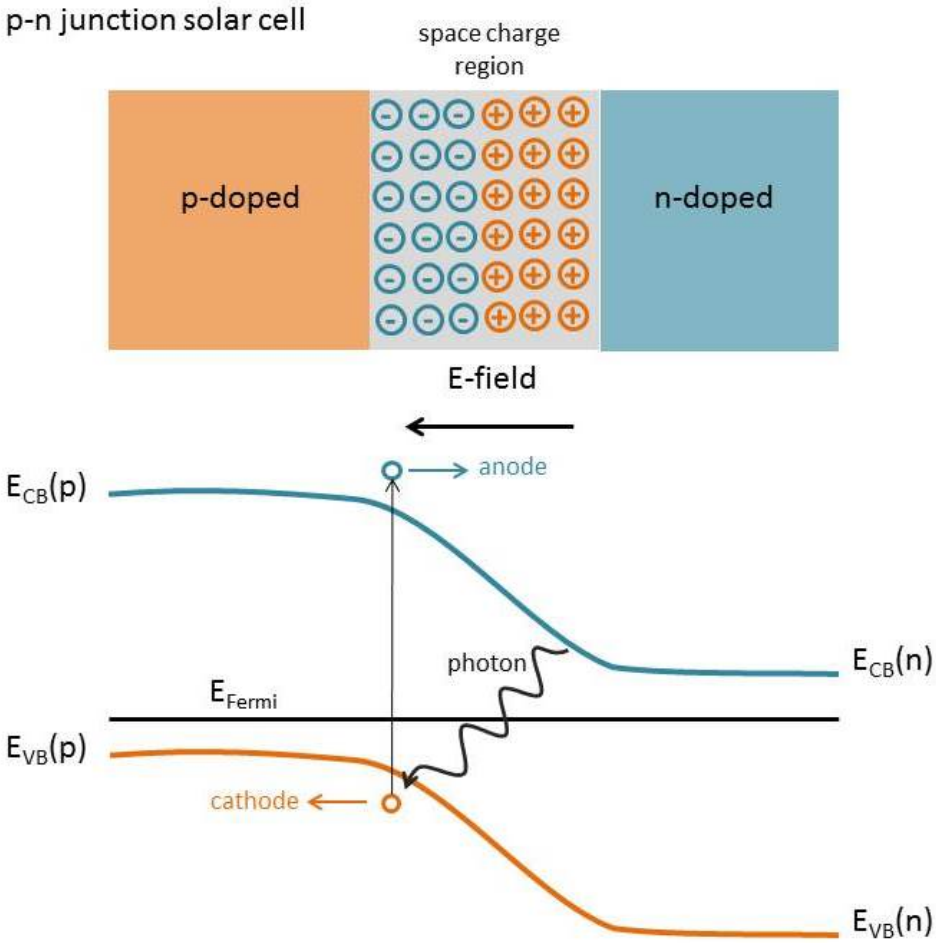

Figure 1-2: Basic operation principle of inorganic solar cells. Step (i): Light (photon) absorption by a valence band electron occurs if the photon energy amounts to at least the band gap energy. The excited electron is then in the conduction band of the semiconductor material and free to move, as is the hole in the valence band. Step (ii): because of the electric field at a pn–junction, photo–excited electrons and holes flow in opposite directions close to the junction. Figure adapted from: http://www.science-kick.com.

As a consequence of the diffusion process, the region close to the junction depletes from mobile charge carriers. This region is called the space–charge region or depleted region. The space charge around the junction leads to the formation of an internal

electric field which forces the charge carriers to flow in the opposite direction of diffusion current. Upon absorption of photons with energies equal or greater than the semiconductor band gap, electrons and holes are created and the presence of this built-in electric field facilitates the charge carriers separation [28].

The current flow continues until the concentration gradient and the internal electrical field acting on the charge carriers compensate each other. To complete the energy conversion process, the separated free electron and hole are conducted toward the cathode and anode contacts to pass through the external circuit and produce electric current.

1.3 Excitonic Solar Cells

Excitonic solar cells have attracted a broad interest in recent years due to their potential to provide an excellent alternative to conventional Si–based PVs. The aim of this section is to focus on excitonic photovoltaic cells, and discuss more details of this technology, various types, basic operation principles and their important challenges.

Excitonic photovoltaic cells are structures that employ organic materials (carbon-based compounds) such as small molecules, polymers, or the hybrids of these material sets to absorb light and produce photovoltaic current. As a general statement, carbon-based semiconductors exhibit desirable light absorption and charge creation properties with the capability of manufacturing by low–temperature processes [29–31].

According to the type of materials used in their structure, excitonic solar cells are classified in two categories: dye–sensitized solar cells (DSC) [32] and organic solar cells (OSC) [33] developed in single–layer [34] and bi–layer [35] including planar [36] and bulk hetero–junction configurations [37]. Quantum dot solar cells (QDSC) are another type of solar cells that have a similar configuration to DSCs or OSCs [38]. A schematic view of different excitonic solar cells is shown in Fig. 1-3.

Historically, in the end of 19th century, by emerging the modern organic chemistry the scientific and industrial interests in the research on organic materials enhanced. The photoconductivity phenomenon by an organic compound "Anthracene" for the

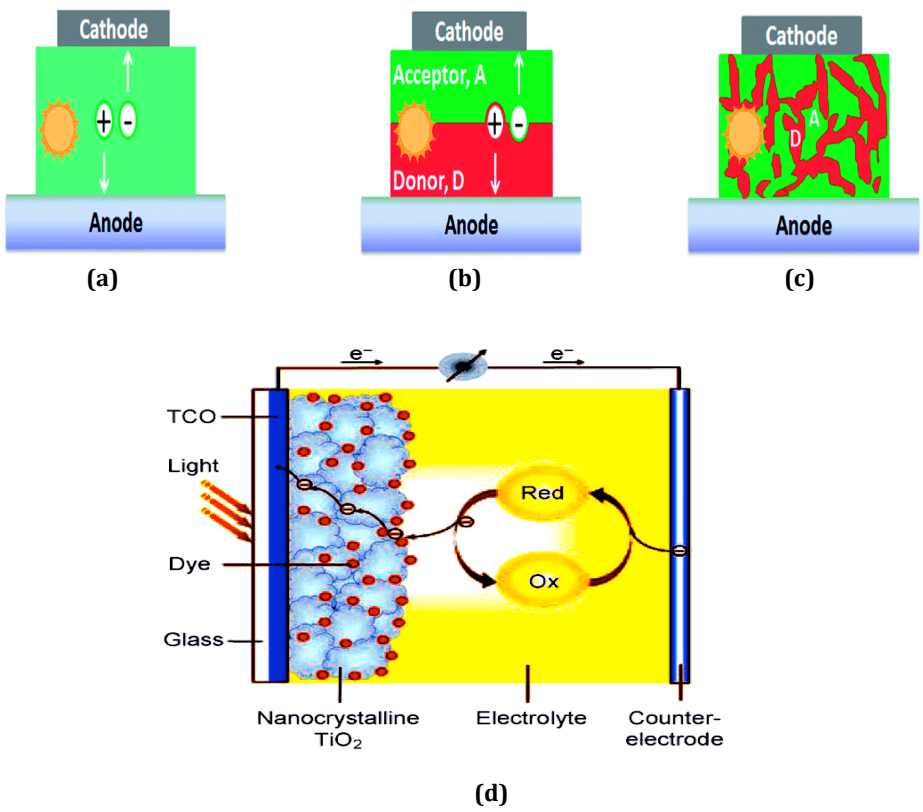

Figure 1-3: Different types of excitonic solar cells. a) Single layer OPV b) Planar OPV c) Bulk hetero–junction OPV d) Dye–sensitized solar cell. Figures adapted from [39, 40].

first time was observed by Pochettino in 1906 [41]. Since then it is realized that many conventional dyes such as methylene blue, can show the semiconducting characteristics [42] and enormous number of organic semiconducting molecules do exist such that their electrical and optical properties can be fine–tuned to address the special applications [43, 44].

In the 1970s (semi)conducting polymers were discovered [45]. Allan J. Heeger, Alan G. MacDiarmid, and Hideki Shirakawa received the Nobel Prize in chemistry in 2000 for the discovery and development of these conductive polymers. The first major breakthrough in the deployment of organic solar cells has been made in 1986 by Tang who developed the donor-acceptor solar cell and reported an efficiency of 1% [46]. The energy conversion efficiency of this cell was very low, but it showed a promising potential of organic photovoltaics when electron donor and acceptor molecules are

used together.

In 1992, Sariciftci et al. [47] displayed the photo–induced charge transfer within organic molecules that led to particular interests in OPVs field. A report of 2.9%–efficient cells based on conducting organic polymers mixed with derivatives of C60 published by Yu et al. in 1995 [48] increased the excitement in this research area. After these achievements the number of publications rose dramatically.

Based on the aforementioned explanations, common organic photovoltaic devices use a donor and an acceptor organic material to build up a hetero–junction favoring the separation of the exciton into free charge carriers. The same organic materials are also responsible for charge transport to their respective leads. That is a material which for organic photovoltaic devices should have both good light absorption and carriers transporting properties which is a hard task to achieve.

On the other hand, the dye–sensitized solar cell technology separates the two requirements as the charge generation is done at the interface of semiconductor–dye and the charge transport is done by the semiconductor and the electrolyte. Therefore, modifying the dye alone can optimize the spectral properties, while carriers transport properties can be improved by optimizing the semiconductor and the electrolyte phases.

The first significant study of dye–sensitization of semiconductors also backs to the 19th century, when Vogel utilized silver halide emulsions sensitized by dyes for providing a black and white photographic film [49]. The mechanism of electron injection from photo–excited dye molecules into the conduction band of the semiconductor dates only from the 1960s [50, 51]. The concept of dye adsorption on the surface of the semiconductor was started in 1976 by Tsuborama et al. [52] and developed in 1981 by Dare–Edwards et al. [53].

However, exploiting the dye–sensitization mechanism in photovoltaic technology was an unsuccessful process until the early 1990's when a breakthrough happened by professor Grätzel and his co–workers at the École Polytechnique Fédérale de Lausanne (EPFL–Switzerland). The Grätzel cell (dye–sensitized solar cell) revealed an energy conversion efficiency exceeding 7% in 1991 [54] and 10% in 1993 [55]. Due to this

invention, Prof. Grätzel has received prestigious awards, including the Balzan Prize in 2009 and the 2010 largest technology prize in the world (Millennium Technology Prize).

DSCs offer large flexibility in color, shape, and transparency [56, 57] and perform relatively better compared with other solar cell technologies at higher temperatures [58]. Furthermore, due to the utilization of cheap and earth–abundant materials and also simple preparation and easy fabrication processes they are highly cost–effective as compared with the conventional inorganic counterparts [59,60]. Due to the interesting characteristics of this family of solar cells, DSC research groups have been established around the world and the field is growing fast [61–63].

These promising characteristics indicate that excitonic solar cells have the capability of being an economically viable source of renewable energy. However, although power conversion efficiencies (PCEs) of XSCs have represented a significant increase over the past ten years, there are still problems in enhancing PCEs and stability to make them commercially available [64–66]. All the cons and pros pointed above make the excitonic solar cells technology a prospective and interesting research and innovation field.

In 2005, the US Department of Energy published a report discussing the point that there exists insufficient microscopic intuition or theory to conduct material and device for better design of new generation photovoltaic devices [67]. According to the mentioned report, developing theories that can provide unified, quantitative and comprehensive understanding of principle processes taking place in solar energy conversion such as photon absorption, exciton formation and dissociation, charge separation and collection are essentially needed. It also predicts that developing theories for sufficient understanding of organic materials and structures have the capability of improving the conversion efficiency of XSCs by a factor of 5–10, and achieving efficiencies of 15–25% in cheap, plastic–type solar cells (Fig. 1-4).

Following this interesting report, in this thesis, we develop a new quantum formalism to describe the performance of excitonic solar cells in the presence of electron–hole interaction, recombination and electron–phonon coupling. To investigate various as-

pects of the model, we choose two examples:

(I) bulk hetero–junction organic photovoltaic cell as a subcategory of organic PVs,

(II) molecular photo–cell which is the simplest model of Grätzel cells (DSCs).

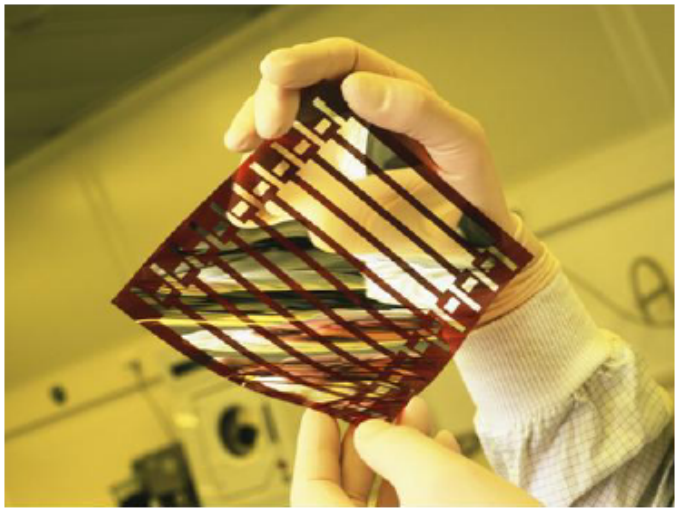

Figure 1-4: Flexible, plastic PV cell. Figure adapted from [67].

1.3.1 Bulk Hetero–Junction (BHJ) Organic Photovoltaic Cells

Exciton generation is the direct consequence of low dielectric constant of organic materials which expresses that there is a strong Coulomb attractive potential between the electron and the hole [22]. Excitons have a short lifetime after which they recombine. Therefore, an important factor that can improve the efficiency of organic solar cells is the exciton dissociation before charge carriers recombination.

To break–up the excitons many approaches have been proposed [68–70]. Among the promising approaches to facilitate the exciton break–up which has a straightforward impact on the energy conversion of OPVs is constructing hetero–junction devices where the absorber layer is made of donor and acceptor (D–A) molecules.

The idea behind the bulk hetero–junction OPVs is increasing the interface through mixing the donor (electron–donating material) and acceptor (electron–accepting material) and consequently increase the number of excitons that get dissociated into free

electrons and holes. Commonly, donors are conjugated polymers and acceptors are based on fullerene derivatives [41, 71, 72].

As the number of dissociated excitons increases, the ratio of generated carriers and the total number of absorbed photons increases as well. This ratio is called the quantum efficiency which is one of the important characteristics used to evaluate the performance of photovoltaic devices.

A schematic depiction of a BHJ photovoltaic cell and its energy levels is shown in Fig. 1-5. The highest occupied molecular orbital and lowest unoccupied molecular orbital are denoted by HOMO and LUMO, respectively. The HOMO and LUMO which are similar to the conduction and valence bands in conventional semiconductors have important effects on optical and electronic properties of organic systems [73, 74].

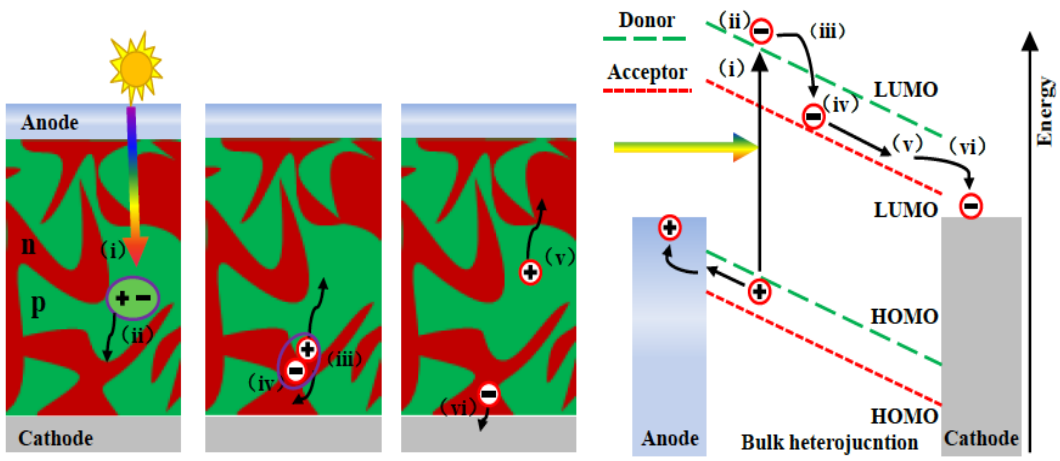

Figure 1-5: Schematic diagram of the photo–current generation mechanism in bulk hetero–junction organic solar cells. (i) Exciton generation arising from the absorption of a photon; (ii) Exciton diffusion to a donor–acceptor interface; (iii) The separation of the charge pair; (iv) Charge transport to the respective electrodes; (v) Charge collection. Left: from a kinetic point of view, right: simplified energy diagram for working principle of OSCs. Figure adapted from [75].

1.3.1.1 Device Physics

In this section, the performance of bulk hetero–junction organic photovoltaic cells is described in detail. As represented in Fig. 1-5, the operation of BHJ OPVs under external illumination can be explained in 6 steps:
(i) light absorption and exciton formation, (ii) exciton diffusion toward the donor–acceptor interface, (iii) exciton dissociation into free charge carriers, (iv) separation of the still Coulomb–bound electron–hole pair, (v) free charge carriers transport through the donor or acceptor materials to the electrodes, (vi) charge carriers collection at the anode and cathode electrodes [76].

1.3.1.2 Light Absorption & Exciton Creation

Usually, the absorption coefficient in the visible range of conventional electron–donating organic materials is much higher than those of their electron–accepting materials, therefore, in BHJ OPVs sunlight is normally absorbed in the donor phase. Organic semiconductors often present high absorption coefficients above $10^7 m^{-1}$, hence, low thicknesses (around 100 and 300 nm) are adequate for sufficiently high photon absorption in organic photovoltaic devices. Whereas, PV cells constructed from the inorganic polycrystalline semiconductor such as $CuInSe_2$ requires a few micrometers thick active layer for good photon absorption, and crystalline silicon solar cells more than 100 μm. On the other hand, inorganic semiconductors have the capability of absorbing the whole visible spectrum of the sunlight, and beyond up to 1000 nm, while conjugated polymers frequently used in organic solar cells typically can only absorb the photons in the visible optical spectrum [77–79].

The absorption coefficient is limited by the semiconductor band–gap which is defined as a difference between its LUMO and HOMO levels such that only photons with energy equal or greater than band–gap can be absorbed. However, some methods through accurate tuning of molecular electronic structure and intermolecular packaging of organic materials can enhance their absorption [80, 81].

It is generally assumed that upon absorption of light an exciton is generated in the donor phase which diffuses toward the donor–acceptor interface. For a long time, there was an argumentative debate about the creation of free electron–hole pairs or tightly bound excitons as a consequence of light absorption [82–85]. According to some simple theories such as the one in [86], by considering the very low dielectric constant of the organic material, the attractive potential between photo–generated electron and hole is too strong such that the electron–hole pair cannot be separated before de-excitation. An alternative assumption is that the dissociation of the exciton at the interface generates an electron–hole pair with an extra vibrational energy that can be utilized to overcome the coulomb attractive potential [87]. However, some other authors believe that the exciton leads directly to relatively delocalized charges [88]. Also, the possibility of dissociation of an exciton which is located at a certain distance from the interface has been discussed [89].

These photo–generated excitons should be dissociated into free charge carriers to contribute in photocurrent. As will be discussed in the next section, a necessity for exciton dissociation into free charge carriers is its diffusion to the D–A interface.

1.3.1.3 Exciton Diffusion & Charge Separation

As shown in Fig. 1-5 (ii), the photo–generated exciton must move to the donor–acceptor interface, which is described as a diffusion process. The exciton which is mainly formed in the donor phase diffuses as long as the recombination processes between the electron and hole forming the exciton do not occur. However, exciton diffusion length, known as a physical characteristic quantity, in the active layer is very short. For instance, based on the experimental results, exciton diffusion length for small molecule donor materials is in the range of 3-30 nm [90], for C60 is 40 nm [90] and for conjugated polymers is around 20 nm [91]. Therefore, due to the short diffusion length and large binding energy of excitons generated in organic semiconductors (greater than 100 meV) [92], thermal excitations cannot effectively dissociate them into free charge carriers [93, 94] which results in a low exciton dissociation yield.

To increase the exciton dissociation yield, the charge transfer process should occur at a much shorter timescale. The bulk hetero–junction structures through providing a large interfacial interface, decreasing domain size of donor and acceptor materials and therefore, decreasing the exciton diffusion length, can facilitate the exciton dissociation. However, after charge carriers arrival at the interface, the positive and negative charges are still bound by a Coulomb attractive potential, as shown in Fig. 1-5 (iv) [95, 96]. Due to the low dielectric constants in organic semiconductors, the binding energy of this pair is relatively strong ($\sim$ 0.1-1.0 eV), such that the thermal activation energy at room temperature is not enough to dissociate them [97]. Hence, an additional step is required for the final charge pair separation.

A general approach to address the pair dissociation is based on a model proposed by Onsager in 1938 [98]. As a general statement, an internal field mainly originating from the different work–functions of the electrodes at the two sides of the device can overcome the Coulomb attraction between the electron–hole pair which are still bound at the D–A interface after the spatial separation. For sufficiently strong fields, charge carrier separation occurs and electrons and holes can diffuse and be transported towards their respective contacts. In other words, excitons can be dissociated due to the energy offset between the lowest unoccupied molecular orbitals (LUMO) in donor and acceptor materials that is adequate to overcome the Coulomb attraction [80].

After the excitons dissociation in BHJ solar cells, electrons go to the lowest unoccupied molecular orbital (LUMO) of the acceptor and holes migrate toward the highest occupied molecular orbital (HOMO) of the donor. Therefore, charge carriers are spatially separated and staying in two different molecules, this decreases the recombination rates.

Here we draw the reader's attention to an important point: usually in D–A structures, the donor material (i.e., polymer) absorbs most of the sunlight and photo–generated charge carriers are separated due to electron transfer to the acceptor material (i.e., fullerene), but in some structures, light can also be absorbed by acceptor material such that a subsequent charge transfer from acceptor to donor has been realized experimentally [99].

1.3.1.4 Charge Carriers Transport & Collection

As shown in Fig. 1-5 (iv, v), once the electrons and holes are separated, the next step is their extraction from the device to yield a photocurrent to perform a work in the external circuit. In order to collect the photogenerated charges, they have to migrate through a set of acceptor and donor sites to the cathode and anode electrodes. In this migration, structural and chemical defects restrict the charge carriers to small segments also referred to as sites and charge carrier transport is based on a hopping mechanism from site to site [100, 101]. Under the optimized morphology, the yield of charges creation and extraction in bulk hetero–junction photovoltaic cells under external illumination can be high [102, 103].

1.3.2 Dye–Sensitized Solar Cells

Dye–sensitized solar cell (DSC) or Grätzel cell is a nano–structured photo–electrochemical device which is composed of sensitized dyes attached to a mesoporous wide band gap semiconductor [104–106]. Dyes harvest the sunlight and the photo–induced injection of an electron from the excited dye into the conduction band of the semiconductor transforms the sunlight into the electricity. The charge carriers move through the semiconductor toward the electrodes and an external circuit. In order to make the process cyclic, the oxidized dye species need to be regenerated and this process is ensured by a redox mediator in the pores [107, 108].

The transparency, large choice of colors, mechanical flexibility, and the parallels to natural photosynthesis all make the DSCs widespread fascinating technology [109–111]. They also propose an inexpensive technology to developing highly efficient photovoltaic cells [112, 113] and due to the utilization of abundant and non–toxic materials, they are considered as an environmentally friendly technology [114, 115]. Due to the great promising potentials of DSCs, some companies have started to invest on this technology to bring that "from the lab to the fab" (e.g., Dyesol, G24i, Sony, Sharp, and Toyota).

1.3.2.1 Device Structure

A schematic depiction of a typical dye–sensitized solar cell is shown in Fig. 1-6. This device consists of two electrodes named the anode and the cathode which are constructed from a specific glass that has a Transparent Conductive Oxide (TCO), usually a thin layer of fluorine–doped tin oxide (FTO), coated on one side. Sunlight can enter to the cell due to the transparency of the substrate while charge collection occurs as a consequence of its conductive surface. In the charge collection process, electrons and holes flow to the cathode and anode electrodes, respectively.

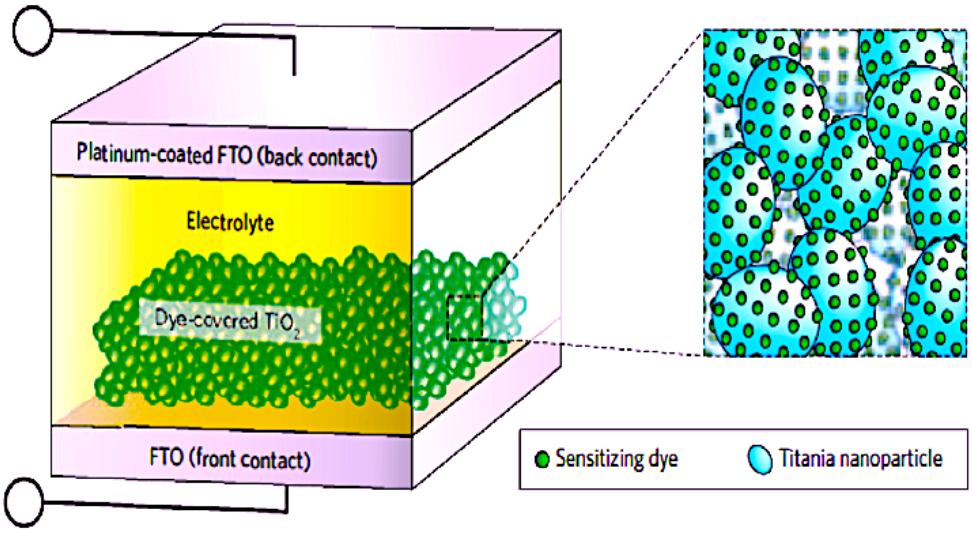

Figure 1-6: Schematic depiction of a dye-sensitized solar cell. Figure adapted from [116].

The anode is the negative terminal of the solar cell, which includes a continuous network of sintered titanium dioxide nanoparticles. Normally, titanium dioxide is a wide band gap semiconductor which is not sensitive to the visible range of solar spectrum. Therefore, to absorb the visible spectrum, the titania particles have to be sensitized with a layer of dye molecules. On the other hand, the cathode which is the positive terminal of the solar cell, is coated with a catalytic material to transfer the electrons. Since a very small amount of catalyst is adequate, the electrode remains transparent. The catalyst is normally based on platinum or carbon based materials

[117, 118]. An electrolyte fills the area between the two electrodes to ensures the charge carriers transportation through a redox couple. The typical electrolytes are based on iodide/tri-iodide in a nitrile solvent. In order to prevent the electrolyte solvent from evaporating, the two electrodes are sealed together. The state-of-the-art Grätzel cells based on liquid electrolyte have displayed power conversion efficiencies of over 11% [119], whereas, reported power conversion efficiencies in DSCs comprised of a solid–state hole conductor are over 5% [120].

1.3.2.2 Basic Operating Principle

Dye–sensitized solar cells are photo–electrochemical and their operating principle is similar to the plant photosynthesis. In contrast to the traditional inorganic solar cells, where light absorption and charge transport occur in the same material, the DSC separates these two functions such that photons are absorbed by the dye molecules and charge carriers transportation takes place in the TiO_2 electrode and in the electrolyte (Fig. 1-7).

The operation of DSCs can be summarized through 7 steps [121, 122]:

1- The sensitizer dye molecule adsorbed on the surface of the semiconductor, absorbs the incident sunlight and as a result an electron becomes excited from the ground state S (Highest Occupied Molecular Orbital (HOMO)) to the excited state S^* (Lowest Unoccupied Molecular Orbital (LUMO)):

$$S + h\nu \rightarrow S^* \tag{1.1}$$

2- The excited molecule injects an electron into the conduction band of the semiconductor resulting in the oxidation of the sensitizer S^+:

$$S^* \rightarrow S^+ + e^-_{CB} \tag{1.2}$$

This process must takes place before the dye can relax back to its ground state.

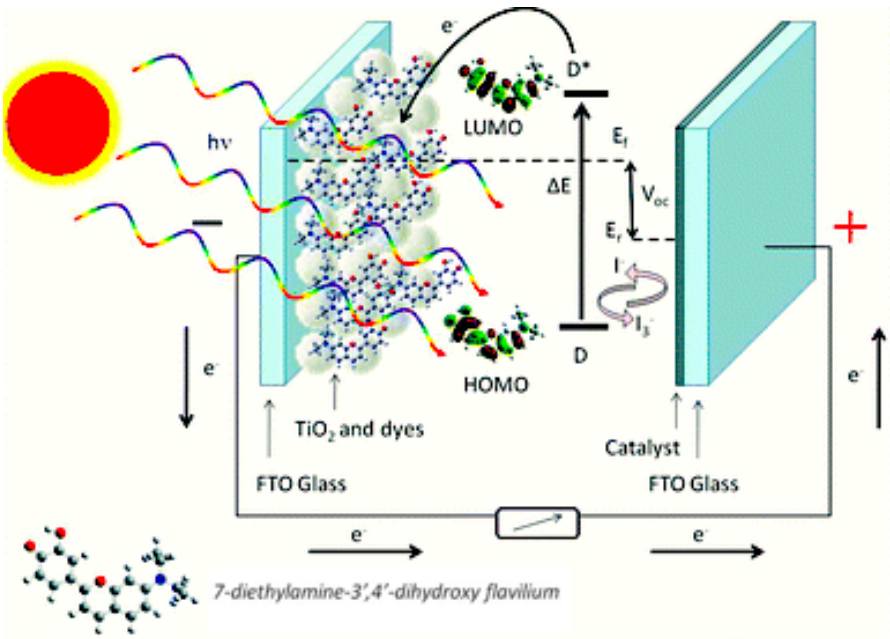

Figure 1-7: Schematic representation of the elementary steps involved in a dye-sensitized solar cells based on 7-diethylamine-3′,4′-dihydroxyflavylium dye. The frontier orbital plots of HOMO and LUMO were drawn and calculated by Gaussian 09 software. Figure adapted from [121].

3- The iodide ion by donating an electron regenerate the oxidized sensitizer (S^+) and turns into tri-iodide :

$$S^+ + \frac{3}{2}I^- \rightarrow S + \frac{1}{2}I^{-3} \tag{1.3}$$

4- The tri-iodide redox mediator diffuses towards the counter electrode and is reduced to iodide:

$$I_3^- + 2e^- \rightarrow 3I^- \tag{1.4}$$

In addition to the mentioned processes, some undesirable reactions resulting in losses in the cell efficiency occur. The loss process includes:

5- Relaxation of the excited dye to the ground state:

$$S^* \rightarrow S \tag{1.5}$$

6- Recombination of the injected electrons with the dye cations:

$$S^+ + e^-_{CB} \rightarrow S \tag{1.6}$$

7- Recombination of the injected electrons with the tri–iodide redox mediator:

$$I^-_3 + 2e^-_{CB} \rightarrow 3I^- \tag{1.7}$$

The aforementioned mechanisms will be discussed in details in the following sections.

1.3.2.3 Light Absorption

In dye–sensitized solar cells, the dye molecule is adsorbed on semiconductor surface due to the special anchoring groups. Light absorption leads to an excitation between the electronic states of the molecule and as a consequence an electron is transferred from the HOMO to the LUMO level. Since there is a partial overlapping between the electron wave functions of the dye LUMO level with the conduction band of the semiconductor material, the electron can be injected in conduction band of semiconductor. To achieve high device performances, the injection process should happen quicker than the decay of the excited state of the dye to the ground state. This is dependent on lifetime of the dye excited state that is different for various complexes. Normally, for typical Ru complexes used in DSCs this lifetime is 20–60 ns [123], obviously for this kind of dye the injection is an ultrafast process.

1.3.2.4 Charge Carriers Separation

Charge separation process in DSCs includes the electron transfer from the dye molecule to the conduction band of semiconductor and movement of the holes from the oxi-

dized dye to the electrolyte. The electronic structure of the dye molecule and the energy level matching between the excited state of the dye and the conduction band of the semiconductor strongly affect the process. The most important mechanism for charge carriers separation in DSC is the relative position of the energetic levels such that for efficient charge separation the excited level of the dye must be higher than the conduction band of the semiconductor, and the HOMO level of the dye must be below the redox potential of the electrolyte.

1.3.2.5 Charge Carriers Transport

In a DSC, charge transport is a result of the electron transport in the nano–structured semiconductor oxide photo–electrode and the hole transport to the electrolyte. It has to be noted that the semiconductor nanoparticle network plays an important role in the DSC performance. On one hand, it provides a large surface area substrate for the dye molecules and on the other hand, it is a transport media for the electrons injected from the dye molecules.

Due to the porous structure of the electrode and the screening effect of the electrolyte, the electrode can be considered as an ensemble of single particles where electrons penetrate by hopping from one particle to the other one [106]. On the other hand, the electrolyte medium in a DSC has a role of hole–conductor. At the photo–electrode, as a consequence of the injection of an electron to the conduction band of the TiO_2, the dye becomes oxidized and I^- present in the electrolyte regenerate the oxidized dye Eq. (1.3). At the counter electrode I_3^- is reduced to I^- in the reaction described by Eq. (1.4).

1.3.2.6 Charge Carriers Recombination

One of the important reasons for lowering the photo–current and consequently the efficiency in DSCs is charge carriers recombination. To address the recombination process, much work has been carried out [124–126]. Solving the charge carriers recombination issue can significantly affect the conversion efficiency of DSCs. The recombination process occurs at both Electrode–Electrolyte and TiO_2–Electrolyte in-

terface. In other words, recombination is possible both after the electron injection to the semiconductor or during its migration in the TiO_2 electrode on its way to the electrical back contact. Since during the charge transfer process the electrons are always within only a few nanometers distance from the interface of semiconductor–electrolyte, the recombination of injected electron is inevitable.

One important point that should be noted is that the recombination is dependent on the different interfaces between elements of the cell junction. As the interfacial area increases a higher photocurrent can be extracted due to more charge–separation sites while it can also increase the number of sites where recombination can occur.

The charge recombination has a significant negative effect on the photovoltaic performance. In order to suppress the disadvantage, much effort has been devoted to optimizing the molecular structure of those organic dyes, through controlling the molecular orientation and assembling modes of the dyes on the TiO_2 surface [127–129].

1.4 Theoretical Models Of Excitonic Solar Cells

The need for optimized XSCs and the fundamental issues about global efficiency enhancement made the experimental XSCs development be accompanied by a constant modeling effort. While understanding the performance of excitonic photovoltaic cells has been a central effort of the scientific community for many years [130–133], theoretical approaches facilitating the understanding of electron–hole interaction and recombination effects on XSCs performance, are needed. Semi–classical theories are inefficient tools to treat interaction problems in nanostructure–based solar cells [134, 135], and on the other hand due to the Coulomb attraction between the photo–generated carriers, the application of standard Non–Equilibrium Green Function (NEGF) theory presents difficulties although some methods allow circumventing this problem in specific cases [136–138]. The different models for XSCs will be briefly reviewed below.

In 2005, Sasa Lacica, et al. [139] developed a theoretical model that enables one to investigate the impact of a number of materials and parameters on device performance. In the same year, Qing Wang, et al. [140] performed an electrochemical

impedance spectroscopy (EIS) to investigate electronic and ionic processes in dye–sensitized solar cells (DSC). In this work, a theoretical model has been elaborated, to interpret the frequency response of the device. In the work published in 2006 by Douglas W. Sievers, et al. [141], the dependence of short circuit current on optical effects and its oscillatory variation on the polymer layer thickness is explained by solving the short circuit current using the drift–diffusion equations, where the light intensity calculated from the optical transfer matrix theory is used as the input for optical carrier generation. Peter K. Watkins and et al. [142] have presented a dynamical Monte Carlo study of the dependence of the internal quantum efficiency (IQE) of an organic bulk hetero–junction solar cell on the device morphology. They showed that there is a relationship between the scale of electron and hole conductor phase separation and device efficiency. In 2012, Guangqi Li, et al. [143] developed a model to describe dissociation of charge transfer excitons in bulk hetero–junction solar cells, and its dependence on the physical parameters of the system. In 2013, Mario Einax, et al. [132] analyzed the factors that affect current–voltage characteristics, power voltage properties and efficiency, and their dependence on non–radiative losses, reorganization of the nuclear environment, and environmental polarization. In 2015, Shigeru Ajisaka, et al. [130] analyzed the non–equilibrium transport properties and energy conversion performance of a molecular photo–cell. In 2016, Oleg V. Kozlov and et al. [144] proposed a model for real–time tracking of singlet exciton diffusion in organic semiconductors. Furthermore, a family of many–body perturbation theories, the so–called GW and Bethe-Salpeter (BSE) formalisms, have been shown recently to yield electronic and optical (excitonic) properties of bulk and gas phase organic systems [145, 146].

We present a novel simple model to describe the performance of excitonic photovoltaic systems especially by focusing on aspects which have received little consideration in the past and we address the effects of electron–hole interaction, recombination and also electron–phonon coupling. We also investigate the effects of hole propagation, symmetric and asymmetric coupling and extra evacuation channels on charge separation yield. This model is based on quantum scattering theory and in particular

on the Lippmann–Schwinger equation [147]. One of its interesting features is developing on the energy domain such that it provides a detailed spectral information to interpret the exciton creation and dissociation phenomena and their effects on device properties as well.

1.5 Organization Of The Thesis

The rest of the thesis is organized as follows:
In chapter two, the new formalism which is based on quantum scattering theory and the Lippmann–Schwinger equation is outlined. It begins with a brief overview of the basic concepts including quantum scattering theory and the Born approximation. The basic idea of this new methodology is shown through the example of two–level excitonic solar cells. These two–level systems are studied in the permanent and transitory regimes of charges separation.

The implementation of the formalism to molecular photo–cells and bulk hetero–junction solar cells is discussed along chapter three and four. Chapter three describes the operation of excitonic solar cells in the presence of short–range electron–hole Coulomb interaction and considers the excitonic solar cells under two different configurations:
(I) Mono–channel system where there is only one evacuation channel for each charge carrier. **(II)** Multi–channel system where there are more than one evacuation channels at least for one of the charge carriers.

In chapter 4 special scenarios are considered due to the non–local interaction. The effects of Coulomb interaction between the photo–generated electron–hole pair while at least one of them is evacuated in its respective lead and also interactions due to the lattice distortion and coupling to the phonon modes are discussed along this chapter.

Finally, chapter 5 presents the general conclusions on the basis of the previous chapters, together with a brief discussion of future work to be done.

Chapter 2

Formalism & Numerical Methods

2.1 Scattering Theory

Our knowledge about microscopic physics almost originates from scattering experiments where the interactions between atomic or sub–atomic particles can be studied. This is done by letting them collide with a fixed target or with each other. In the scattering formalism, an incident particle in state Ψ_0 is scattered by the potential V, resulting in a scattered state Ψ_S [148, 149]. The incident state Ψ_0 is assumed to be an eigenstate of the Hamiltonian H_0, with eigenvalue E. This is expressed mathematically as

$$(E - H_0)\Psi_0 = 0 \tag{2.1}$$

Usually, H_0 is the Hamiltonian of a free–particle,

$$H_0 = \frac{P^2}{2M} \tag{2.2}$$

The goal of scattering theory is then to solve the full energy–eigenstate problem

$$(E - H_0 - V)\Psi = 0 \tag{2.3}$$

where Ψ is the eigenstate of the full Hamiltonian $H = H_0 + V$ with energy E. It has to be noted that there is a different Ψ_0 and correspondingly, a different Ψ for each

energy E.

2.1.1 The Lippmann–Schwinger Equation

The relation between incident and scattered states can be determined by the Lippmann–Schwinger equation [150]. We start by defining the scattered state, Ψ_S, via

$$\Psi_S = \Psi - \Psi_0 \tag{2.4}$$

The full Scrödinger equation (Eq. 2.3) can be written as

$$(E - H_0)\Psi = V\Psi \tag{2.5}$$

By substituting $\Psi = \Psi_S + \Psi_0$ in equation (2.5) and making use of (2.1) one obtains

$$(E - H_0)\Psi_S = V\Psi \tag{2.6}$$

Operating on both sides with $(E - H_0)^{-1}$ leads to

$$\Psi_S = (E - H_0)^{-1}V\Psi \tag{2.7}$$

which, by adding Ψ_0 to both sides, becomes

$$\Psi = \Psi_0 + (E - H_0)^{-1}V\Psi \tag{2.8}$$

This is known as the Lippmann–Schwinger equation.

2.1.2 Green's Function Method

Many of the interesting quantities in scattering theory can be expressed in terms of the exact Green's function or operator for the system [151, 152]. In these notes, we apply Green's functions to scattering problem. Let us recall the definitions of the

resolvent operators,

$$G_0(z) = (z - H_0)^{-1} \tag{2.9}$$

which is Green's function for the free–particle Hamiltonian H_0 and

$$G(z) = (z - H)^{-1} \tag{2.10}$$

is the perturbed Green's function. z is an arbitrary complex number.
With this notation, the Lippmann–Schwinger equation becomes

$$\Psi = \Psi_0 + G_0 V \Psi \tag{2.11}$$

where $z = E + i\epsilon$ and ϵ is an infinitesimal positive number. This choice ensures that the scattered wave Ψ_S is an outgoing wave.

2.1.3 The Born Series

The Lippmann–Schwinger equation is an exact equation for the scattering problem and that needs to be solved. In a general statement, there is no simple way to find exact solutions of the Lippmann–Schwinger equation. One possible way to solve this equation is by perturbation theory, i.e., a power series expansion in the potential V such that in the absence of potential, $\Psi = \Psi_0$.

$$\Psi = \Psi_0 + G_0 V \Psi_0 + G_0 V G_0 V \Psi_0 + G_0 V G_0 V G_0 V \Psi_0 + ... \tag{2.12}$$

Therefore, the lowest order approximation can be written as

$$\Psi = \Psi_0 + G_0 V \Psi_0 + O(V^2) \tag{2.13}$$

and neglect $O(V^2)$ correction. This is called the first–order Born approximation. This approximation works well only in a situation where the scattering is weak.

2.2 Two–level Photovoltaic Systems

The basic idea of our methodology is described through the example of two–level photovoltaic systems with the electron–hole interaction and non–radiative recombination. The two–level system characterized by the HOMO (highest occupied molecular orbital) and the LUMO (lowest unoccupied molecular orbital) can be in the permanent or in the transitory regime.

Here, for the photovoltaic devices in the permanent regime, we consider the molecular photo–cells where the energy conversion process takes place in a single molecular donor–acceptor complex attached to electrodes. Initially, the whole system is in the ground state with filled valence bands and empty conduction bands. Following the photon absorption by the molecule, one electron and one hole are created in LUMO and HOMO, respectively. Both charge carriers interact via the Coulomb potential and can be recombined in the molecule or can be transferred to their respective channels where they produce photovoltaic current (See Fig. 2-1).

Furthermore, as pointed above, this formalism can be applied to the photovoltaic systems working in the transitory regime. As an example for the photovoltaic devices in the transitory regime, we consider the Bulk Hetero–Junction (BHJ) organic solar cells. The full system includes two semi–infinite leads of acceptor (A) and donor (D) sites. For both leads, the initial sites correspond to the interface, and the rest represent the electron or hole evacuation leads. All the A and D molecules have been taken as a single level energy, corresponding to the LUMO and HOMO, respectively. In the BHJ structure, upon absorption of a photon one exciton is created in the donor side of the cell at one negative time, and then it diffuses up to the interface (the two–level system). This exciton arrives at the interface at time $t = 0$ and our aim is to evaluate the total charge injected in each contact due to the exciton dissociation after a sufficiently large time.

In our study, the energy difference between LUMO and HOMO levels on the absorber molecule (permanent regime) or on the interface (transitory regime) is taken equal to Δ. The coupling matrix elements between the molecular or interface states

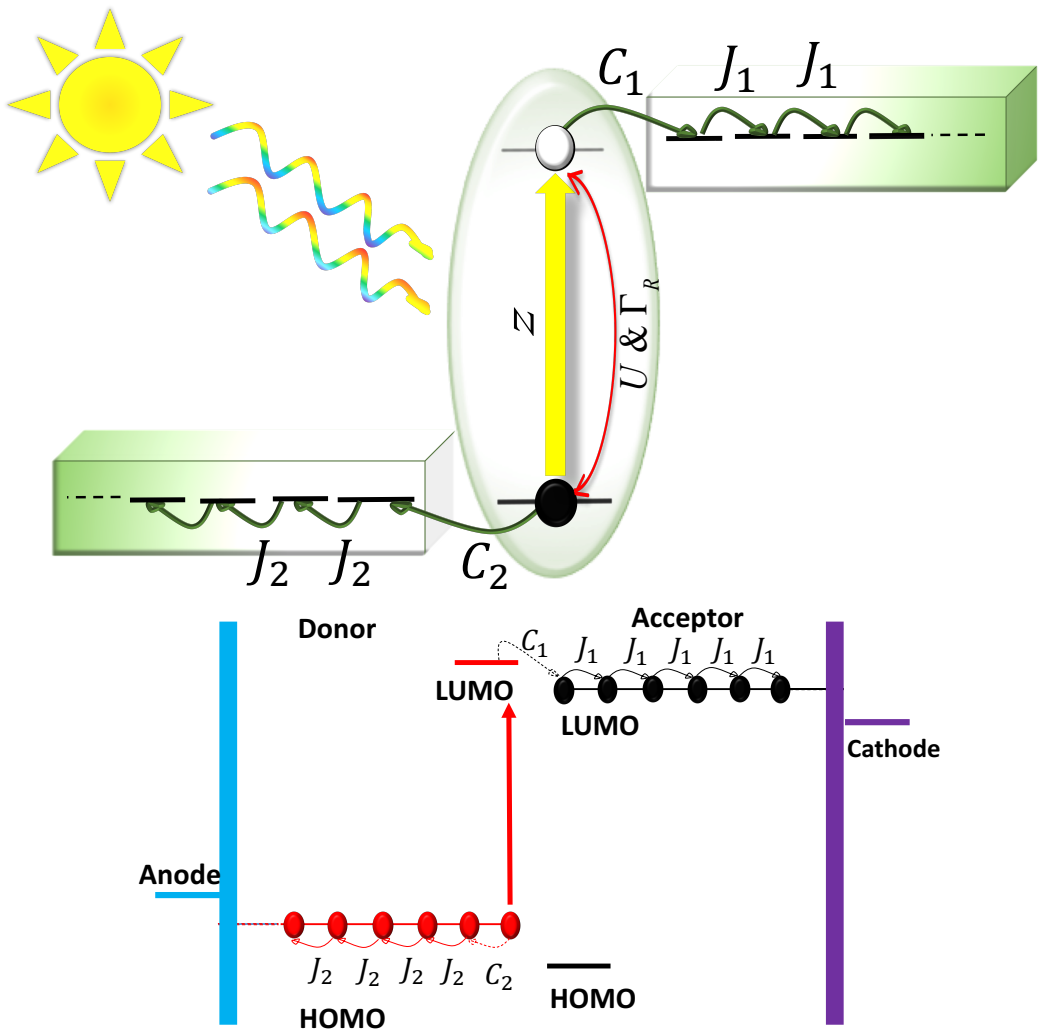

Figure 2-1: The two–level model in the permanent (Top panel) and transitory (Bottom panel) regime of illumination. (Top panel) A molecular photo–cell with one HOMO and one LUMO orbitals attached to the electrodes. The red line represents the electron–hole interaction and recombination inside the molecule and the hopping integrals of electron and hole are denoted by C and J. Z is the energy of absorbed photon. U and Γ_R represent respectively the electron–hole interaction and recombination inside the molecule. (Bottom panel) Schematic representation of a donor–acceptor system. Charge evacuation leads are considered as semi–infinite chains. Here, J_1 and J_2 are the coupling energies between two adjacent sites in the electron and hole chains, respectively. Also, C_1 and C_2 represent the first coupling energies between the interface states and charge evacuation chains.

and the possible evacuation channels are denoted by C. The hopping matrix elements inside each evacuation channel are considered uniform and denoted by J. The onsite energies of the electron at site (x) and the hole at site (y) are assumed to be $\varepsilon_e(x)$ and

$\varepsilon_h(y)$, respectively. Additionally, their Coulomb–type interaction $I(x, y)$ is modeled by

$$I(x,y) = \begin{cases} U, & \text{if } x = 0 \quad \textit{and} \quad y = 0, \\ \frac{V}{(x+y)}, & \text{if } x \neq 0 \quad \textit{or} \quad y \neq 0. \end{cases} \tag{2.14}$$

x and y are the site numbers on the mentioned square lattice.

Since $I(x, y)$ is an attractive Coulomb potential, U and V have negative values. In the above equation, U represents the strength of short–range electron–hole interaction, i.e., the situation where both charge carriers are in the same place either absorber molecule or D–A interface. On the other hand, V is the strength of long–range electron–hole interaction, i.e., the situation where at least one of the charge carriers is in its respective lead.

2.3 Hilbert Space Of The Electron–Hole Pair

The Hilbert space of the mentioned two–level structures can be mapped onto a square lattice (Fig. 2-2). For the PV devices in the permanent regime, x (y) represents the position of the electron (hole), in the molecule or in the attached leads such that site ($x = 0,\ y = 0$) is the electron–hole pair position in the molecule that is simply the initial state just after the photon absorption, i.e., the excited state and site $x > 0$ ($y > 0$) represents the electron (hole) position in its respective lead. Similarly, for the PV devices in the transitory regime, x (y) represents the position of the electron (hole), in the interface or in the attached leads.

2.3.1 The Electron–Hole Pair Hamiltonian

The effective Hamiltonian of the system is of the tight–binding type [153] additionally including the electron–hole interaction term

$$H = \sum_i \varepsilon_i \left|i\right\rangle\!\left\langle i\right| + \sum_{i,j} J_{i,j} \left|i\right\rangle\!\left\langle j\right| \tag{2.15}$$

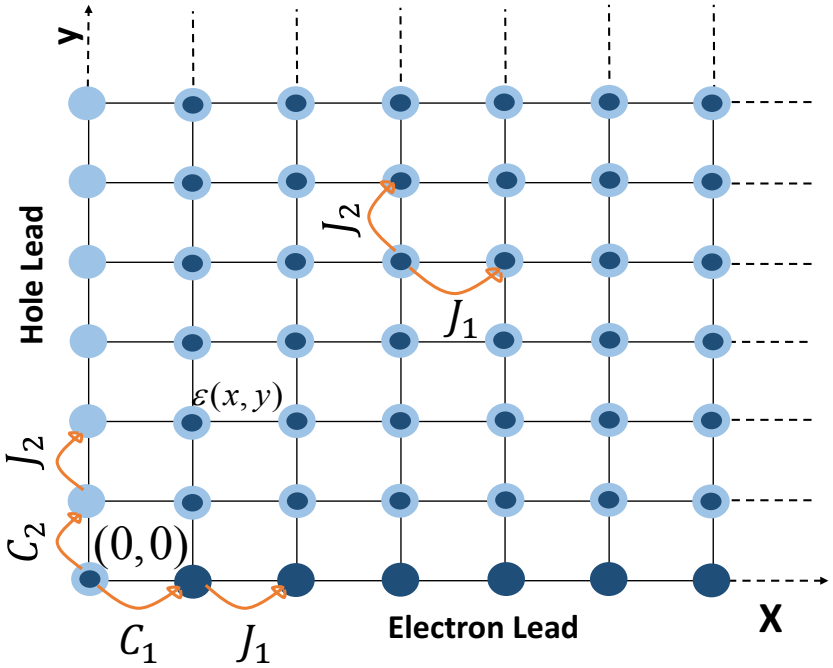

Figure 2-2: The Hilbert space of the electron–hole pair by considering just one evacuation channel for each charge carrier, with one state at each point (x, y) of the lattice. The coordinates x and y of a given state represent the position of electron and hole in their respective leads. $\varepsilon(x, y)$ is the onsite energy of each site of the square lattice and the hopping integrals (C and J) are along the bonds of the square lattice.

Here the first term indicates the total onsite energy of each square lattice basis state which is defined as a summation over the electron onsite energy, the hole onsite energy and the Coulomb interaction energy between them

$$\varepsilon(x, y) = \varepsilon(x) + \varepsilon(y) + I(x, y) \tag{2.16}$$

The probability of photo–generated electron–hole pair local–recombination inside the absorber molecule or in the D–A interface is taken into account by adding an imaginary part $-i\Gamma_R/2$ to the onsite energy of the site $(0, 0)$, where Γ_R is the recombination parameter. Finally, the second term in equation (2.15) represents the coupling energy between two adjacent basis states on the square lattice. As pointed above, the coupling energies between molecular states or interface states (i.e., site

$(0,0)$) and their first neighbors are taken different from the other coupling energies.

2.4 Expression Of Spectral Weight (Density Of States)

For most of this thesis we shall be concerned with calculating the local density of state (LDOS) for an orbital Φ_0 from a tight–binding or localized orbital model Hamiltonian H. The LDOS is used to understand what effect the rest of the solid is having on a local region such as an atom. The definition for the LDOS is given by the definition of the total density of states (DOS) weighted by the probability of the excitation being in a particular orbital. For a system described by a Hamiltonian H and normalized eigenfunctions Ψ_m and eigenvalues E_m, the mathematical definition of the LDOS is

$$n_0(E) = \sum_m |\langle\Phi_0|\Psi_m\rangle|^2 \delta(E - E_m) \tag{2.17}$$

such that the total density of states is the sum of the density of states projected over a full orthonormal set $|\Phi_m\rangle$.

Equation (2.17) is a rather formal definition of the local density of states. However this definition can be related to the Green's operator $G(z) = (z - H)^{-1}$ and since we want to calculate only the local density of states associated with an orbital Φ_0 we just need the element $G_{00}(z)$. This diagonal matrix elements of Green's function is given by

$$G_{00}(E + i\epsilon) = \langle\Phi_0|\frac{1}{E + i\epsilon - H}|\Phi_0\rangle \tag{2.18}$$

where ϵ is an infinitesimal positive number. By inserting the identity operator $\sum_m |\Psi_m\rangle\langle\Psi_m|$ to this equation and using $H|\Psi_m\rangle = E_m|\Psi_m\rangle$, one obtains

$$G_{00}(E + i\epsilon) = \sum_m |\langle\Phi_0|\Psi_m\rangle|^2 \frac{E - E_m - i\epsilon}{(E - E_m)^2 + \epsilon^2} \tag{2.19}$$

where the real part indicates the poles which correspond to the discrete eigenvalues

of H and the imaginary part results in type δ singularities

$$\lim_{\epsilon \to 0} \frac{1}{\pi} \frac{\epsilon}{(E - E_m)^2 + \epsilon^2} = \delta(E - E_m) \tag{2.20}$$

Figure (2-3) represents the typical behavior of real and imaginary parts of the Green's function close to a pole.

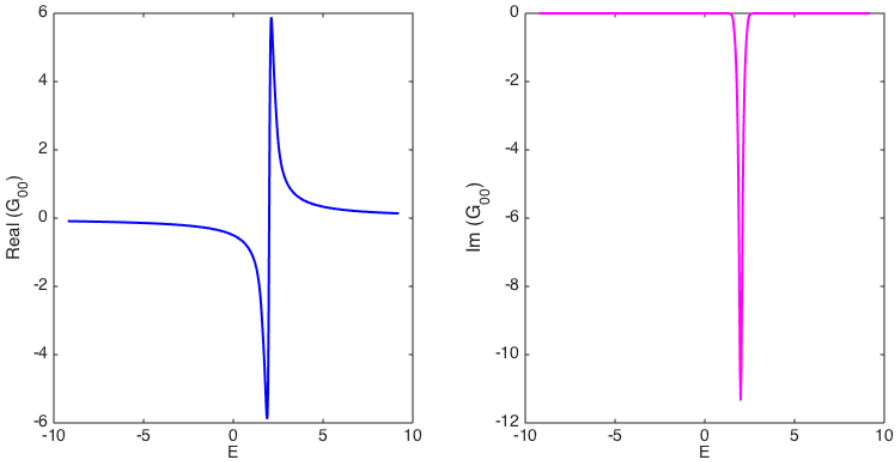

Figure 2-3: Real and imaginary parts of Green's function $G_{00}(E)$.

The above mentioned equations indicate the standard spectral theorem

$$n_0(E) = \sum_m |\langle \Phi_0 | \Psi_m \rangle|^2 \lim_{\epsilon \to 0} \frac{1}{\pi} \frac{\epsilon}{(E - E_m)^2 + \epsilon^2} \tag{2.21}$$

$$\rightarrow n_0(E) = -\frac{1}{\pi} \lim_{\epsilon \to 0} \operatorname{Im} G_{00}(E + i\epsilon) \tag{2.22}$$

Therefore, the imaginary part of the Green's function $G_{00}(z)$ describes the intensity of each eigenstate on a chosen orbital Φ_0. $G_{00}(z)$ can be calculated using a continuous fraction approach which will be explained later in this chapter. It has to be noted here that in this formalism the density of states indicate all the possible energy states for the electron–hole pair.

2.4.1 The Krylov Space

Let us consider a state $|\Psi_1\rangle$ and a Hamiltonian H in a given Hilbert space. The Krylov space of order N is simply the space spanned by the vectors $|\Psi_1\rangle$, $H|\Psi_1\rangle$, $H^2|\Psi_1\rangle$ ... $H^{N-1}|\Psi_1\rangle$. In a general statement, the Krylov space is composed of the states of the form $Q_n(H)|\Psi_1\rangle$ where Q_n is any polynomial of degree n [154, 155].

The Krylov space plays a central role in the study of operators of the form $f(H)$ such that it allows to calculate vectors $|\Psi\rangle$ of the form $|\Psi\rangle = f(H)|\Psi_1\rangle$. We present the famous recursion basis states in the Krylov space which is obtained from an initial basis by a Schmidt orthogonalization procedure. It allows numerical evaluation of Green's operators.

2.4.2 The Recursion Method

Efficient computational recursion and order N methods have been successfully developed in solid–state physics since their introduction by R. Haydock [156–158]. The recursion methods are based on an eigenvalue approach of Lanczos [159], and rely on the computation of Green's functions matrix elements by continuous fraction expansion and allow to calculate the projected densities of states for a given Hamiltonian. An initial–state vector, on whose projection one wishes to compute a density of states, is selected [160]. One can build a new basis set and a series of recursion coefficients starting from the mentioned initial state. In this new basis, the Hamiltonian becomes tri–diagonal and the recursion coefficients are the matrix elements of the Hamiltonian [161–165]. In the following, the recursion method is explained in details.

We consider a system described by a tight–binding Hamiltonian H. To a given normalized state $|\Psi_0\rangle$ we can always associate a recursion basis which is constructed by a Schmidt orthogonalization procedure [**?**, **?**], starting from the set of states $|\Psi_0\rangle$, $H|\Psi_0\rangle$, $H^2|\Psi_0\rangle$ ... $H^{N-1}|\Psi_0\rangle$ ... . Let us consider $H|\Psi_0\rangle$ and decompose it into two components: first component parallel to $|\Psi_0\rangle$ and the second one orthogonal to $|\Psi_0\rangle$. Therefore, we can write

$$H|\Psi_0\rangle = a_0|\Psi_0\rangle + b_0|\Psi_1\rangle \tag{2.23}$$

where $\langle\Psi_0|\Psi_1\rangle = 0$ and $\langle\Psi_1|\Psi_1\rangle = 1$. If the coefficient b_0 is chosen real and positive then $|\Psi_1\rangle$ can be defined in a unique way. In the next step, we consider $H\,|\Psi_1\rangle$ which can be decomposed into a component parallel to the space spanned by $|\Psi_0\rangle$, $|\Psi_1\rangle$ and a component orthogonal to this space. We obtain

$$H\,|\Psi_1\rangle = a_1\,|\Psi_1\rangle + b_0'\,|\Psi_0\rangle + b_1\,|\Psi_2\rangle \tag{2.24}$$

with $\langle\Psi_0|\Psi_2\rangle = 0$, $\langle\Psi_1|\Psi_2\rangle = 0$ and $\langle\Psi_2|\Psi_2\rangle = 1$. Since, H is a Hermitian operator we deduce that $b_0 = b_0'$. If the coefficient b_1 is chosen real and positive then $|\Psi_2\rangle$ can be defined in a unique way.
The process can be repeated and leads to the construction of a set of states $|\Psi_n\rangle$ which are orthonormal and satisfy the equation below

$$H\,|\Psi_n\rangle = a_n\,|\Psi_n\rangle + b_{n-1}\,|\Psi_{n-1}\rangle + b_n\,|\Psi_{n+1}\rangle \tag{2.25}$$

A typical recursion chain is shown in Fig. 2-4. Parameters a_n and b_n are called recursion coefficients and represent the onsite energy of each state and the hopping integrals between two adjacent states, respectively. Ψ_n are the recursion wave vectors.

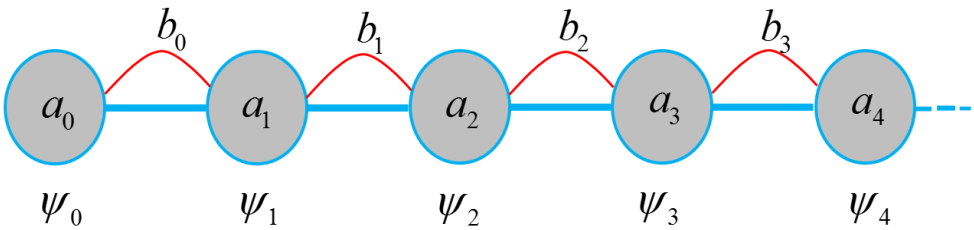

Figure 2-4: A typical recursion chain. The parameters a_n represents the onsite energy of each state, while the parameters b_n are the hopping energies between two adjacent states. $|\Psi_n\rangle$ is the wave function associated to the state n.

At any step n, the recursion coefficient a_n is determined by $\langle\Psi_n|H|\Psi_n\rangle$ which is a real number. Then, the recursion coefficient b_n and recursion wave vector Ψ_{n+1} are obtained by the normalization condition for Ψ_{n+1} and the choice of a real positive b_n. An important property of the states $|\Psi_n\rangle$ is that they spread progressively from

an initial state. In Fig. 2-5, the propagation of recursion wave vectors on a square lattice where the initial state $|\Psi_0\rangle$ supposed to be on site $(1, 1)$ is shown.

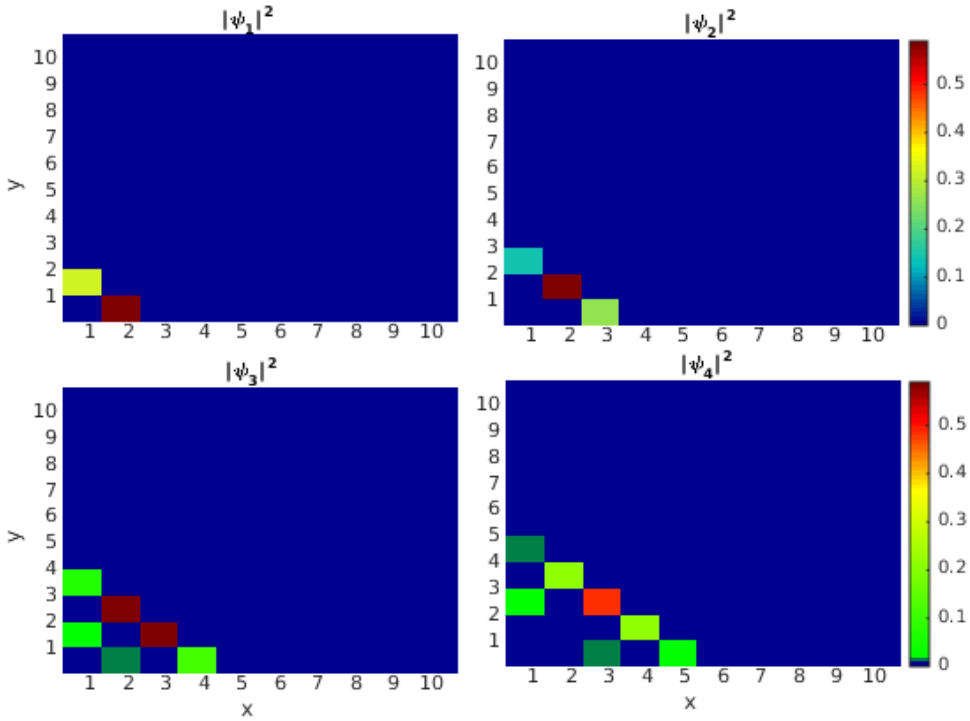

Figure 2-5: Propagation of different order of recursion wave vectors $|\Psi_n\rangle$.

The significant achievement of the recursion method is that the Hamiltonian H on the basis ($|\Psi_0\rangle$, $|\Psi_1\rangle$, $|\Psi_2\rangle$, ...) can be written in a tri–diagonal form

$$H = \begin{bmatrix} a_0 & b_0 & 0 & \dots & \\ b_0 & a_1 & b_1 & \dots & \\ 0 & b_1 & a_2 & b_2 & \dots \\ \vdots & \ddots & \ddots & \ddots & \ddots \\ & & & b_n & a_n \end{bmatrix} \tag{2.26}$$

where the recursion coefficients are the matrix elements.

Here we draw the reader's attention to the physical interpretation of the chain model represented in Fig. (2-4). The physics behind this chain model is that the orbital Ψ_0 represents the initial state of the system, for example an electron on one

particular atom. The chain model permits the system to hop from Ψ_0 to Ψ_1, where Ψ_1 represents a linear combination of orbitals of atoms neighboring Ψ_0. Having reached Ψ_1 the system has the possibility to either hop back to Ψ_0 or on to Ψ_2, where Ψ_2 represents second nearest neighbors of the original atom. Therefore the chain model establishes an ordering of states of the basis in terms of how many intermediate states must be passed to reach a given state. Thus the system must pass through Ψ_n to reach state Ψ_{n+1} and so forth. Therefore, the behavior of Ψ_0 is most strongly influenced by Ψ_1 and less and less by each succeeding orbital in the chain. The stronger influence on orbitals of the systems comes from orbitals nearer in the sense of being accessible via fewer intermediate orbitals. Chain model is the mathematical expression of the concept of local environment. Each orbital on the chain represents a more distant part of the environment of the initial orbital Ψ_0, whereas the parameters of the recursion specify the effects of that environment on the motion of the system.

2.4.3 Continued Fraction

Based on the definition of projection operators on the recursion chain (see Appendix B), the Green's function expressed by Eq. (2.18) can be written in the continued fraction form

$$G_{00}(z) = \cfrac{1}{z - a_0 - \cfrac{b_0^2}{z - a_1 - \cfrac{b_1^2}{z - a_2 - \ddots}}} \tag{2.27}$$

The calculation of recursion coefficients should be continued up to the convergence occurrence. Suppose that the convergence occurs in the recursion step (Rec). Then, to terminate the continuous fraction we define the terminator $T(z)$ which includes

the effects of the all the terms after the convergence occurrence step

$$T(z) = \cfrac{1}{z - a_{Rec} - \cfrac{b_{Rec}^2}{z - a_{Rec} - \cfrac{b_{Rec}^2}{z - a_{Rec} - \ddots}}} \tag{2.28}$$

where the index "Rec" indicates all the recursion steps after the convergence occurrence step. The terminator $T(z)$ can be rewritten by a closed form including itself as follows

$$T(z) = \frac{1}{z - a_{Rec} - b_{Rec}^2 T(z)} \tag{2.29}$$

By solving Eq. (2.29) regarding $T(z)$, then we get a well known square root terminator

$$T(z) = \frac{z - a_{Rec} \pm \sqrt{(z - a_{Rec})^2 - 4b_{Rec}^2}}{2b_{Rec}^2} \tag{2.30}$$

Choosing the negative or positive sign in front of the root according to the condition where $T(E + i\epsilon) \to 0$ if $E \to \infty$ we derive the terminator

$$\begin{aligned} \text{if } |E - a_{Rec}| < 2b_{Rec} \quad T(E + i\epsilon)_{\mathbb{C}} &= \frac{E - a_{Rec} - i\sqrt{4b_{Rec}^2 - (E - a_{Rec})^2}}{2b_{Rec}^2} \\ \text{if } |E - a_{Rec}| > 2b_{Rec} \quad T(E + i\epsilon)_{\mathbb{R}} &= \frac{E - a_{Rec} \pm \sqrt{(E - a_{Rec})^2 - 4b_{Rec}^2}}{2b_{Rec}^2} \end{aligned} \tag{2.31}$$

The energy continuum is therefore between $|E - a_{Rec}| < 2b_{Rec}$.
Using Eqs. (2.31) and (2.27) as well as the coefficients a_n and b_n, finally the Green's function $G_{00}(z)$ can be calculated iteratively. The local density of states obtained this way converges very fast and numerically almost exact results can be obtained within the order of hundreds iterations steps.
It has to be noted here that the Green's function expressed by Eq. (2.27) can be

written in a compact form as shown below

$$G_{00}(z) = \frac{1}{z - a_0 - \Sigma_0(z)} \tag{2.32}$$

where $\Sigma_0(z)$, so–called the self–energy, is an energy due to the coupling to other degrees of freedom. In other words, the self–energy represents the contribution to the particle's energy resulting from its interactions with its environment.

2.4.4 Spectral Decomposition

By spectral decomposition, one can consider the Green's function as a summation over localized and continuous spectrums. In the case of just one localized state which is the case of main interest here, one can write

$$G(z) = \frac{1}{z - H} = \frac{|\Psi_{lz}\rangle\langle\Psi_{lz}|}{z - E_{lz}} + \int \frac{|\Psi_{cn}\rangle\langle\Psi_{cn}|}{z - E} dE \tag{2.33}$$

where "lz" stands for the localized state and "cn" indicates the continuous part. In the limit of "$z \to E_{lz}$" one has

$$\lim_{z \to E_{lz}} (z - E_{lz}) G(z) = |\Psi_{lz}\rangle\langle\Psi_{lz}| \tag{2.34}$$

Multiplying both sides of this equation on the right and on the left by $|0,0\rangle$ results in

$$\lim_{z - E_{lz}} (z - E_{lz}) G_{00}(z) = |\langle\Psi_{lz}|0,0\rangle|^2 = P \tag{2.35}$$

where $P = |\langle\Psi_{lz}|0,0\rangle|^2$ is the weight of localized state on the state $|0,0\rangle$. Making use of Eq. (2.32) one obtains

$$G_{00}^{-1}(z) = z - a_0 - \Sigma_0 = (z - E_{lz}) - [\Sigma_0(z) - \Sigma_0(E_{lz})] \tag{2.36}$$

$$\to z - a_0 - \Sigma_0(z) = (z - E_{lz})[1 - \frac{\partial \Sigma_0}{\partial z}|_{z=E_{lz}}] \tag{2.37}$$

Therefore, the weight of localized state can be determined by

$$P = \lim_{z-E_{lz}} (z - E_{lz}) G_{00}(z) = \frac{1}{1 - \frac{\partial \Sigma_0}{\partial z}|_{z=E_{lz}}} \tag{2.38}$$

The weight of localized states has a strong impact on the charge separation yield as will be discussed in details in the next chapters.

2.5 Fluxes & Quantum Yield

2.5.1 Scattering State

In this formalism, we consider a photovoltaic cell as a system subjected to an incident flux of photons and assume that the whole system (PV cell + electromagnetic field) is in a stationary state that obeys the fundamental Lippmann–Schwinger equation. By applying quantum scattering theory, in particular the Lippmann–Schwinger equation, the photovoltaic system is described by a wave function. The incoming state of the theory $|\Phi_{inc}\rangle$ represents the photon field with the PV cell in its ground state. By the dipolar interaction between the photovoltaic system and the electromagnetic field this incident state $|\Phi_{inc}\rangle$ is coupled to a state where one photon is absorbed and one electron–hole pair is created.

Based on the Lippmann–Schwinger equation the total wave function of the system with incident photons of energy E is

$$|\Psi(E)\rangle = |\Phi_{inc}\rangle + G_0 V |\Psi(E)\rangle \tag{2.39}$$

In the second quantization notation, V can be expressed by

$$V = \alpha(d^\dagger a + d a^\dagger) \tag{2.40}$$

where a and $a^\dagger$ are the photon annihilation and creation operators, respectively. Furthermore, the dipolar transition operators are denoted by d and $d^\dagger$.

α is defined as

$$\alpha^2(E) = \frac{d^2\rho(E)}{2\epsilon_0} \tag{2.41}$$

where d and $\rho(E)$ are respectively the dipole matrix element of the molecular transition and the electromagnetic energy density of photons with energy E. ϵ_0 represents the vacuum permittivity.

Then based on the first–order Born approximation, the total wave function can be described by

$$|\Psi(E)\rangle = |\Phi_{inc}\rangle + G_0 V |\Phi_{inc}\rangle \tag{2.42}$$

which can be rewritten as follows

$$|\Psi(E)\rangle = |\Phi_{inc}\rangle + |\Psi_P(E)\rangle \tag{2.43}$$

The second term in the right hand side of the above equation, $|\Psi_P(E)\rangle$, is called the scattered wave function which represents the charge carriers photo–generated by absorption of a photon with energy E and plays an important role in this formalism. The scattered wave function $\Psi_P(E)$ is defined by the following equation

$$|\Psi_P(E)\rangle = \frac{1}{z - H_0} |exc\rangle \tag{2.44}$$

where $z = E + i\epsilon$ is a complex energy with an infinitesimal positive imaginary part ϵ and $|exc\rangle = V |\Phi_{inc}\rangle$ represents the excited state after the photon absorption for the PV devices in the permanent regime (or the donor–acceptor interface for the PV devices in the transitory regime), i.e., $|0, 0\rangle$ on the mentioned square lattice. H_0 is the Hamiltonian of the electron–hole pair which is defined by the tight–binding model. The recursion formalism allows to compute $|\Psi_P(E)\rangle$ in an interesting way.

Let us write

$$G(E)\,|0,0\rangle = \sum_{n=0}^{\infty} |\Psi_n\rangle \langle\Psi_n|\, G(E)\,|0,0\rangle \tag{2.45}$$

where $|\Psi_n\rangle$ are the vectors of the recursion chain computed from the initial site $|0,0\rangle$. By introducing a new parameter named β the above mentioned equation can be rewritten as

$$G(E)\,|0,0\rangle = \sum_{n=0}^{\infty} \beta_n(E)\,|\Psi_n\rangle \tag{2.46}$$

where

$$\beta_n(E) = \langle\Psi_n|\, G(E)\,|\Psi_0\rangle \tag{2.47}$$

therefore we need to compute the off–diagonal elements of the Green's function. By considering the recursion chain introduced in the previous sections and defining proper projection operators on this chain, our formalism allows us to compute the off–diagonal elements using the product of recursion parameters as

$$\beta_n(E) = \frac{1}{b_n} \prod_{p=0}^{n} b_p G_p(E) \tag{2.48}$$

According to Eq. (2.48) one has

$$\beta_0(E) = G_0 \tag{2.49}$$

$$\beta_1(E) = G_0 G_1 b_0 \tag{2.50}$$

$$\beta_2(E) = G_0 G_1 G_2 b_0 b_1 \tag{2.51}$$

$$\vdots \tag{2.52}$$

where G_0 is the Green's function starting from site 0, similarly G_1 starts from site 1 and so on. b_n are the recursion coefficients.

To have an idea about the behavior of scattered wave function $|\Psi_P(E)\rangle$, Fig. 2-6 represents the weight of $|\Psi_P(E)\rangle$ on different sites (x, y) of the square lattice normalized to its value on the initial site $\frac{|\langle x,y|\Psi_P(E)\rangle|^2}{|\langle 0,0|\Psi_P(E)\rangle|^2}$ by considering various absorbed photon energies (z) for a cell with energy continuum (EC) lying between 1.2 and 2.8 eV. The energy continuum indicates all allowed energies for the electron–hole pair. As can be seen, for the photon energies outside the continuum or on the band edge, the scattered wave function is nearly localized on the site $|0, 0\rangle$ which is simply the absorber molecule (in the permanent regime) or the D–A interface state (in the transitory regime). As the photon energy E increases such that E lies within the continuum, the scattered wave function extends on the various sites of the square lattice.

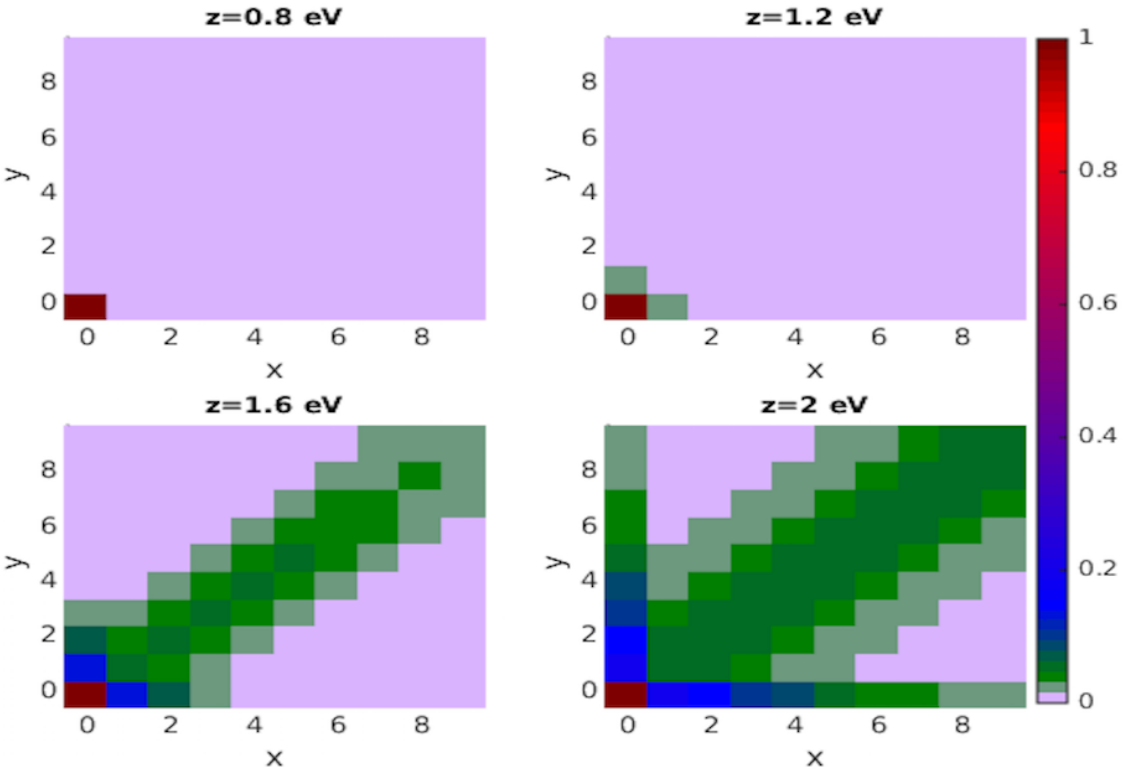

Figure 2-6: Weight of the scattered wave function $|\Psi_P(z)\rangle$ on different sites (x, y) of the square lattice normalized to its value on the initial site $(\frac{|\langle x,y|\Psi_P(z)\rangle|^2}{|\langle 0,0|\Psi_P(z)\rangle|^2})$ for various absorbed photon energies (z). The cell parameters are $J_1 = J_2 = 0.2$, $C_1 = C_2 = 0.1$ and the energy difference between LUMO and HOMO energy levels (Δ) is equal to 2, therefore the energy continuum (EC) is between 1.2 and 2.8 (All energies are in eV unit).

Knowledge of $|\Psi_P(E)\rangle$ allows one to compute the average values of the cell parameters. Let us look at to the evaluation of the average photovoltaic current "A". Since the intensity of the incident sunlight is not as strong as some other light sources (such as lasers), we can stay in the Born approximation and keep the terms which are of linear order with respect to the light intensity. The average values of current operator A can be expressed by

$$\langle A(E)\rangle = \langle\Psi(E)|\, A\, |\Psi(E)\rangle \tag{2.53}$$

which can be developed based on the Eq. (2.43) as follows

$$\langle A(E)\rangle = \langle\Phi_{inc}|A|\Phi_{inc}\rangle + \langle\Psi_P(E)|\, A\, |\Phi_{inc}\rangle + \langle\Phi_{inc}|\, A\, |\Psi_P(E)\rangle + \langle\Psi_P(E)|A|\Psi_P(E)\rangle \tag{2.54}$$

where only the last term gives non–zero contribution because $A\,|\Phi_{inc}\rangle = 0$ in the models considered here. Therefore,

$$\langle A(E)\rangle = \langle\Psi_P(E)|\, A\, |\Psi_P(E)\rangle \tag{2.55}$$

Note that there are several incident electromagnetic modes such that the total photovoltaic current is the sum of the contributions of all modes $\langle A(E)\rangle$. Furthermore, here the average current is given per spin.

2.5.2 Fluxes

In this formalism, the cell performance can be described through the definition of a series of fluxes. The main three fluxes are: (1) the flux of absorbed photons $\Phi_{ph}(E)$, which is the number of absorbed photons per unit time. (2) the fluxes of electron–hole pairs that recombine in the molecule $\Phi_R(E)$, and (3) the flux of pairs whose escape from the molecule result in the photovoltaic current $\Phi_C(E)$.

By knowing $|\Psi_P(E)\rangle$, one can compute the fluxes of absorbed photons, of recombined electron–hole pairs and of charges injected in the evacuation channels. The determination of these quantities gives access to a detailed analysis of the photovoltaic

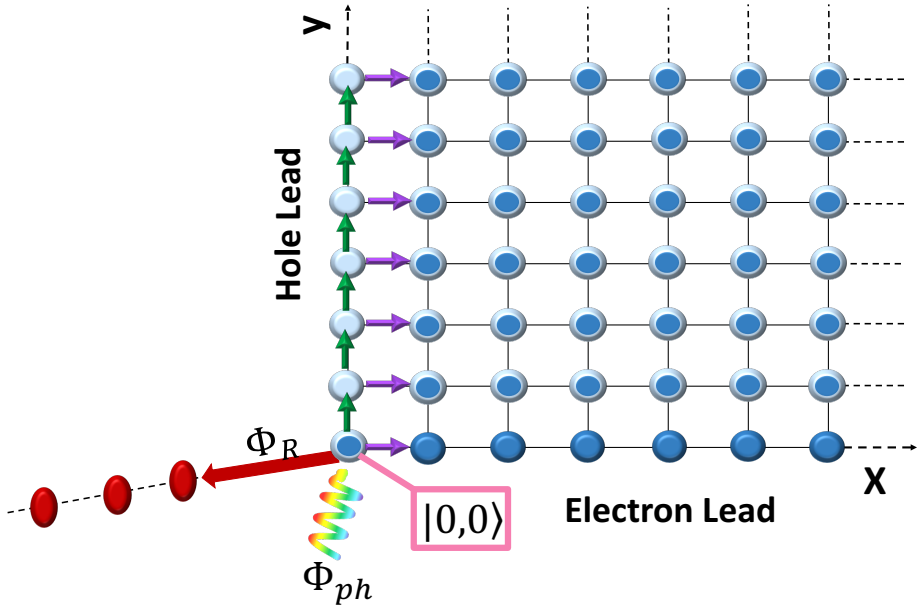

Figure 2-7: Flux conservation. Flux of current, recombination and photons are represented on the square lattice. The sum of the two fluxes starting from site (0,0) (violet and green) is equal to the flux of electron–hole pairs injected in the material. The sum of all the violet contributions is equal to the flux of electron injected in its lead. If there are no localized states these two fluxes are equal. The recombination flux is denoted by red arrow. $|0,0\rangle$ determines either the first excited state or the D–A interface.

cell performance.

2.5.2.1 Flux Of Absorbed Photons

As pointed above, the scattered wave function of photo–generated electron–hole pair can be expressed by

$$\Psi_P(E) = G_0(E)\,|0,0\rangle \tag{2.56}$$

the density matrix related to this wave function is

$$\rho = \alpha(E)^2\,|\Psi_P(E)\rangle\langle\Psi_P(E)| = \alpha(E)^2(\frac{1}{z-H}\,|0,0\rangle\,\langle 0,0|\,\frac{1}{z^*-H}) \tag{2.57}$$

A simple way to derive the expression of the fluxes is to write the time evolution of the density matrix which can be formally computed according to

$$\frac{\mathrm{d}\rho}{\mathrm{d}t} = \frac{-i}{\hbar}[H, \rho] \tag{2.58}$$

where H is the Hamiltonian of the system and the brackets denote a commutator. As can be seen clearly from the above equation, density matrix satisfies the von Neumann Equation. Also, the time evaluation of the density matrix on a given state k can be expressed by

$$\frac{\mathrm{d}\rho_{kk}}{\mathrm{d}t} = \frac{\langle k|[H, \rho]|k\rangle}{i\hbar} \tag{2.59}$$

where,

$$\langle k|[H, \rho]|k\rangle = \langle k|H\rho|k\rangle - \langle k|\rho H|k\rangle \tag{2.60}$$

Finally, after few algebra processes and making use of Eq. (2.57), one obtains

$$\langle k|[H, \rho]|k\rangle = \alpha^2(E)\left\{[\langle k|\frac{1}{z-H}|0,0\rangle\langle 0,0|k\rangle] - h.c.\right\} + (z - z^*)\rho_{kk} \tag{2.61}$$

Since the imaginary part in the z definition (ϵ) is negligible, we can write

$$\sum_j \Phi_{j\to k} = \frac{2\alpha^2(E)}{\hbar}\,\mathrm{Im}\{\langle k|\Psi_P(E)\rangle\langle 0,0|k\rangle\} \tag{2.62}$$

where the flux from site j to site k is given by

$$\Phi_{j\to k}(E) = \alpha^2(E)\frac{2}{\hbar}H_{k,j}\,\mathrm{Im}(\langle j|\Psi_P(E)\rangle\langle\Psi_P(E)|k\rangle) \tag{2.63}$$

Based on Eq. (2.62), if $\langle k|0,0\rangle = 0$ then the total flux is equal to zero as well. On the other hand, if $|k\rangle = |0,0\rangle$, we obtain

$$\Phi = \sum_j \Phi_{j\to k} = \frac{2\alpha^2(E)}{\hbar}\,\mathrm{Im}\{\langle 0,0|\Psi_P(E)\rangle\} \tag{2.64}$$

which can be rewritten as

$$\Phi = \frac{2\alpha^2(E)}{\hbar}\,\mathrm{Im}\{\,\langle 0,0|G(E)|0,0\rangle\} \tag{2.65}$$

As pointed before, the local density of states on a given state, for instance $|0,0\rangle$, can be expressed by

$$n(E) = -\frac{1}{\pi}\,\mathrm{Im}\{\,\langle 0,0|G(E)|0,0\rangle\} \tag{2.66}$$

Merging Eqs. (2.65) and (2.66) gives

$$\Phi = -\frac{2\pi\alpha^2(E)}{\hbar}n(E) \tag{2.67}$$

Based on Eq. (2.67), the flux of absorbed photons is related to the local density of states $n(E)$ which is equivalent to the Fermi's Golden Rule. $n(E)$ can also be expressed as follows

$$n(E) = \frac{1}{\pi}\frac{\Gamma_R + \Gamma_p(E)}{(E - \Delta + U - E_p(E))^2 + (\Gamma_R + \Gamma_p(E))^2} \tag{2.68}$$

where $U(U < 0)$ and $\Gamma_R(E)$ are electron–hole local interaction energy and local recombination parameter, respectively. $E_p(E)$ and $\Gamma_p(E)$ are the real and imaginary parts of the self–energy of site $|0,0\rangle$. It should be noted that for sufficiently small coupling parameter C compared to bandwidth, the value of $n(E)$ is important only near the resonance energy E_{res} such that

$$E_{res} \approx \varepsilon(0,0) = \Delta + U \tag{2.69}$$

Δ is the energy difference between HOMO and LUMO and $\varepsilon(0,0)$ represents the onsite energy of the state $(0,0)$ of the square lattice.

2.5.2.2 Flux Of Current & Recombination

By applying the recursion procedure on the square lattice basis, as explained previously, one can obtain the expression of $|\Psi_P(E)\rangle$. From this expression we can compute the flux of electron–hole pairs along the bonds between nearest neighbors. The flux of electron–hole pair $\Phi_{l\to k}(E)$ from site l to site k on the square lattice is given by [168]

$$\Phi_{l\to k}(E) = \alpha^2(E)\frac{2}{\hbar}H_{k,l}\,\mathrm{Im}(\langle l|\Psi_P(E)\rangle\,\langle\Psi_P(E)|k\rangle) \tag{2.70}$$

where $H_{k,l}$ is the matrix element of the Hamiltonian between site k and l (hopping integral) which is real in the present model. It is also possible to compute the flux of electrons or holes using the fluxes of electron–hole pair $\Phi_{l\to k}(E)$. For example, the flux of electron from site a to site b is computed as

$$\Phi_{a\to b}(E) = \sum_{l_h}\Phi_{a,l_h\to b,l_h}(E) \tag{2.71}$$

which is the sum over all possible positions of the hole l_h of the electron–hole flux $\Phi_{a,l_h\to b,l_h}(E)$. Similarly, the flux of holes from site c to site d can be expressed by

$$\Phi_{c\to d}(E) = \sum_{l_e}\Phi_{l_e,c\to l_e,d}(E) \tag{2.72}$$

The above formulas are general and provide an efficient numerical tool to evaluate the flux of particles.

We introduce Φ_R and Φ_p which are the fluxes of electron–hole pairs that recombine on the site $(0,0)$ of the square lattice and pairs that escape from the site $(0,0)$, respectively. To remind, site $(0,0)$ of the square lattice represents either the absorber molecule of the PV devices in the permanent regime of illumination or the donor–acceptor interface of the PV devices in the transitory regime. The ratio between Φ_R

and Φ_p is given by the ratio between recombination and escaping rates. Based on the flux conservation one has $\Phi_{ph}(E) = \Phi_R(E) + \Phi_p(E)$, therefore the flux of outgoing charges can be related to the total photon flux through the equation

$$\Phi_p(E) = \Phi_{ph}(E) \times \frac{\Gamma_p(E)}{\Gamma_R + \Gamma_p(E)} \tag{2.73}$$

This formula has a classical form but let us recall that the different rates are computed through a quantum model. The current intensity in material I induced by photons of energy E is $I(E) = -e\Phi_C(E)$, where $-e$ is the electron charge. $\Phi_C(E)$ is defined by

$$\Phi_C(E) = \Phi_P(E)R(E) \tag{2.74}$$

where $R(E)$ indicates the proportion of the electrons and holes giving rise to the photovoltaic current. In general, one can define $R(E) = p_{e1}(E) - p_{h1}(E)$ where $p_{e1}(E)$ and $p_{h1}(E)$ are the proportion of electrons and holes evacuated from the molecule or form the D–A interface to the channel in material I. If there is only one evacuation channel for electron in material I and one channel in material II for the hole, $R(E) = 1$.

In case the number of available evacuation channels for at least one of the charge carriers is more than one, $R(E)$ again can be expressed by $R(E) = p_{e1}(E) - p_{h1}(E)$ where $p_{e1}(E)$ and $p_{h1}(E)$ are the proportion of electrons and holes evacuated from the molecule or from the D–A interface to the channel in material I. $R(E)$ can be computed from the electron–hole pair scattered wave function.

We discuss now the particular case of local electron–hole interaction and local electron–hole recombination. When there is only local interaction (i.e., just inside the molecule or on the interface) between the electron and the hole, an interesting analytical expression can be derived. In this case, the scattered wave function $\Psi_{PI}(z)$ for photons of energy z can be expressed simply in terms of the scattered wave function without electron–hole interaction $\Psi_{p0}(z)$ [168]

$$\Psi_{PI}(z) = \frac{G_I(E)}{G_0(E)}\Psi_{P0}(E) \tag{2.75}$$

where $G_I(E)$ and $G_0(E)$ are the local Green's function on site $|0,0\rangle$ with and without interaction. This implies that the ratio between different fluxes on the square lattice is unaffected by local interaction. Therefore the relative proportion $p_{eI}(z)$ of electrons that go to material I compared to material II is independent of local interaction and recombination.

Since for the non–interacting electron–hole pair this ratio can be expressed analytically, we get a way to estimate it even if there are interaction and recombination in the molecule or on the D–A interface. We have [168]

$$p_{eI}(z) = \left\langle \frac{\Gamma_{eI}(z)}{\Gamma_{eI}(z) + \Gamma_{eII}(z)} \right\rangle \tag{2.76}$$

where the bracket indicates an average over energies E such that

$$\langle f(z) \rangle = \frac{\int f(z-E) n_e(z-E) n_h(z) dE}{\int n_e(z-E) n_h(E) dE} \tag{2.77}$$

with $n_h(E) = {}_h\langle 0| \delta(E - H_h) |0\rangle_h$ and $n_e(E) = {}_e\langle 0| \delta(E - H_e) |0\rangle_e$ being the densities of states of holes and electrons on the HOMO and LUMO orbitals. Note that $n(z) = \int n_e(z-E) n_h(z) dE$ is the density of states on site $|0,0\rangle$ of the square lattice and is therefore proportional to the flux of absorbed photons. The meaning of the equation (2.77) is simply that the energy of the photon is divided into a part E for the hole and $(z-E)$ for the electron. Therefore, one has to perform an average of the operator $f(z-E)$ (which depends only on the energy $(z-E)$ of the electron state) over all possible repartitions of energy between electron and hole.
$\Gamma_{eI}(E)$ is the electron injection rate between the LUMO orbital, on site $(0,0)$ and the first site in material I which is given by

$$\Gamma_{eI}(E) = \pi |J_{0I}|^2 \tilde{n}_1(E) \tag{2.78}$$

Similarly, $\Gamma_{eII}(E)$ indicates the electron injection rate between the LUMO orbital, on

site $(0,0)$ and the first site in material II

$$\Gamma_{eII}(E) = \pi |J_{0II}|^2 \tilde{n}_2(E) \tag{2.79}$$

Here, the hopping integrals between the molecular states or interface states and the electron channels are denoted by C. $\tilde{n}_1(E)$ ($\tilde{n}_2(E)$) is the density of state of the first site of the isolated material I (II) (without considering the absorber molecule or D–A interface) but all other terms are unchanged. One can also define the fraction of holes that go to material I.

In the case where the two channels in material I and II have identical hoping integral J but different coupling to the molecular states or interface states then the density term $\tilde{n}_1(E)$ and $\tilde{n}_2(E)$ are the same

$$p_{eI}(z) = \left\langle \frac{\pi {J_{0I}}^2 \tilde{n}_1(E)}{\pi {J_{0I}}^2 \tilde{n}_1(E) + \pi {J_{0II}}^2 \tilde{n}_1(E)} \right\rangle = \frac{J_{0I}^2}{J_{0I}^2 + J_{0II}^2} \tag{2.80}$$

An interesting case is the wide band limit where $C < J$. In this limit, $\tilde{n}_1(E)$ can be considered as constant and since $\Gamma_{eI}(E)$ and $\Gamma_{eII}(E)$ are independent of E, one has

$$p_{eI}(z) = \left\langle \frac{\Gamma_{eI}}{\Gamma_{eI} + \Gamma_{eII}} \right\rangle = \frac{\Gamma_{eI}}{\Gamma_{eI} + \Gamma_{eII}} \tag{2.81}$$

Here, a simple analytical expression can be extracted for $R(E)$

$$R(E) \approx \left(\frac{\Gamma_{eI}}{\Gamma_{eI} + \Gamma_{eII}} - \frac{\Gamma_{hI}}{\Gamma_{hI} + \Gamma_{hII}}\right) \tag{2.82}$$

where $\Gamma_{eI,eII,hI,hII}$ are the injection rates of electrons or holes (e/h) in material I/II. Furthermore, in the wide band limit the escape rate $\Gamma_p(E)$ is energy independent and satisfies $\Gamma_p = \Gamma_{eI} + \Gamma_{eII} + \Gamma_{hI} + \Gamma_{hII}$. In this limit, the current injected in material I is $I(E) = -e\Phi_C(E)$ with

$$\Phi_C(E) = \alpha^2(E) \frac{2}{\hbar} \left[\frac{\Gamma_P}{(E - \Delta - U)^2 + (\Gamma_p + \Gamma_R)^2}\right] \times \left[\frac{\Gamma_{eI}}{\Gamma_{eI} + \Gamma_{eII}} - \frac{\Gamma_{hI}}{\Gamma_{hI} + \Gamma_{hII}}\right] \tag{2.83}$$

This equation, comprising the effects of electron–hole interaction (U) and recombination parameter (Γ_R), is an extension of the formula obtained in reference [166] for non–interacting and non–recombining electron–hole pairs. The interaction energy (U) shifts the resonance energy at which photons are absorbed and the recombination processes (Γ_R) decrease the total amount of current injected in the channels. Note that the relative proportion of charges carriers injected in the different channels are unchanged by the local interaction and local recombination processes.

2.5.3 Expression Of The Quantum Yield

2.5.3.1 Permanent Regime

At a given photon energy E, the quantum yield $Y(E)$ is equal to the ratio between the number of photo–generated electrons or holes and the number of absorbed photons at this given energy

$$Y(E) = \frac{\Phi_C(E)}{\Phi_{ph}(E)} \tag{2.84}$$

Based on the equation mentioned before one obtains

$$Y(E) = (\frac{\Gamma_p(E)}{\Gamma_p(E) + \Gamma_R}) \times R(E) \tag{2.85}$$

Here, we suppose that $\alpha^2(E) = \alpha^2$ in the region where $n(E)$ (i.e., photon absorption) is important. Therefore, the average yield or in other words, the charge separation yield, which is the proportion of the all electron–hole pairs, generated by different photons and giving rise to the photovoltaic current can be defined as

$$Y = \frac{\Phi_C}{\Phi_{ph}} = \int n(E)Y(E)dE \tag{2.86}$$

where Φ_{ph} the total flux of absorbed photons is equal to $\Phi_{ph} = \int \Phi_{ph} dE = \frac{2\pi\alpha^2}{\hbar}$. This quantity depends only on the light intensity and dipole matrix element of the molecular transition. Furthermore, the total current flux is $\Phi_C = \int \Phi_C dE$ depends

on the parameters of the cell.

Without loss of generality, if $n(E)$(i.e., photon absorption) is significant in a narrow region around the resonance energy E_{res} then $Y \approx Y(E_{res})$. Based on the Eq. (2.85), $Y(E_{res})$ depends not only on the ratio between recombination and escaping rates Γ_R and $\Gamma_p(E_{res})$, but also on $R(E_{res})$.

Here, we draw the reader's attention to an interesting point: in the limit of small recombination parameter, if the photon energy E lies within the energy continuum then there is a transformation into an electron–hole pair and therefore yield $Y(E)$ is one. Whereas, if E corresponds to an excitonic state, recombination happens anyway and $Y(E)$ is zero. As a consequence, the average yield Y given by Eq. (2.86) can be expressed by $Y = 1 - P$, with P representing the total weight of localized states on the state $|0, 0\rangle$ of the square lattice.

2.5.3.2 Transitory Regime

For the PV devices in the transitory regime we consider that the system at time zero is in the state $|0, 0\rangle$ and the aim is to evaluate the total charge injected in the leads at large time. In the absence of recombination, we expect that the yield Y is related to the probability P that the excitonic state $(0, 0)$ is in a localized state. Therefore,

$$Y = 1 - P \tag{2.87}$$

Indeed the part of the initial state which is localized cannot evolve with time, except for a phase factor, and will give no current in the lead at large time. From this point of view, it is clear that the yield is intimately related to the spectral properties of the electron–hole Hamiltonian (H), i.e., H defined on the square lattice. More generally, we shall consider quantities such as Q

$$Q = \int_0^\infty dt \, \langle \Psi(t) | \hat{A} | \Psi(t) \rangle \tag{2.88}$$

where

$$|\Psi(t)\rangle = U(t)\,|\Psi\rangle \tag{2.89}$$

and

$$U(t) = e^{-iHt/\hbar} \tag{2.90}$$

Where Ψ is any wave function and $U(t)$ is the time evolution operator. Here, we consider $\hat{A}$ as an operator which measures the current along a bind so that Q is the total charge (in units of the electron charge) passing through a given bind during the process of exciton dissociation or recombination. Introducing the total electron number Q_e or hole number Q_h injected in the contacts we obtain

$$Y = Q_e = Q_h \tag{2.91}$$

In order to compute or analyse the behavior of Q, we use a general relation, which relates the integrals of an operator in time and energy domains

$$\int_0^\infty dt\,\langle\Psi(t)|\hat{A}|\Psi(t)\rangle = \frac{\hbar}{2\pi}\int_{-\infty}^{\infty} dz\,\langle\Psi(z)|\hat{A}|\Psi(z)\rangle \tag{2.92}$$

$$\tilde{\Psi}(z) = G(z)\,|\Psi\rangle\,\&G(z) = \frac{1}{z-H} \tag{2.93}$$

Here $z = E + i\epsilon$ is a complex energy with an infinitesimal positive imaginary part ϵ and $G(z)$ is the so–called resolvent. In the following a central quantity will be

$$G_{00}(z) = \langle 0,0|\frac{1}{z-H}|0,0\rangle \tag{2.94}$$

which is a diagonal element of the resolvent (or Green's function $G(z)$) on the site (0,0). As explained before, $G_{00}(z)$ can be written as below

$$G_{00}(z) = \frac{1}{z - \varepsilon(0,0) + i\frac{\Gamma_R}{2} - \Sigma_0(z)} \tag{2.95}$$

Where, $\Sigma_0(z)$ is the self–energy that can be computed based on the recursion method, $\varepsilon(0,0)$ is the onsite energy of the site $(0,0)$ and Γ_R represents the rate of non–radiative recombination process of the electron–hole on site $(0,0)$. The local DOS for electron and hole pair is

$$n(E) = -\frac{1}{\pi}\operatorname{Im} G_{00}(z) = \frac{1}{\pi}|G_{00}(z)|^2(\frac{\Gamma_R}{2} - \operatorname{Im}\Sigma_0(z)) \tag{2.96}$$

The characteristic behavior of $n(E)$ provides essential information about the existence of energy continuum and excitonic states. We define a flux of the recombination $\Phi_R(z)$ and similarly a flux of the electron–hole pairs (Current flux) $\Phi_C(z)$

$$\Phi_R(z) = \langle 0,0|G^\dagger(z)\hat{A}G(z)|0,0\rangle = |G_{00}(z)|^2\frac{\Gamma_R}{\hbar} \tag{2.97}$$

$$\Phi_C(z) = |G_{00}(z)|^2\frac{-2\operatorname{Im}\Sigma_0(z)}{\Gamma_R} \tag{2.98}$$

Using Eqs. (2.96), (2.97) and (2.98) one obtains

$$Q_e = Q_h = \frac{\hbar}{2\pi}\int_{-\infty}^{\infty} dz \left\langle \tilde{\Psi}(z)\middle|\hat{A}\middle|\tilde{\Psi}(z)\right\rangle = \int_{-\infty}^{\infty} dz\Phi_C(z) \tag{2.99}$$

The charge separation yield, which is proportional to the portion of the charge carriers arriving at the electrodes, can be computed by the following equation

$$Y = \int_{Continuum} \frac{-\operatorname{Im}\Sigma_0(E)}{\frac{\Gamma_R}{2} - \operatorname{Im}\Sigma_0(E)} n(E)dE \tag{2.100}$$

Equation (2.100) is a general formula, obviously when the recombination parameter is zero, the yield is simply equal to the weight of the LDOS in the energy continuum. In that case we recover $Y = 1 - P$, where P is the weight of localized

states.

Chapter 3

Two–Level Systems With Local Interaction

Relying on the new formalism described in the second chapter of the thesis, here we are going to investigate the effects of short–range electron–hole interaction on the performance of photovoltaic cells in the permanent and transitory regimes. As mentioned previously, the molecular photo–cell and Bulk Hetero–Junction (BHJ) organic solar cell are respectively our selected examples for the photovoltaic devices in the permanent and transitory regimes (See Fig. 3-1).

The short–range interaction term implies that interaction between the electron and the hole occurs only when they both are in the same place, i.e., either inside the absorber molecule or at the D–A interface. We model and analyze the photon absorption, exciton creation, dissociation and subsequent effects on quantum yield in the energy domain. To illustrate various aspects of the model, we consider the two–level photovoltaic systems in three type of configurations [167–169]:

(A) Mono–channel case where there is just one possible evacuation channel for each charge carrier and it is studied in two different conditions:
(I) the asymmetric coupling condition (i.e., $C_1 \neq C_2$) and
(II) the symmetric coupling condition (i.e., $C_1 = C_2$).
The asymmetric term refers to the situation where the coupling parameters of the

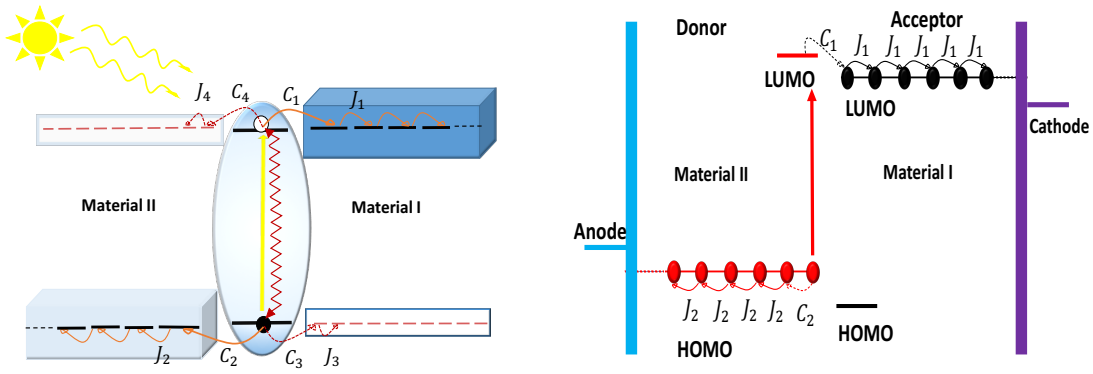

Figure 3-1: The two–level model in the permanent (Left panel) and transitory (Right panel) regime of illumination. (Left panel) A molecular photo-cell with one HOMO and one LUMO orbitals attached to the electrodes in materials I (right) and II (left). The red line represents the electron–hole interaction (U) and recombination (Γ_R) inside the molecule and the hopping integrals of electron and hole are denoted by C and J. Z is the energy of absorbed photon. (Right panel) Schematic representation of a donor–acceptor system. Charge evacuation channels are considered as semi-infinite chains. Here, J_1 and J_2 are the coupling energies between two adjacent sites in the electron and hole chains, respectively. Also, C_1 and C_2 represent the first coupling energies between the interface states and charge evacuation chains.

electron and hole to their respective channels are different whereas, these parameters are the same in the symmetric coupling condition.

(B) Multi-channel case where there are more than one evacuation channel for at least one charge carrier. We suppose there are two evacuation channels in materials I and II for the hole while there is just one evacuation channel in material I for the electron. Here, the widths of the energy continuum EC_1 (electron injected in material I and hole in material II) and EC_2 (electron and hole injected in material I) are important parameters and they play an essential role. Hence, in the multi–channel case we investigate the performance of the system under two specified conditions:
(B1) multi–channel system with identical energy continuums (i.e., $EC_1 = EC_2$) and
(B2) multi–channel system with different energy continuums (i.e., $EC_1 \neq EC_2$).

(C) Non–resonant coupling to the leads: In the first two parts ((A) and (B) cases), the coupling of each orbitals of the two–level system with the leads is resonant.

It means that the onsite energies of the orbitals of the two–level systems are identical to those of the orbitals that constitute the leads. In addition the coupling parameters C are smaller than the hopping parameters J inside the leads. In part (C) we study the effect of a non–resonant coupling obtained either by increasing C to high values compared to J or by considering an offset between the orbital energies of the two–level system and of the lead. The results presented in this part are preliminary but indicate that interesting behaviour can stem from this non–resonant conditions.

3.1 Mono–Channel Condition

As pointed above, the performance of mono–channel system will be investigated in the asymmetric and symmetric coupling conditions. Since in most of the studies done so far the effects of hole propagation in BHJ OPV are neglected [143], we apply the asymmetric coupling condition to this structure to provide a comprehensive insight to the effects of hole immobility and propagation. To broaden the viewpoint, the symmetric coupling condition is applied to molecular photo–cells.

3.1.1 Asymmetric Coupling : Bulk Hetero–Junction

As discussed in the first chapter, excitonic solar cells (XSCs) are currently a focus of intense interests because of their potential advantages, such as flexibility, low material cost, and processability. One interesting class of XSCs is the bulk hetero–junction solar cells, where the donor and acceptor zones are mixed. In the BHJ solar cells, an absorbed photon creates a bound electron–hole pair, so called exciton, which migrates at the interface. After exciton arrival at the interface and ignoring the trapping and de–trapping of charge carriers, there are two main possibilities: (i) The first one is that the exciton dissociates at the donor–acceptor (D–A) interface and separated charge carriers leave the interface, then by moving along a set of acceptor and donor sites arrive at the electrodes. (ii) In the second scenario the short–range and long–range Coulomb interaction between the charge carriers are strong enough, such that charge

carriers remain bound at the D–A interface [80, 170]. In this second scenario, charge carriers may ultimately undergo a recombination that reduces the photovoltaic yield. In order to investigate and subsequently improve the charge separation yield in the BHJ photo–cells, the material design is one important aspect. Besides, focusing on the device physics by developing models that capture the physical mechanism involved in the cell is another efficient way to improve the energy conversion yield [143, 171]. In this section, we use the simple efficient model described in the second chapter of the thesis to analyze the performance of the BHJ organic photo–cell which is considered in this study as a cell in the transitory regime.

We try to pedagogically explain the main aspects of the model and use it to calculate the charge separation yield. The yield can be treated based on this formalism by considering the effects of electron–hole interaction and non–radiative recombination. As pointed previously, of specific interests of this model is that both charge carriers (i.e., the electron and the hole) are considered mobile whereas in most of the studies [143, 172], the hole is studied as a fixed carrier. To have detailed knowledge about the hole propagation, here in this section, the asymmetric coupling is considered.

The present study can be compared to ref [143]. However, among the interesting characteristics of the theoretical model developed in this thesis is that the exciton creation, dissociation and subsequent effects on charge separation yield are discussed in the energy domain. This provides an insight that is not obtained through the numerical calculations in the time domain that are performed in the previous studies [143].

3.1.1.1 Local Density Of States (LDOS)

In order to analyze the charge separation we first consider the spectral properties and in particular, the local DOS on the site (0,0). Here, for the numerical simulation, we use $J_1 = J_2 = 0.2\,eV$ and $C_1 = 0.1\,eV$. The DOS is given in the unit of states per eV. With this choice of the cell parameters, the bandwidth of electrons and holes in their respective channels are 0.8 eV. Therefore, the total bandwidth of electron–hole pair is 1.6 eV.

We choose the same enrgies for all the LUMO orbitals (occupied by electrons) and all the HOMO orbitals (occupied by the holes). Only the sum of these energies is relevant and we take

$$\varepsilon_e(x) + \varepsilon_h(y) = 2 \ eV \tag{3.1}$$

which is independent of orbitals occupied by the electron and the hole. As pointed above, the approach developed here allows us to go beyond the restrictive condition for the hole (i.e., $C_2 = 0 \ eV$). Four values including $C_2 = 0 \, eV$ for the fixed hole case and $C_2 = 0.05, 0.1$ and $0.15 \ eV$ corresponding to the mobile hole under the $C_2 < J_2$ condition are considered.

First we consider the case where there is no interaction between the electron and the hole. In that case the local DOS on site (0,0) is the convolution of local DOS for electron and for hole on the initial sites of their respective semi–infinite chains. When the coupling energies C_1 and C_2 are not too strong compared to the hopping integrals J_1 and J_2 we know that the DOS for each charge carrier has a Lorentzian line–shape.

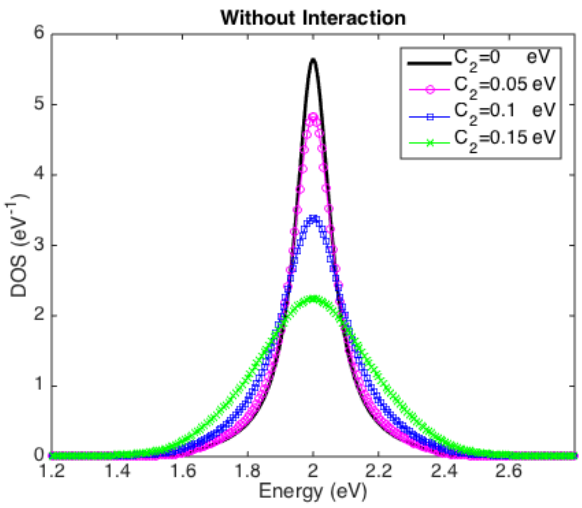

Figure 3-2: Local density of states for electron–hole pair in non–interacting condition.

Therefore, the local DOS for the electron–hole pair on site $(0, 0)$ has also a Lorentzian line–shape with a width that is sum of the both widths. This is consistent with the result of Fig. 3-2 which is obtained for non–interacting charge carriers. In

addition, as the coupling energy increases, the width of the DOS increases as well. In the following we shall find resonant shapes for the DOS which are centered at an energy which we call the resonance energy E_{res}. Mathematically, in the limit of small coupling to the leads (small C), the line–shape is centered around the onsite energy of site $(0,0)$ which is $E_{res} \simeq 2eV$.

Figure 3-3 examines the effect of short–range Coulomb interaction between charge carriers at the D–A interface. We suppose that the strength of short–range Coulomb interaction is $U = -0.4\,eV$ and the same values of the parameters as Fig. 3-2 are taken. Panel (a) depicts that the short–range interaction with $U = -0.4\,eV$ can lead to an excitonic state outside the energy continuum in the fixed hole condition. In that case the bandwidth of the holes has no effects and only the electron bandwidth matters. Hence, the continuum of states is between 1.6 and 2.4 eV and the excitonic peak is just below the band minimum. As can be seen in panel (b), $U = -0.4\,eV$ is not strong enough to generate such a localized state in the mobile hole conditions. It can be understood based on the fact that the bandwidth of electron–hole pairs in the mobile hole condition is between 1.2 and 2.8 eV.

As a general statement, in order to observe an excitonic peak outside the energy continuum, the strength of interaction should be greater than a critical value (i.e., $|U| \geq |U_{Critical}|$). Mathematically an excitonic peak appears at the energy E outside the continuum, if

$$E - (\varepsilon_e(0) + \varepsilon_h(0)) - U - \Sigma_0(E) = 0 \tag{3.2}$$

as shown previously by Eq. (2.95) (with $\Gamma_R = 0$).

Note that the resonance energy E_{res} is this time the energy of the exciton. In the limit of small coupling to the leads the self–energy $\Sigma_0(E)$ is negligible and E_{res} is given by $E_{res} \simeq \varepsilon_e(0) + \varepsilon_h(0) + U$ which is the onsite energy of site $(0,0)$ on the square lattice (see chapter 2) as already seen above.

Since $\Sigma_0(E)$ is always a decreasing function of energy outside the continuum this shows that the energy of the excitonic peak decreases when U becomes more negative. For $U = U_{Critical}$ the energy of the excitonic peak takes its maximum value, i.e., just

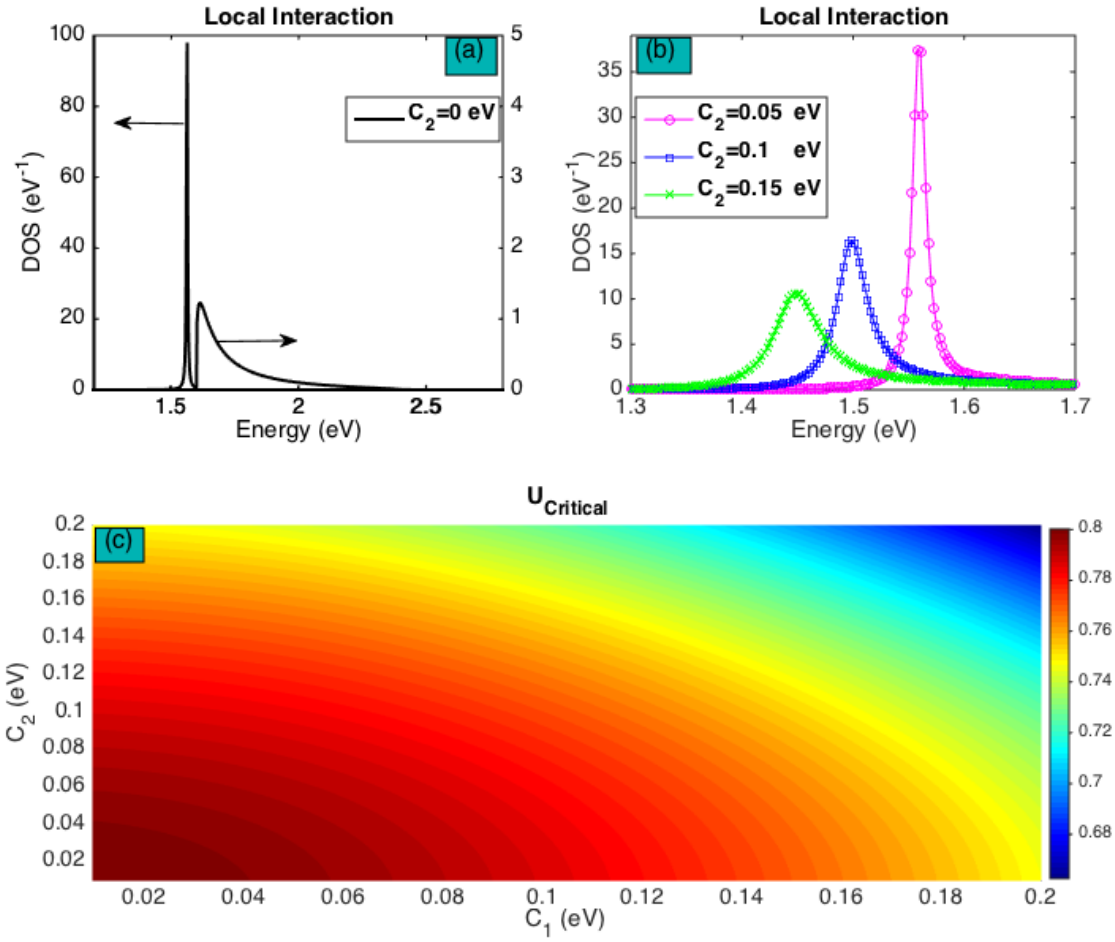

Figure 3-3: DOS for electron–hole pair under short–range interaction condition. (a) Fixed–hole case (b) Mobile–hole cases. (c) Variation of the $U_{Critical}$ as a function of C_1 and C_2.

at the bottom of the continuum band (E_{min})

$$E_{min} - (\varepsilon_e(0) + \varepsilon_h(0)) - U_{Critical} - \Sigma_0(E_{min}) = 0 \tag{3.3}$$

E_{min} depends on the hopping integrals and the onsite energies of electron (ε_e) and hole (ε_h) far from the interface

$$E_{min} = (\varepsilon_e + \varepsilon_h) - 2J_1 - 2J_2 = 1.2\, eV \tag{3.4}$$

In order to have ideas about the dependence of $U_{Critical}$ on the cell parameters, in

panel (c) of Fig. 3-3, this quantity is plotted as a function of C_1 and C_2 for a given set of J_1 and J_2. Based on the results shown in this figure, for different sets of C_1 and C_2, the value of $U_{Critical}$ varies, but in a relatively small proportion. In fact, the limiting value of $U_{Critical}$ for small C_1 and C_2 is easily obtained. Indeed, in that case the Eq. (3.3) is satisfied with the self–energy $\Sigma_0(E_{min})$ being essentially zero. Therefore, in this limit

$$U_{Critical} \approx E_{min} - (\varepsilon_e(0) + \varepsilon_h(0)) \tag{3.5}$$

In the present case, Eq. (3.5) gives $U_{Critical} = -2J_1 - 2J_2 = -0.8\, eV$.

3.1.1.2 Weight Of Excitonic States & Charge Separation Yield

As discussed in chapter two, one can compute the weight of localized states by $P = \frac{1}{1-\frac{\partial\Sigma_0}{\partial z}|_{z=E_{lz}}}$. Making use of Eq. (3.2) one has

$$\frac{\mathrm{d}U}{\mathrm{d}E} = 1 - \frac{\partial\Sigma_0}{\partial E} \tag{3.6}$$

which results in

$$P = \frac{1}{(dU/dE)} \tag{3.7}$$

Obviously, weight of excitonic peak emerged due to $U_{Critical}$, can be determined by the following equation

$$P_{Critical} = \frac{1}{(dU/dE)|_{E=E_{min}}} \tag{3.8}$$

From these expressions one shows easily that the weight P increases as the exciton energy decreases or equivalently when U becomes more negative. It can be shown also that $P_{Critical}$ is non–zero for mobile hole but is zero for fixed hole. This is confirmed by numerical results as shown below.

The variation of $P_{Critical}$ as a function of coupling parameters C_1 and C_2 is shown in Fig. 3-4. As can be seen, upon increasing the coupling parameter, the $P_{Critical}$ decreases. This can be understood through the fact that the strong coupling parameters facilitate the charge evacuation process which straightly decreases the possibility of localized states formation.

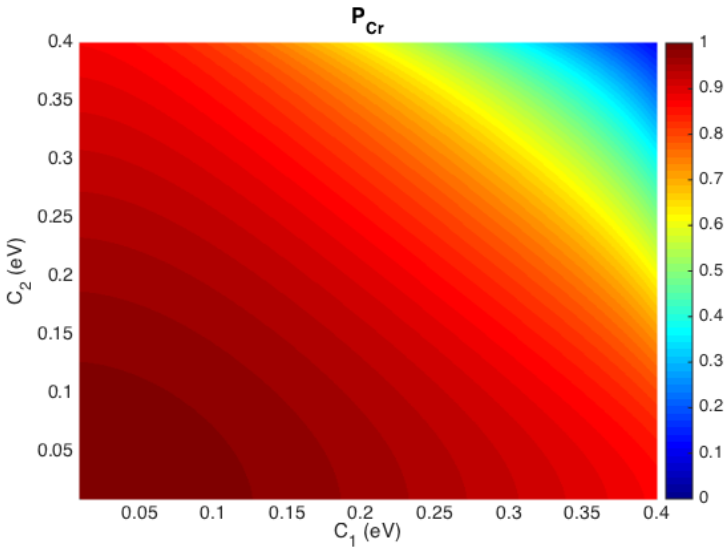

Figure 3-4: Variation of the $P_{Critical}$ as a function of coupling parameters C_1 and C_2.

In the absence of recombination the yield is determined by $Y = 1 - P$, therefore the effect of excitonic states on the yield Y depends on the total weight of these peaks P. In Fig. 3-5, the total weight of the excitonic peaks under short–range Coulomb interaction condition is investigated as a function of U by considering $C_1 = 0.2\ eV$ and C_2 including 0, 0.05, 0.1 and 0.15 eV.

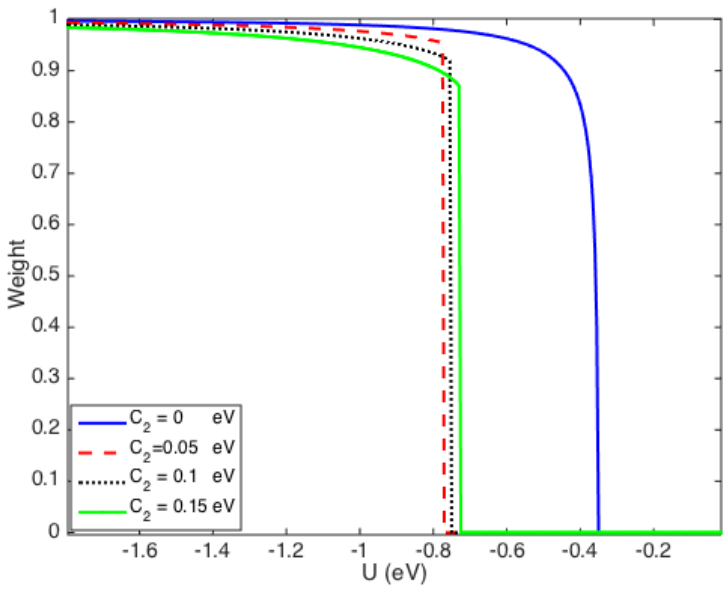

Figure 3-5: Weight of the excitonic peaks (P) as a function of short–range interaction strength (U) for different values of hole coupling parameter (C_2).

Figure 3-5 depicts an abrupt variation of the total weight when U goes through some critical value. Under the short–range interaction condition, the theory predicts that the total weight of the excitonic states is $P = 1$ for $|U| > |U_{Critical}|$ and $P = 0$ for $|U| < |U_{Critical}|$ and $U_{Critical}$ is given by Eq. (3.5).

Based on the fact that the minimum energy E_{min} of the continuum of electron–hole pair states is not the same in the fixed and in the mobile hole conditions, the variation of the $U_{Critical}$ between these two situations can be understood.

However, based on the results shown through this figure one can conclude that the strength of the short–range Coulomb interaction U and the coupling energies are important parameters that can significantly affect the weight of excitonic peaks and subsequently the charge separation yield. In general, for a given electron–hole interaction the yield is much improved if the motion of the hole is taken into account. Therefore, improving the mobility of the hole could be an important ingredient to get experimentally much larger exciton dissociation than usually expected [173–175]. Qualitatively, efficient coupling to the channels facilitates the charge carrier transport and hence the possibility of localized state appearance decreases.

Figure 3-6 represents the charge separation yield as a function of short–range interaction strength U, for several hole coupling energy C_2 and local recombination parameter Γ_R. Our results show that by considering the hole as a fixed carrier, since $|U_{Critical}|$ is underestimated, the yield of the cell has a smaller value, particularly for high recombination parameter. In general, one can conclude that the effect of non–radiative recombination is to reduce the yield and its impact is more significant in the weak coupling condition. In fact, under relaxation processes, less charge carriers are able to exit through the electrodes, hence the yield decreases.

3.1.2 Symmetric Coupling : Molecular Photo-cell

Here we consider the mono–channel molecular photo-cell in the symmetric coupling condition, i.e., $C = C_1 = C_2$. In the molecular photo-cells, the energy conversion process takes place by a single molecular donor–acceptor complex attached to electrodes. In this structure, initially the whole system is in the ground state with filled valence

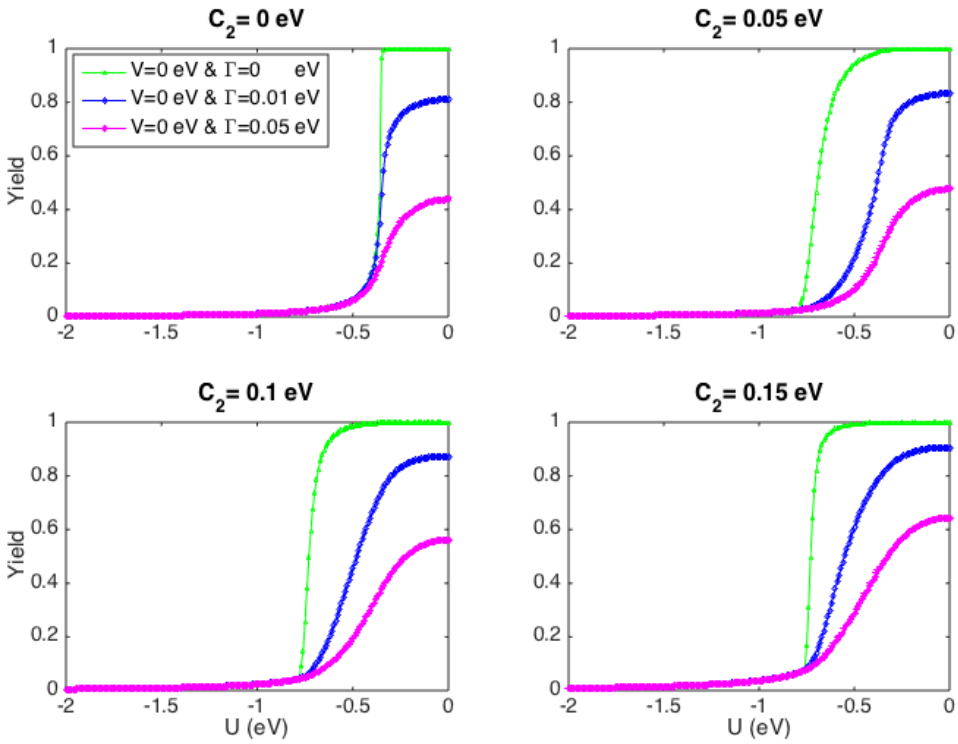

Figure 3-6: Yield (Y) of charge separation as a function of short–range interaction energy U obtained with different first coupling energies to the hole lead. The legend presented in the first panel, is valid for all the other panels. Γ_R is the recombination parameter. The strength of long–range interaction V is assumed to be zero.

bands and empty conduction bands. After photon absorption by the molecule, one electron and one hole are created in LUMO and HOMO, respectively. Both charge carriers interact via the Coulomb potential and can be recombined in the molecule or can be transferred to their respective channels where they produce photovoltaic current. A schematic depiction of a molecular photo-cell is shown in Fig. 3-1.

3.1.2.1 Local Density Of States (LDOS)

In this case, we use $J_1 = J_2 = 0.2\ eV$ and $\Delta = 2\ eV$, therefore the energy continuum lies between 1.2 and 2.8 eV. In addition, $R(E) = p_{e1}(E) - p_{h1}(E)$, which represents the proportion of electrons and holes evacuated from the molecule to the channel in material I, is equal to one (see chapter two). In Fig. 3-7, the LDOS is plotted as a function of the absorbed photon energy.

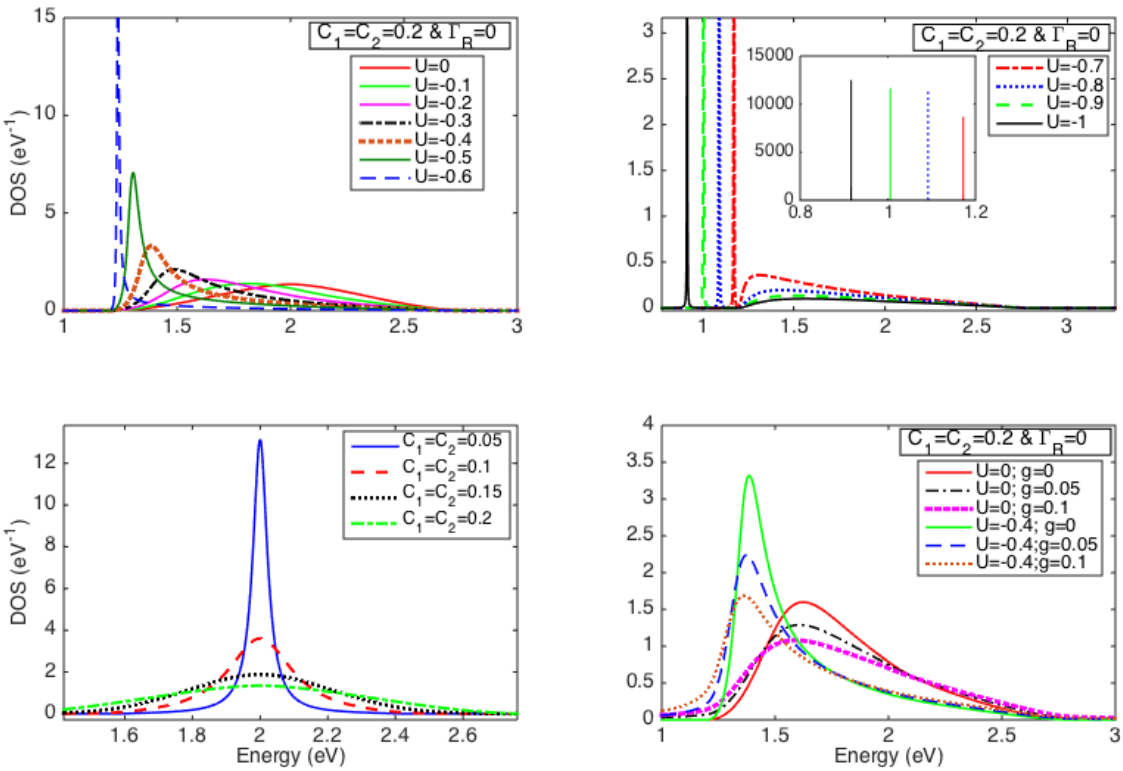

Figure 3-7: Density of States as a function of absorbed photon energy in a mono–channel system under different conditions. (a, b) For different values of interaction energy (U). (c) For different coupling parameters (C_1&C_2). (d) For different interaction energies and recombination parameters (U&Γ_R).

In these plots, the dependence of LDOS on short–range interaction energy (U), strength of coupling parameters (C) and recombination parameter (Γ_R) is examined. As can be seen from panels (a) and (b), for a given set of coupling parameters and in the absence of recombination, the number of LDOS peaks is dependent on the interaction strength. For small values of $|U|$, there is a single peak which tends to become narrower for larger $|U|$. This peak appears at an energy E_{res} which is close to the onsite energy of site $(0,0)$ of the square lattice. Therefore, $E_{res} \simeq \varepsilon_e(0)+\varepsilon_h(0)-U$. Indeed in the context of the molecular photo-cell, E_{res} is the energy at which photons are most easily absorbed. As expected this energy is close to the transition energy of the isolated molecule which is given by $\varepsilon_e(0) + \varepsilon_h(0) - U$. The peak eventually splits into two for growing values of $|U|$ and the resulting two peaks separate further with increasing $|U|$ as depicted in panel (b). The narrow peak outside the continuum

(EC) is called excitonic state, which blocks the charge carrier injection to the energy continuum.

Next, we study the effects of the coupling parameters. The corresponding LDOS is shown in panel (c). Increasing C enhances charge carrier transfer from HOMO and LOMO to the respective evacuation channels; it can be detected through the extended width of the LDOS line–shape. In panel (d), the effect of varying the recombination parameter (Γ_R) for interacting and non–interacting cases is shown. In both cases, the effect of Γ_R is to slightly shifts the LDOS peak to the left and slightly broadening of the line–shape width.

3.1.2.2 Charge Separation Yield

Figure 3-8 represents the dependence of the yield, $Y(E)$, on the energy of absorbed photons and recombination parameter, Γ_R, for different values of coupling parameters ($C = C_1 = C_2$). As can be seen, for photon energies inside the continuum, i.e., $1.2 \leq E \leq 2.8\ eV$, the yield remains 1 for $\Gamma_R = 0$, while the effect of non–zero Γ_R is to reduce the yield.

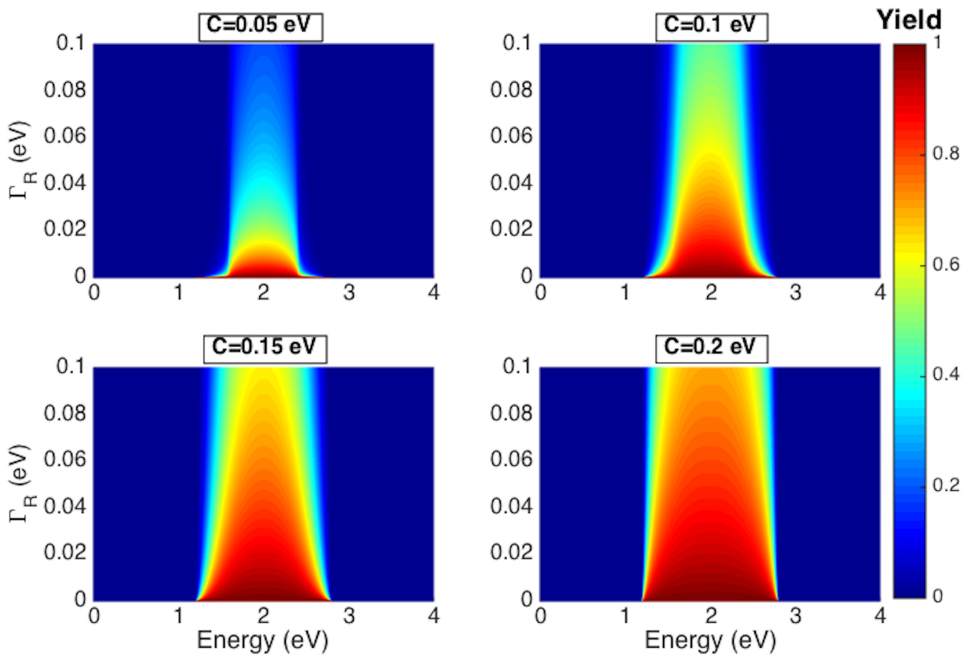

Figure 3-8: Photovoltaic yield as a function of absorbed photon energy and recombination parameter (Γ_R) for different values of coupling parameter C.

In the energy continuum regime, as C increases, the curve broadens and the yield increases. Therefore, one can conclude that by increasing the coupling strength, charge carriers transfer more quickly to the evacuation channels and hence the cell remains efficient over a wider range of recombination parameters. For photon energies outside the continuum charge carriers stay on the molecule forming a localized state and hence, the yield goes to zero. This observation is compatible with the LDOS behavior.

The other important quantity that can be investigated is the average yield or in the other words, the charge separation yield Y, which is computed as an average over all the absorbed photon energies. The dependence of the charge separation yield of the interacting electron–hole pair is examined as a function of short–range interaction strength U and recombination parameter Γ_R, for different coupling parameter C. As can be seen from Fig. 3-9, in all cases, for small values of interaction energy, the yield remains 1 for $\Gamma_R = 0$. The effect of Γ_R and U is to reduce the yield.

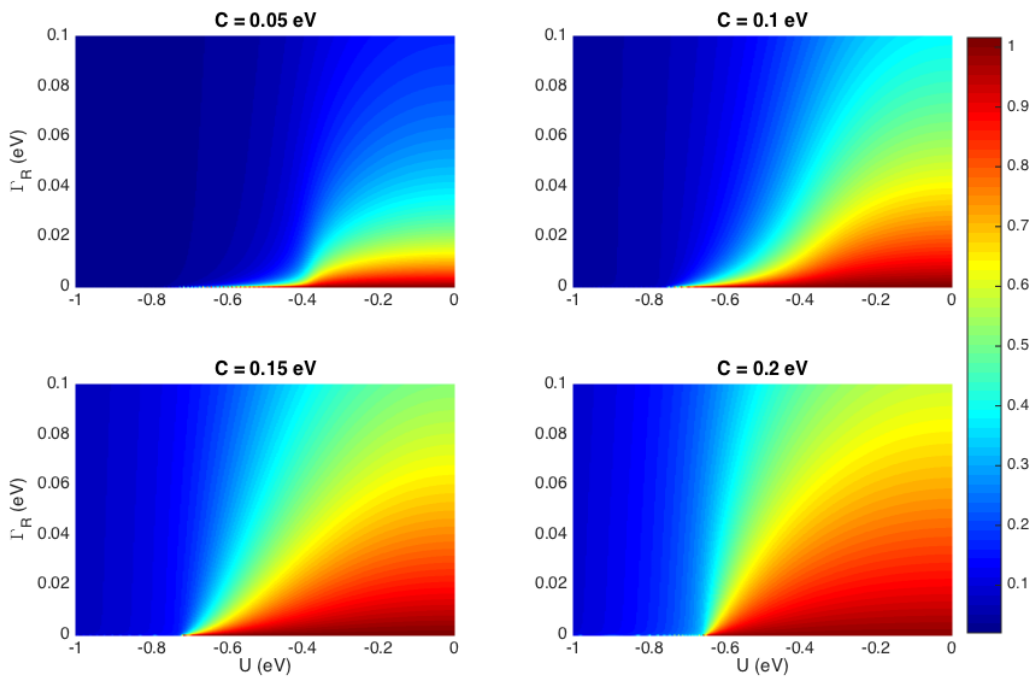

Figure 3-9: Photovoltaic yield as a function of interaction energy (U) and recombination parameter (Γ_R) in a mono–channel system for different values of coupling parameters (C_1 and C_2).

The behavior can be understood based on the information provided in Figure 3-7. For larger values of $|U|$, the charge carriers will stay on the molecule to form a localized state because their energy does not lie in the energy continuum of the contacts. Besides, for large values of the coupling parameters (C_1 and C_2), more charge carriers will transfer to the evacuation channels and hence the cell remains efficient over a wider range of the recombination parameter.

3.1.3 Message To Take Home

We used the simple novel model explored in chapter two to examine the performance of mono–channel BHJ OPVs and molecular photo-cells under the influence of asymmetric and symmetric electron and hole coupling conditions. This analysis is based on the energy spectrum of the electron–hole pair. Our results show that the yield strongly depends on the short–range interaction energy strength U. There is a critical interaction energy $U_{Critical}$, which depends essentially on the band edges of the electron–hole excitations, and the HOMO–LUMO energy offset on the initial site. We find that if $|U| < |U_{Critical}|$ yield values are higher compared to the $|U| > |U_{Critical}|$ where the localized states are created and hence the yield is strongly decreased. More interestingly, our results show that the mobility of the hole is an important parameter to improve the charge separation yield such that by considering the hole as a fixed carrier, one underestimate the $|U_{Critical}|$ and therefore the yield of the cell can be disesteemed.

3.2 Multi–Channel System

In the following, the process of charge separation is studied by considering coupling to two different evacuation channels for the hole and only one evacuation channel for the electron. The system performance is investigated by considering first two identical and then two different energy continuums.

3.2.1 Two Identical Energy Continuums

In Fig. 3-10, charge separation yield as a function of short–range interaction energy (U) and recombination parameter (Γ_R) and corresponding LDOS as a function of absorbed photon energy are examined by considering two energy continuums (EC_1 and EC_2) with identical bandwidths. To recognize the parameters re-look at the Fig. 3-1.

The cell parameters $J_1 = 0.2$, $J_2 = 0.4$, $J_3 = 0.4$, $C_1 = 0.2$ and $\Delta = 2$ (all in eV unit) are kept constant whereas C_2 and C_3 are varied. Therefore, EC_1 and EC_2 both are between 0.8 and 3.2 eV. Here, $R(E)$ is given by $R(E) = R = C_2^2/(C_2^2 + C_3^2)$ and is energy independent (see the second chapter of the thesis). Similarly to the mono–channel case, the yield decreases when $|U|$ or Γ_R increase. Based on the spectral information provided in the second row of this figure, due to the electron–hole interaction, charge carriers tend to localize to form an exciton outside the energy continuums and by increasing $|U|$, more charge carriers will be localized. Therefore, the global behaviour is essentially that of the mono–channel case except that the current is renormalized by a factor $R < 1$. Indeed when an electron–hole pair is injected in the leads the current produced is diminished by the factor R because part of the hole goes in the same material as the electron and therefore diminishes the charge injected by the factor $R < 1$.

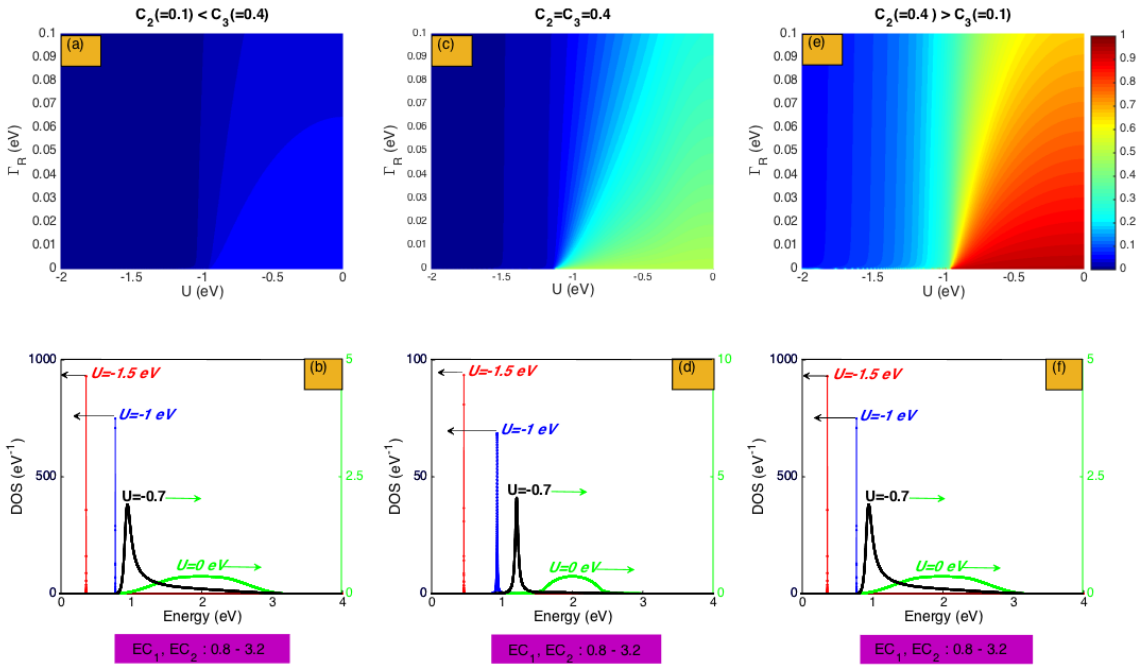

Figure 3-10: Photovoltaic yield and LDOS in a multi–channel system with identical energy continuums. (a, c, e) Photovoltaic yield as a function of interaction energy (U) and recombination parameter (Γ_R) for different values of coupling parameters of the hole to material II and material I (C_2 and C_3). (b, d, f) DOS as a function of incident photon energy for different values of interaction energy. The energy continuum range is indicated by coloured band below the DOS plots.

3.2.2 Two Different Energy Continuums

Next, in Figs. 3-11, LDOS and the corresponding charge separation yield are examined by considering two energy continuums (EC_1 and EC_2) with different bandwidths. The cell parameters $J_1 = 0.2, J_2 = 0.4, J_3 = 0.1, C_1 = 0.2$ and $\Delta = 2$ (all in eV unit) are kept constant whereas C_2 and C_3 are varied. As depicted in panel (a), for small values of $|U|$, $E_{res} \simeq \varepsilon_e(0) + \varepsilon_h(0) - U$ falls within EC_1 and EC_2, hence holes can be injected in materials I and II, depending on the values of the coupling parameters.

With increasing $|U|$, E_{res} is outside the EC_2 while it is still within the EC_1. Therefore, regardless the strength of the coupling parameter the hole will be evacuated only in material II. Finally, for strong enough U, E_{res} is outside the two continuums and charge carriers will be localized inside the molecule.

In panels (b) and (c), for $U = -1\ eV$ the effects of varying C_2 and C_3 are examined.

Their influences are detected by changing the position of resonance energy (E_{res}) and width of the line–shape. In the figure inset the behavior of the line–shape inside the second energy continuum (EC_2) is shown. As can be seen, the variation inside the EC_2 is negligible. Spectral information shown through panels (a)-(c) provides an appropriate framework to interpret the behavior of the photo-cell yield.

Through panels (d-f) of Fig. 3-11, we examine the yield by taking three different sets of HOMO coupling parameters to material I and material II (C_2 and C_3). The yield variations can be understood by separation of the interval of charge interaction energy (U) into three zones. The first zone considers $U \in [0, -0.5]$, where the resonance energy is coupled to two continuums EC_1 and EC_2, therefore the coupling parameters determine the appropriate channel and the yield values.

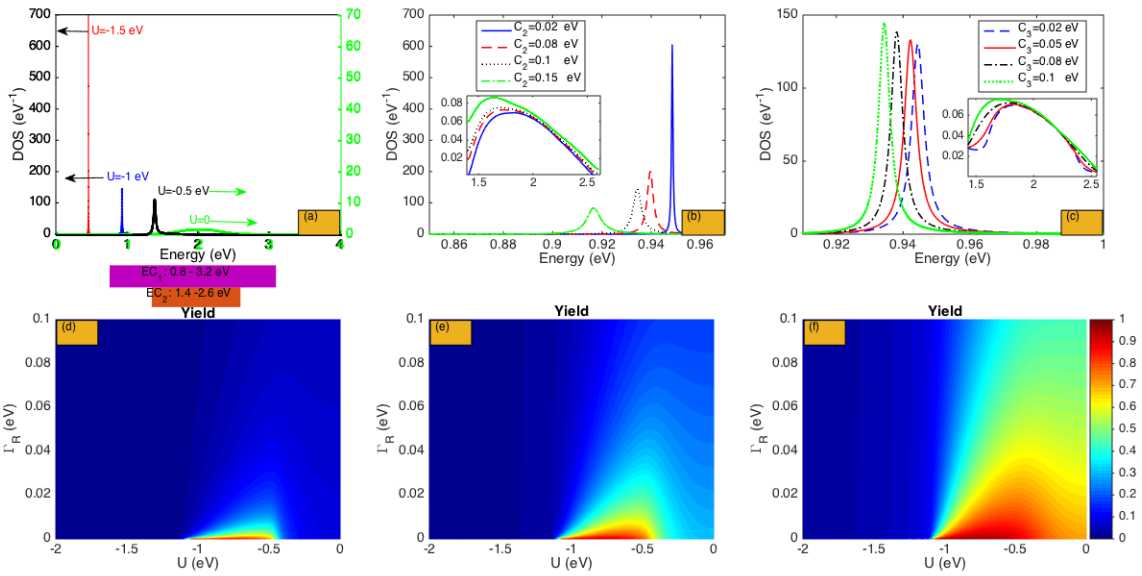

Figure 3-11: LDOS and yield in a multi–channel system with different energy continuums. (a) LDOS as a function of absorbed photon energy for different values of U. The energy continuums EC_1 (electron in material I and hole in material II) and EC_2 (electron and hole in material I) ranges are shown by colored bands below the plot. Here, $C_2 = C_3 = 0.1eV$. (b) LDOS computed for $C_3 = 0.1eV$, $U = -1eV$ and different values of C_2. (c) LDOS computed for $C_2 = 0.1eV$, $U = -1eV$ and different values of C_3. (d, e, f) Photovoltaic yield in a multi–channel system with different energy continuums as a function of interaction energy (U) and recombination parameter (Γ_R) for different values of coupling parameters of the hole to material II and material I (C_2 and C_3).

As can be seen, the cell can be efficient in this range of U if and only if $C_2 \geq C_3$. The maximum value of the yield in all cases is detected in the interval of $U \in [-0.5, -1.1]$. Based on the spectral information (panel (a)), in this range of U values, the resonance energy just lies in the continuum EC_2, therefore the hole either jumps into material II or stays at the molecule. Increasing C_2 enhances the yield. For larger interaction parameter values, $U \in [-1.1, -2]$, the resonance energy does not lie in any continuum, therefore the yield of the cell tends to be zero. In addition, the effect of the recombination parameter (Γ_R) is to reduce the yield.

3.2.3 Message To Take Home

We have presented a theoretical model based on the wave function of a coherent molecular photo-cell. This theory is well adapted to analyse molecular photo-cells in the presence of strong Coulomb interaction between the electron and the hole. We show that there is a competition between injection of charge carriers in the channels and recombination. This competition depends sensitively on the parameters of the model such as the short–range electron–hole interaction in the molecule, the recombination parameter, the coupling to the channels and the band structure of the channels. When there are several evacuation channels for the charge carriers (electrons or holes) there is, in addition, a competition between injections in the different channels. Although some of the results presented here show similarity with kinetic models, the value for the final current and therefore the cell efficiency can be obtained only through a complete quantum calculation. The formalism can also be applied to molecules with more complex electronic structures. This method should help to understand the conditions needed for a high yield of a molecular photovoltaic system, such as single molecule junctions or a molecular monolayer.

3.3 Non–resonant Coupling To The Leads

So far we have considered that the interface or molecular orbitals are at the same energy as the orbitals that constitute the leads to which they are coupled. In addition, we have considered also that the hopping integral between these orbitals and those of the leads are smaller than those between orbitals of the leads ($C \leq J$). Under these conditions the central (interface or molecular) orbital coupled to the continuum of states in the leads produces a resonant state. Yet in some circumstances it may be that these resonant conditions are not fulfilled. It is the aim of this part to discuss the consequences for the efficiency of these non–resonant conditions.

If the coupling between the central orbital and the leads is much larger than that between orbitals of the leads ($C >> J$) then there is no more resonant state. Indeed as a first approximation one may neglect the coupling inside the lead compared to that between the central orbital and the first state of the lead. Then one is left with a two–level system which gives rise to two eigenstates separated by an energy much larger than the bandwidth of the lead. These localized states are obviously not favorable for charge injection and this situation is expected to be unfavorable for the efficiency. In chap 4 we show that this situation could happen when there is strong electron–phonon coupling. Indeed the strong electron–phonon coupling leads to very narrow polaronic bands for which this strong coupling regime ($C >> J$) can be reached.

Even if the strong coupling regime is not reached one can have a non–resonant condition if there is a strong energy offset between the molecular (or interface) orbital and the orbitals of the corresponding leads. Depending on the value of the offset the number of bound states can be zero, or one (we cannot have two bound state because we do not consider the strong coupling regime briefly described above).

Here we focus on the effects of LUMO–LUMO offset δ and we shall study in particular the combined role of the offset energy δ and of the short–range interaction energy U on the DOS and on the charge separation yield. We consider a mono–channel molecular photo-cell and try to clarify the interrelationships between the energetic

characteristics of the acceptor material, and the conditions those characteristics impose on cell performance. For the numerical simulation, we use $J_1 = J_2 = 0.2\ eV$ and $C_1 = C_2 = 0.2\ eV$. The onsite energy ε_e and ε_h of the electron and hole sites in the acceptor and donor materials are taken equal to 2 eV and 0 eV, respectively. With this choice of the cell parameters, the bandwidth of electrons lies between $1.6 : 2.4\ eV$ and of hole is between $-0.4 : 0.4\ eV$. The onsite energy of the electron on the LUMO orbital of the photo-cell is $\varepsilon_e + \delta$ where δ is the LUMO–LUMO offset.

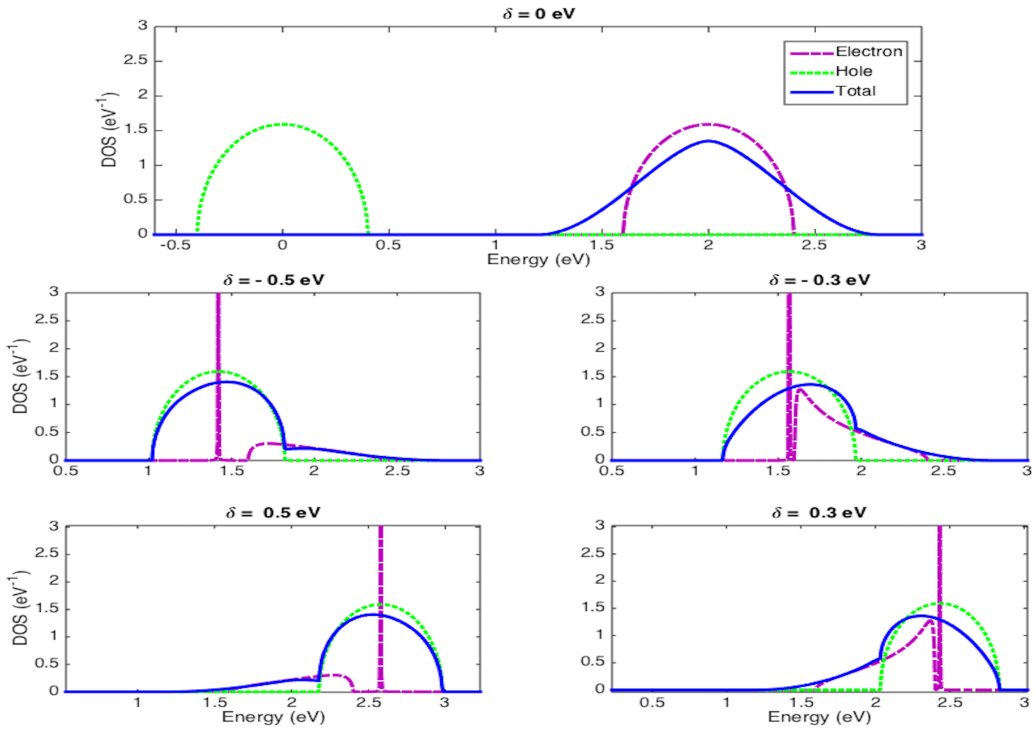

Figure 3-12: Local density of states as a function of absorbed photon energy for different values of LUMO–LUMO offset.

We show now that the resonance energy $E_{res} = \varepsilon_e + \delta + \varepsilon_h + U$ is a determinant parameter for the cell. Indeed this resonance energy is about the energy of all the photons that are absorbed by the two–level system. Because of energy conservation these absorbed photons give rise to electron and hole in their respective leads with a conserved total energy. Therefore, an important criteria for efficiency is that E_{res} belongs to the electron–hole energy continuum (EC). The electron–hole energy continuum (EC) is determined from the spectrum of electrons and holes in their re-

spective channels. Here with the chosen parameters EC lies between 1.2 and 2.8 eV. This argument is qualitatively confirmed by the calculations described below.

In Fig. 3-12, the non–interacting electron–hole LDOS and also the spectrum of bare electron and hole chains are plotted as a function of energy. In these panels, all the parameters are the same and we vary the LUMO–LUMO offset δ which represents the energy difference between the LUMO level of the molecule and of the acceptor material. In all cases, the hole density of states is a broad resonance because we took here $C = J$. On the contrary the electron DOS is a broad resonance if $\delta = 0$ but as $|\delta|$ increases, a localized state can appear in the spectrum. This is represented by a Delta peak which separates further from the electron continuum with increasing $|\delta|$. The energy of this peak is around E'_{res} given by $E'_{res} = \varepsilon_e + \delta$.

Figure 3-13 represents the weight of the bound state of the electron spectrum. As can be seen, for small values of $|\delta|$ the resonant condition is valid and therefore there is no possibility of bound state. For large enough offset the resonant condition is no more valid and the localized state appears. As $|\delta|$ increases, the weight of this bound state enhances as well.

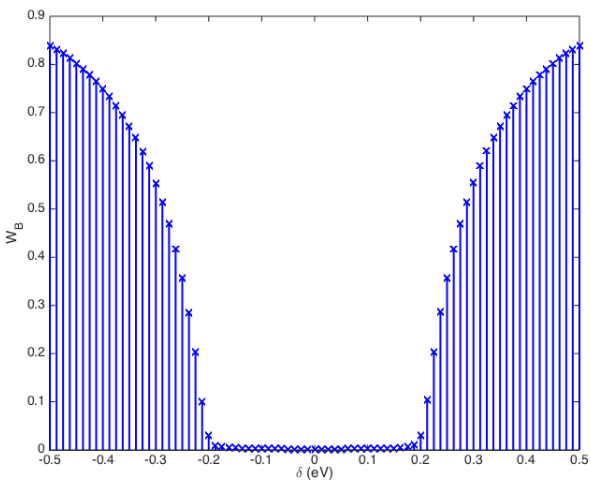

Figure 3-13: Weight of bound state in the electron spectrum as a function of LUMO–LUMO offset.

We consider now the case where there is interaction between electron and hole. The dependence of LDOS on short–range interaction energy (U) is depicted in Fig.

3-14. As can be seen, for zero and negative values of δ, the number of LDOS peaks is dependent on the interaction strength. For small values of $|U|$, there is a single peak which tends to become narrower for larger $|U|$. For growing values of $|U|$, the peak eventually splits into two and the resulting two peaks separate further with increasing $|U|$. The narrow excitonic peak outside the continuum (EC) is expected to block the charge carrier injection to the energy continuum.

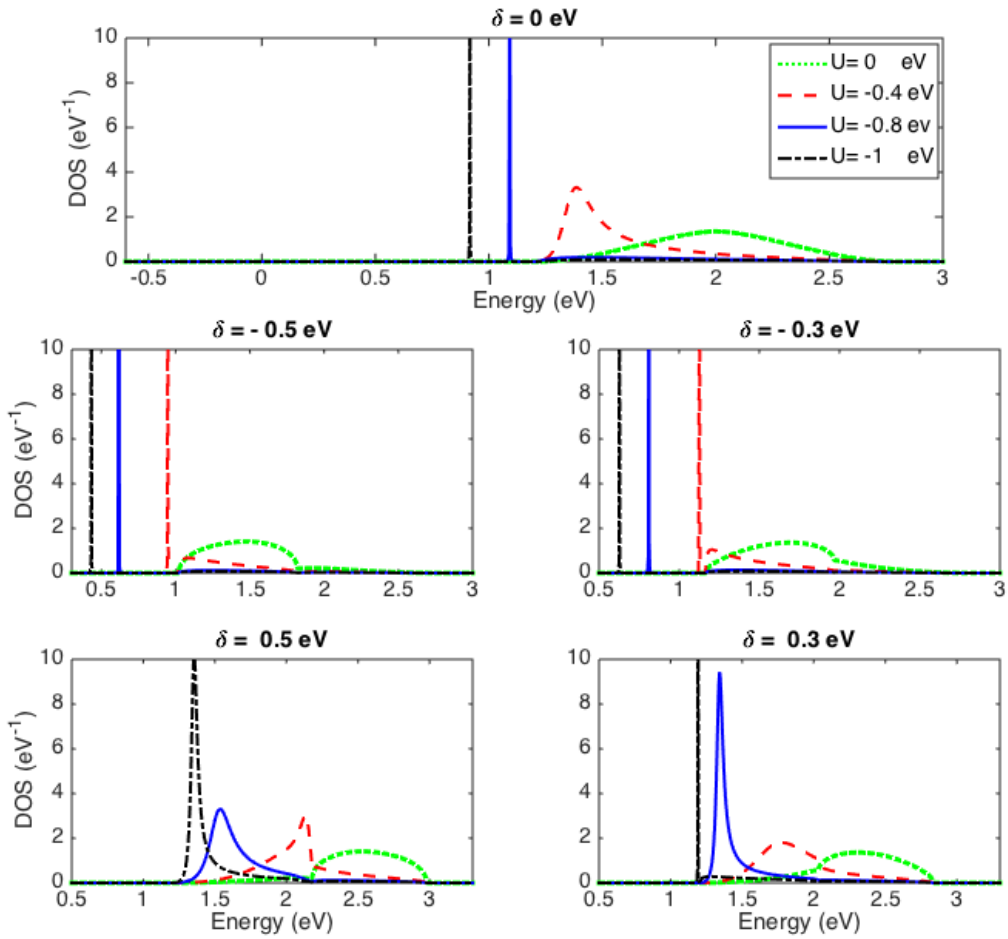

Figure 3-14: Local density of states as a function of absorbed photon energy for different values of LUMO–LUMO offset and different strength of interaction energy.

Therefore, we can conclude that effect of the Coulomb interaction and of a negative LUMO–LUMO offset tend to create a localized state outside the continuum below the lower band edge. The energy of the localized state is roughly given by the resonance energy $E_{res} \simeq \varepsilon_e + \delta + \varepsilon_h + U$.

On the other hand, for positive non–zero δ, the presence of interaction can compensate the effect of the offset, and the resonance energies that are initially above the continuum EC can shift inside the continuum. For even larger $|U|$, again the resonance energy does not lie in continuum and hence a localized state appears blow the lower band edge. Here also the energy of the localized state is roughly given by the resonance energy $E_{res} \simeq \varepsilon_e + \delta + \varepsilon_h + U$.

Spectral information shown through Figs. 3-12 and 3-14 provides an appropriate framework to interpret the behavior of the photo-cell yield. Through the different panels of Fig. 3-15, we examine the yield as a function of interaction energy U and recombination parameter Γ_R by taking different values of LUMO–LUMO offset δ. As can be seen, in the absence of LUMO–LUMO offset ($\delta = 0\ eV$) for small values of interaction energy, the yield remains 1 for $\Gamma_R = 0$. The effect of Γ_R and U is to reduce the yield. This behavior can be understood based on the information provided in Fig. 3-12. For larger values of $|U|$, the charge carriers will stay on the molecule to form a localized state because their energy does not lie in the energy continuum of the contacts.

For negative δ values, similar to the $\delta = 0$ case, the yield takes its maximum value when $|U|$ and Γ_R are both zero and when $|U|$ or Γ_R increases, the yield decreases. However, there is an important difference which is that in the negative δ case, the yield never reaches one.

An interesting case happens when the offset parameter has a high positive value. In this condition, for $U = 0$, E_{res} falls initially above the Energy Continuum of electron–hole pairs (EC). Therefore the yield is low. Upon increasing the interaction energy $|U|$, the yield increases, since E_{res} decreases and start to enter in EC. Therefore, charge carriers will be evacuated in the contacts. On the other hand, for larger values of interaction energy U, the resonance energy E_{res} does not lie in the continuum and charge carriers will be localized inside the molecule; therefore, the yield of the cell tends to be zero. In addition, the effect of the recombination parameter (Γ_R) is to reduce the yield.

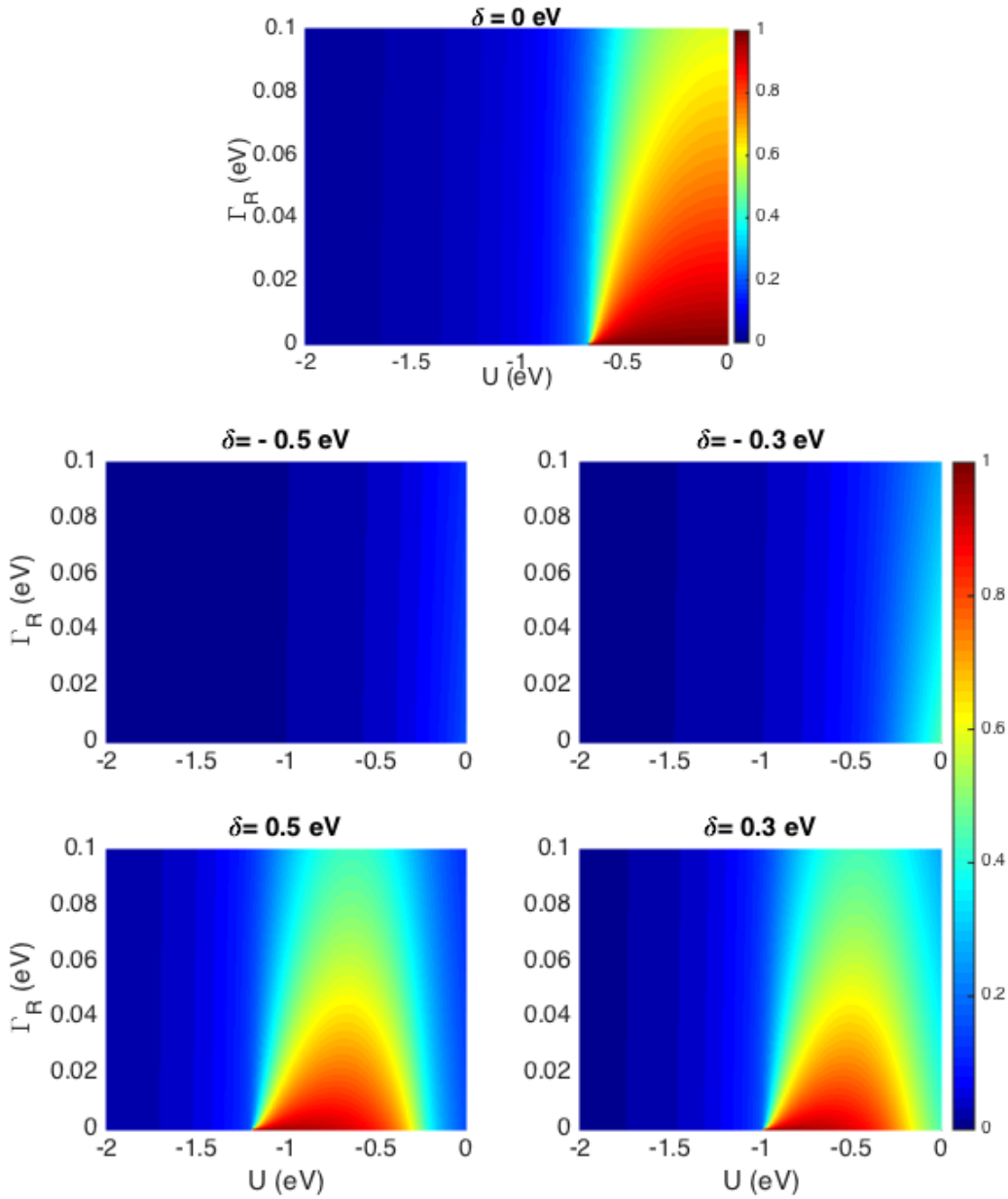

Figure 3-15: Photovoltaic yield as a function of short–range interaction energy U and recombination parameter Γ_R for different values of LUMO–LUMO offset δ.

3.3.1 Message To Take Home

To conclude we showed that if the coupling between the molecular orbitals and the leads is not resonant this may deeply affect the yield. We studied in particular the role of the LUMO–LUMO energy offset. If this offset is negative (onsite energy of the molecular LUMO orbital below the onsite energies of the orbitals of the electron lead)

then the electron–hole interaction tends to deteriorate even more the yield. Yet if the offset is positive there can be a kind of compensation between the effect of the offset and that of the interaction. This means that interaction can help to restore a high yield. A simple physical argument is to consider that photons are essentially absorbed around the resonance energy $E_{res} \simeq \varepsilon_e + \delta + \varepsilon_h + U$ and that the best efficiency is obtained if this energy is well within the Energy Continuum (EC) of electron–hole pairs states.

Our conclusions drawn here for the molecular photo-cell immediately apply to the Bulk Hetero–Junction. We therefore conclude that a positive LUMO–LUMO offset is favorable for a good charge separation at the interface. This positive offset is usually considered as a necessary condition in real material but then the argument is that this is due to the loss of electron energy (by transfer to phonon energy and ultimately transformation into heat) when going from the interface to the acceptor side. Clearly the understanding of the role of the offset deserves further studies.

Chapter 4

Two-Levels Systems With Non–Local Interaction

This chapter is intended to investigate the effects of non–local interaction on the performance of photovoltaic cells in the permanent (molecular photo-cells) and transitory (bulk hetero–junction organic solar cells) regimes. This means that in contrast to the results presented in the previous chapter there are interactions even if the charge carriers are out of the molecule (in the permanent regime) or away from the interface (in the transitory regime). An important case of non–local interaction is the long–range Coulomb interaction between the photo–generated electron and hole. This means that the electron and the hole do interact even if they are not both inside the molecule or just at the interface. Here of course the Coulomb interaction is not the bare interaction but is screened by all the charges of the material around the electron–hole pair. This screening effect is well represented by considering an effective dielectric constant of the medium. The other case of non–local interaction is the coupling between the electron (or the hole) with the lattice distortion around it when the electron (or the hole) moves out of the initial two–levels system. We study this case by considering the Holstein model for electron–phonon interaction. This model describes essentially the interaction of charge carriers with optical phonon modes.
The first part of this chapter is devoted to the long–range Coulomb interaction case and the second part deals with the coupling to the optical phonon modes.

4.1 Long–Range Electron–Hole Coulomb Interaction

recombination parameter One of the major effects of long–range Coulomb interaction is to create excitonic states that are localized states of the electron–hole pair. We discuss first the occurrence of these states in the context of our tight–binding like models and then study the systems with asymmetric or symmetric roles of electron and hole.

4.1.1 Energy Levels Of The Hydrogen Atom & Of The Tight–Binding Chain

Conceptually an exciton is similar to a hydrogen atom: one electron orbiting one proton (i.e., a hole), bound together by Coulomb interaction. Due to the analogy between the energy levels of the Hydrogen atom and bound states appearance in the presence of long–range Coulomb interaction, we start the discussion by recalling the basic concepts related to the spectrum of the hydrogen atom. Through the discussions given below, one can figure out the similarity between the Hamiltonian of the Hydrogen atom and the tight–binding Hamiltonian of the electron–hole pair.

The Hydrogen atom represents the simplest possible atom, since it consists of only one proton and one electron. Its potential energy function $V(r)$ expresses its electrostatic energy as a function of its distance r between the electron and the proton. Following the variable separation, the wave function of the Hydrogen atom can be written as

$$\Phi(\vec{r},\theta,\phi) = \frac{1}{r}u(r)Y_l^m(\theta,\phi) \tag{4.1}$$

where r is the distance from proton to the electron, θ and ϕ are respectively the Polar and Azimuthal angles. The radial differential equation for $r > 0$ can be expressed by

$$[\frac{-\hbar^2}{2\mu}\frac{d^2}{dr^2} + \frac{l(l+1)\hbar^2}{2\mu r^2} + V(\vec{r})]u(\vec{r}) = Eu(\vec{r}) \tag{4.2}$$

Here μ is the reduced mass of the electron–proton system. For isotropic levels ($l = 0$),

the Hamiltonian can be written in the following form

$$H = \alpha k^2 - \frac{\beta}{r} \tag{4.3}$$

and the negative eigen–energies are given by

$$E_n = -\frac{\beta^2/4\alpha}{n^2} \tag{4.4}$$

where n (an integer counter) is the principal quantum number, and varies from 1 to infinity. The lowest energy level or ground state for an electron bound to a Hydrogen–like nucleus can be realized in the $n = 1$ case. Therefore, the solution of the Schrödinger's equation in the presence of the Coulomb potential reveals the existence of quantized or discrete bound–state energy levels. At positive energies there are extended states that spread in the full 3D space. A schematic depiction of the Hydrogen atom bound levels is shown in Fig. 4-1. As can be seen, upon increasing n, the radius of wave function increases as well.

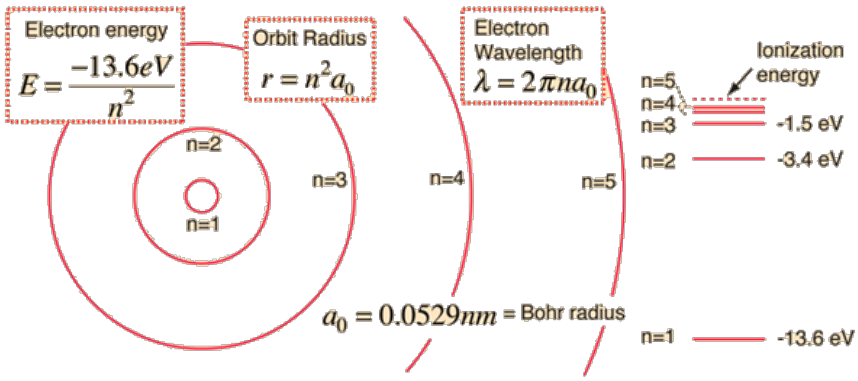

Figure 4-1: The energy levels of Hydrogen atom based on the Bohr model. Each main shell is associated with a value of the principal quantum number n [176].

Now, we consider a tight–binding chain with onsite energies ε and hopping energy t. The onsite energy of each site can be expressed by $\varepsilon = \frac{V}{(n+1)a} \simeq \frac{V}{r}$, where V is the Coulomb binding energy, n is the site number which starts from zero, a is the interatomic distance which is taken equal to one in our study and r is the distance

from the initial site ($n = 0$) of the chain.

For this chain, it is easy to verify, by expanding the tight–binding energies near the bottom of the band in power of k, that the Hamiltonian for long wavelengths can be written as follows

$$H_{TB} = |t|a^2k^2 - \frac{V}{r} \tag{4.5}$$

and after the results from the Hydrogen atom (see Eq. (4.4)) the negative eigen-energies are for sufficiently large n given by

$$\tilde{E_n} = -\frac{(V/a)^2}{4|t|n^2} \tag{4.6}$$

Figure 4-2 represents the local density of states, on site $n = 0$, of a one–dimensional tight–binding chain for different values of Coulomb potential. The appearance of bound states is similar to the energy levels of the Hydrogen atom. As the interaction strength increases, the weight of localized states increases as well. In addition, the plots of $1/E_n$ as a function of n^2 obtained by the LDOS calculations and by equation (4.6) are compared in figures' insets. As can be seen, the results obtained by the calculation are in a good accordance with the theory.

4.1.2 Asymmetric Coupling: Bulk Hetero–Junction Organic Photovoltaic Cells

In this section, we use the formalism developed in the second chapter of the thesis to analyze the performance of BHJ organic photovoltaic cells under the influence of long–range electron–hole Coulomb interaction and non–radiative recombination. We consider both charge carriers (i.e., the electron and the hole) mobile whereas in most of the studies [143, 172], the hole is studied as a fixed carrier. Although there is a correspondence between the permanent and the transitory regime cases; the asymmetric regime situation considered here seems to us to correspond better to the BHJ OPVs.

Before our study the other theoretical works have analyzed the situation by doing

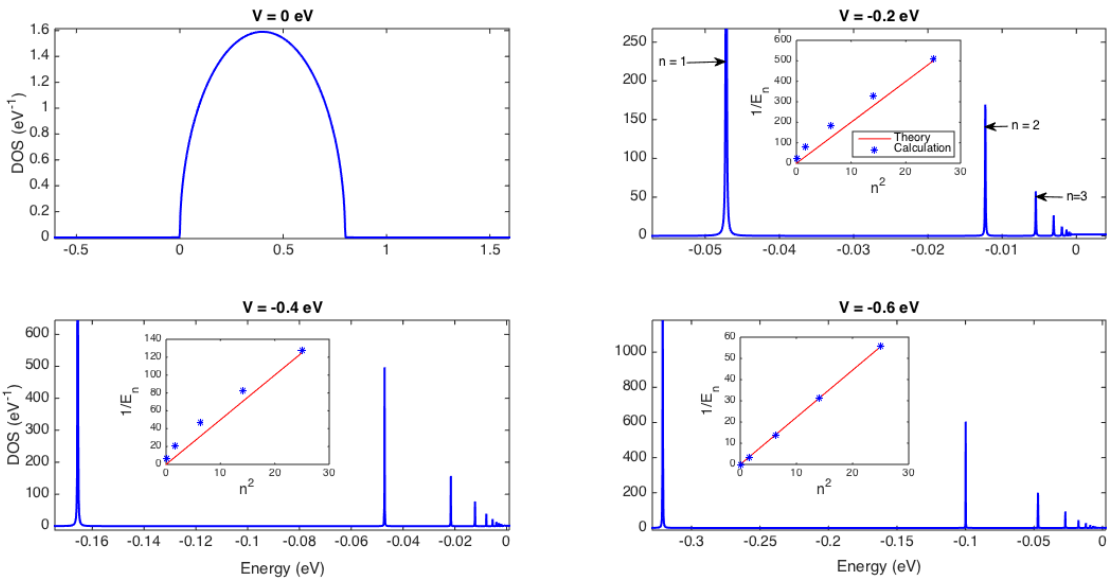

Figure 4-2: Local Density Of States (LDOS) as a function of energy for a one–dimensional tight–binding chain by considering different values of Coulomb interaction energy V.

computations in the time domain [143, 177]. The new formalism of this thesis enables one to investigate the exciton creation and dissociation in the energy domain, therefore, it provides useful spectral information in particular about the existence or absence of localized states which are at the heart of the exciton dissociation process. Hence, one can investigate the weight of excitonic states and charge separation yield and their dependence on the cell parameters. We discuss how the long–range interaction strength, recombination parameter and coupling energies can affect the charge separation yield in the BHJ organic photovoltaic cells.

4.1.2.1 Local Density Of States (LDOS)

In order to provide a spectral information to analyze the cell performance, we first consider the local DOS on the site $(0, 0)$ of the square lattice (Fig. 2-2). The cell parameters are chosen as $J_1 = J_2 = 0.2\ eV$ and $C_1 = 0.1\ eV$. Therefore, the bandwidth of electrons and holes in their respective leads are $0.8\ eV$ and the total bandwidth of electron–hole pair is $1.6\ eV$.

As a reminder, J_1 and J_2 are the coupling energies between two adjacent sites in

the electron and hole chains, respectively. Also, C_1 and C_2 represent the first coupling energies between the states of the two–level system and charge evacuation chains.

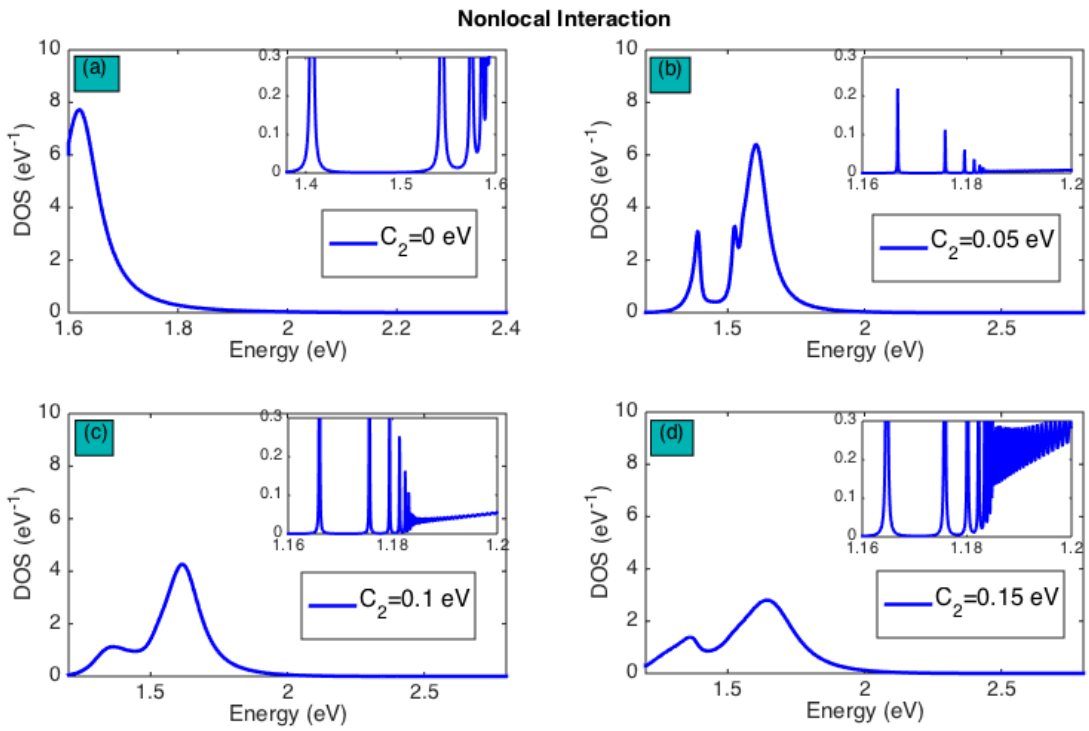

Figure 4-3: Density of states for electron–hole pair under long–range Coulomb interaction condition. These figures are obtained for $U = V = -0.4\,eV$ and different hole coupling parameter C_2 as indicated in the figure.

We choose

$$\varepsilon_e(x) + \varepsilon_h(y) = 2eV \tag{4.7}$$

and the hole coupling parameters include $C_2 = 0\ eV$ for the fixed hole case and $C_2 = 0.05, 0.1$ and $0.15\ eV$ for the mobile hole under the $C_2 < J_2$ condition.

Figure 4-3 represents the LDOS in an interesting and general situation with long–range Coulomb interaction between charge carriers. As explained frequently in the previous chapters, U and V denote the strength of short–range and long–range Coulomb interaction, respectively. In that case we find that a series of excitonic peaks appear below the lower band of the energy continuum. This is expected since the long–range Coulomb attraction can create localized states as discussed above. In panels (c) and (d) in Fig. 4-3, all the excitonic peaks close to the lower band edge

cannot be resolved.

4.1.2.2 Charge Separation Yield

Figure 4-4 represents the exciton dissociation yield, which is proportional to the portion of the charge carriers arriving at the electrodes, as a function of U, for several hole coupling parameter C_2, long–range interaction strength V and local recombination parameter Γ_R.

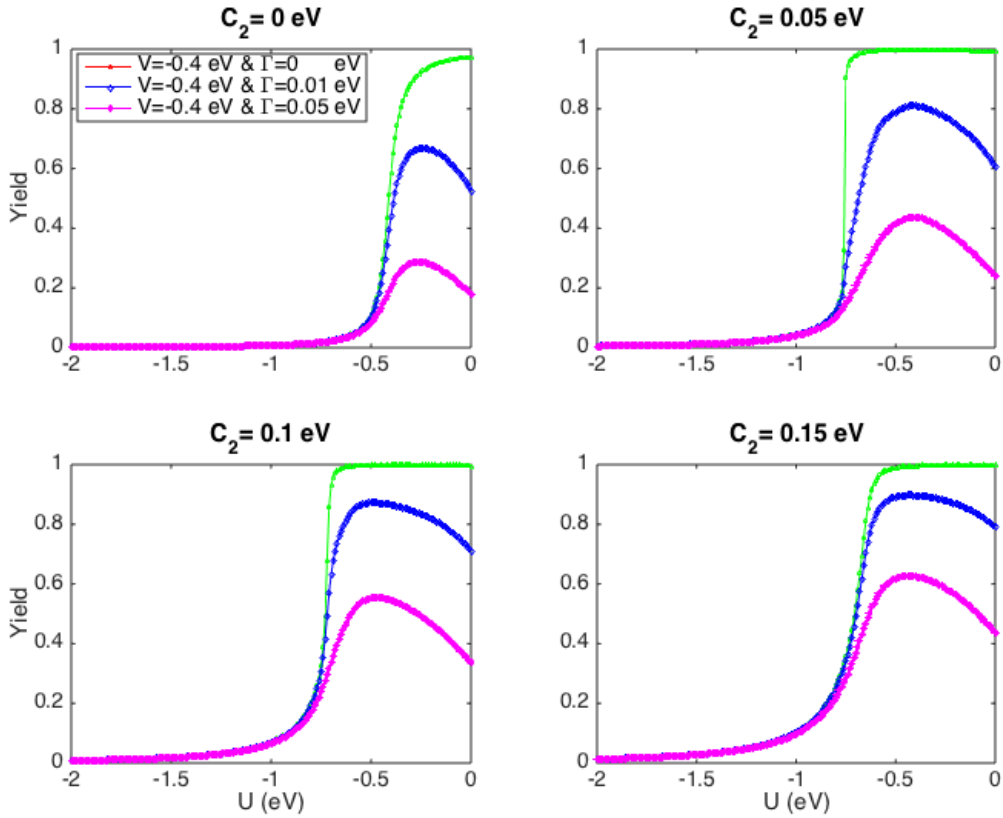

Figure 4-4: Yield (Y) of charge separation as a function of U obtained with different first coupling parameters to the hole lead C_2. The legend presented in the first panel, is valid for all the other panels. Γ_R represents the recombination parameter and V is the strength of long–range Coulomb interaction.

In the fixed hole condition, the total bandwidth of the electron–hole pair is simply equal to the electron bandwidth. Therefore, it is possible to create localized states with a smaller absolute value of the local interaction U. As a consequence

of the decrease of $|U_{Critical}|$ the yield of the cell quickly drops and goes toward zero (The concept of $U_{Critical}$ explained previously in Section. 3.1.1.1). Whereas by increasing the coupling energy C_2 of the hole one enhances the threshold of localized states appearence and as a consequence, the cell is efficient over a larger short–range interaction strength.

An important point that should be noted here is that under the influence of long–range interaction in contrast to the short–range interaction case, the maximum of the cell efficiency is not at $U = 0\ eV$, but at $U \approx V$ because the effect of the Coulomb interaction is to diminish globally the onsite energy close to the initial site of the square lattice.

Additionally, one sees from figure 4-4 that the effect of non–radiative recombination is to reduce the yield and that its impact is more significant in the weak coupling condition C_2. This can be understood based on the fact that charge evacuation becomes a difficult process in the weak coupling regime and hence the yield tends to decrease for a fixed recombination parameter.

4.1.2.3 Message To Take Home

In this section, we examined the performance of BHJ organic photovoltaic cells under the influence of long–range electron–hole interaction. In that case, we found that a series of excitonic peaks appear below the lower band of energy continuum. Additionally, since the effect of the Coulomb interaction is to diminish globally the potential around the site (0,0) of the square lattice, the maximum of the cell efficiency is not at $U = 0\ eV$, but at $U \approx V$. When the modulus of U increases the physics is dominated by the creation of a bound electron–hole pair with a very small spatial extension and the yield becomes poor, independently of the recombination parameter.

4.1.3 Symmetric Coupling: Molecular Photo-cells

The system under consideration consists of a single two–level molecule, represented by its HOMO and LUMO, situated between two leads (Fig. 4-5). The LUMO–HOMO gap plays an important role and in this study is denoted by Δ. We consider the mono–channel case where there is only one evacuation channel for each charge carrier. The first coupling parameters to the charge evacuation leads, i.e., between molecular states and evacuation leads, are denoted by C_1 and C_2. The hopping matrix elements inside each evacuation lead are considered independent of electron–hole positions and indicated by J_1 and J_2. We analyze photon absorption, energy conversion and quantum yield of a molecular photo-cell by considering the effects of long–range electron–hole interaction and non–radiative recombination. We model the exciton creation, dissociation and subsequent effects on quantum yield in the energy domain.

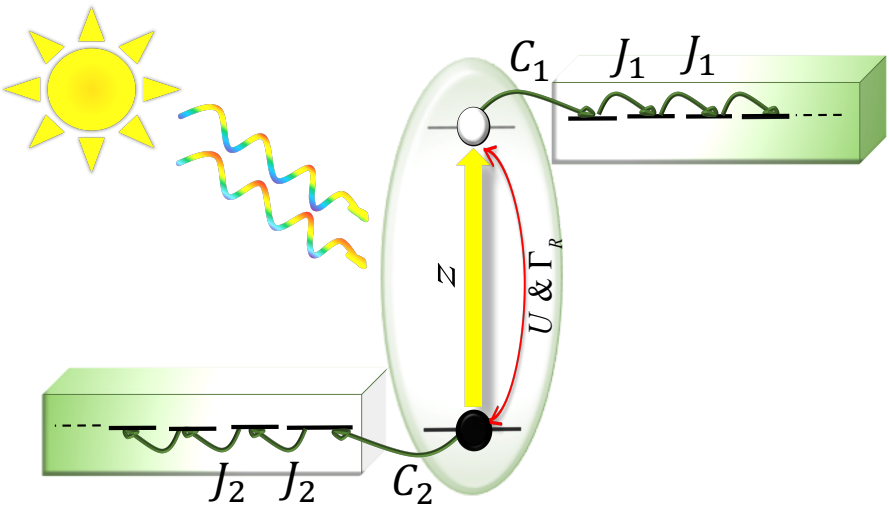

Figure 4-5: The two–level model for a molecular photo-cell with one HOMO and one LUMO orbitals attached to the electrodes. The red line represents the electron–hole interaction and recombination inside the molecule and the hopping integrals of electron and hole are denoted by C and J.

4.1.3.1 Local Density Of States (LDOS)

For the numerical simulation, we use $J_1 = J_2 = 0.2\,eV$ and $\Delta = 2\,eV$, therefore the continuum of electron–hole pair energies lies between 1.2 and 2.8 eV. In all the

calculations, C stands for the first coupling parameters and we treat the symmetric condition, i.e., $C_1 = C_2 = C$. Here, we study the effects of electron–hole interaction and introduce a long–range Coulomb interaction and examine its impact on the spectral properties (LDOS) and the charge separation yield.

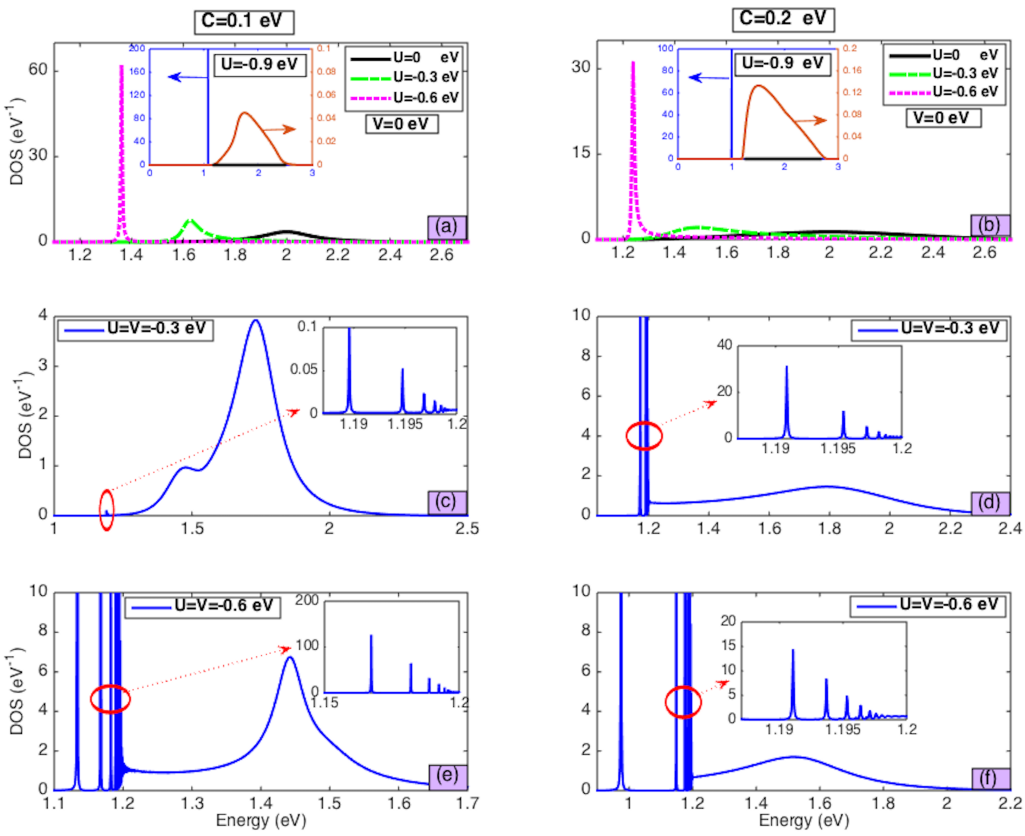

Figure 4-6: LDOS as a function of the energy of the absorbed photon. The impact of the coupling parameter C and the strength of the electron–hole interaction is illustrated in the various panels.

In order to understand the role of long–range electron–hole interaction, we consider also the non–interacting and local interacting electron–hole pairs to provide the necessary framework. In Fig. 4-6, the LDOS is plotted as a function of the absorbed photon energy. In these plots, the dependence of LDOS on short- and long- range interaction energy (U and V) and strength of coupling parameters (C) is examined. Here, the coupling parameter related to the panels of left and right columns is $C = 0.1\ eV$ and $C = 0.2\ eV$, respectively.

We can see that for non–interacting electron–hole pairs, the variation of LDOS is completely inside the energy continuum and as C increases, the width of DOS line–shape increases as well. Nevertheless, the position of DOS resonance energy E_{res} is unchanged. The increased DOS width facilitates the charge carrier transfer from the HOMO and LUMO to the respective leads. In the first two panels (panels (a) and (b)), the short–range electron–hole interaction, i.e., electron–hole interaction only inside the molecule, is considered.

As can be seen, for a given coupling parameter, the short–range interaction strength U indicates the number of LDOS peaks such that for small values of $|U|$, there is a single peak which becomes narrower as $|U|$ increases. As depicted in the inset, for growing values of $|U|$ the peak splits into two. The narrow peak outside the continuum is called excitonic state, which suppresses the charge carrier injection to the energy continuum. The effect of long–range interaction is examined through the panels (c)-(f).

As can be seen, under the influence of the long–range interaction a series of excitonic peaks appears outside the energy continuum, below the lower band edge. This is expected, as it is known that the long–range Coulomb interaction creates localized states. It should be noted that upon increasing the interaction strength, the total weight of excitonic states increases. Furthermore, in all cases, as the coupling parameter increases, the width of LDOS peak inside the energy continuum increases as well.

4.1.3.2 Weight Of Excitonic States & Charge Separation Yield

As pointed previously, in the limit of small recombination parameter, the relation $Y = 1 - P$ is valid which expresses that the charge separation yield is dependent on the weight of excitonic states. Figure 4-7 represents the weight of localized states as a function of resonance energy. We see that, as the modulus of interaction strength V increases, the weight of localized states increases as well.

Furthermore, for a given interaction strength, increasing the coupling parameter leads to localized state creation at higher values of resonance energies (i.e., smaller

values of U). For instance, in the case of $V = -0.3\ eV$, for $C = 0.1\ eV$ localized state formation occurs at interaction energy around $U = -0.75\ eV$, whereas this value in the case of $C = 0.2\ eV$ is around $U = -0.15\ eV$.

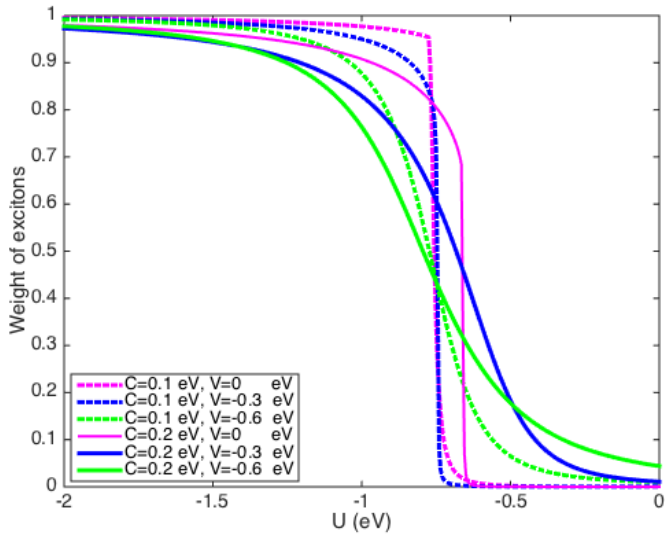

Figure 4-7: Weight of the excitonic peaks (P) as a function of U. The various curves are obtained upon variation of the coupling parameter C and the strength of the long–range electron–hole interaction V.

This behavior can be understood based on the discussion given in the pervious discussion, which shows that there is a critical value for interaction energy to create localized states. The mentioned discussion shows as the coupling parameter to the leads enhances, the modulus of critical interaction energy decreases, i.e., localized state formation occurs at lower values of interaction energies (See Section. 3.1.1.1).

As can be seen, upon increasing the interaction strength inside the molecule (U), less charge carriers exit through the contacts because of localized–state formation and hence the yield decreases. The interesting point is that in case of $U = V$, the effect of the Coulomb interaction is to diminish the global potential nearly uniformly, which has a small effect on the localization of electron–hole pair. Therefore the maximum of the charge separation yield is at $U \approx V$ as shown in Fig. 4-8. In panels (a) and (b) where the effect of long–range interaction has been neglected ($V = 0\ eV$), the maximum in the charge separation yield is at $U = V = 0\ eV$, in the other panels, as

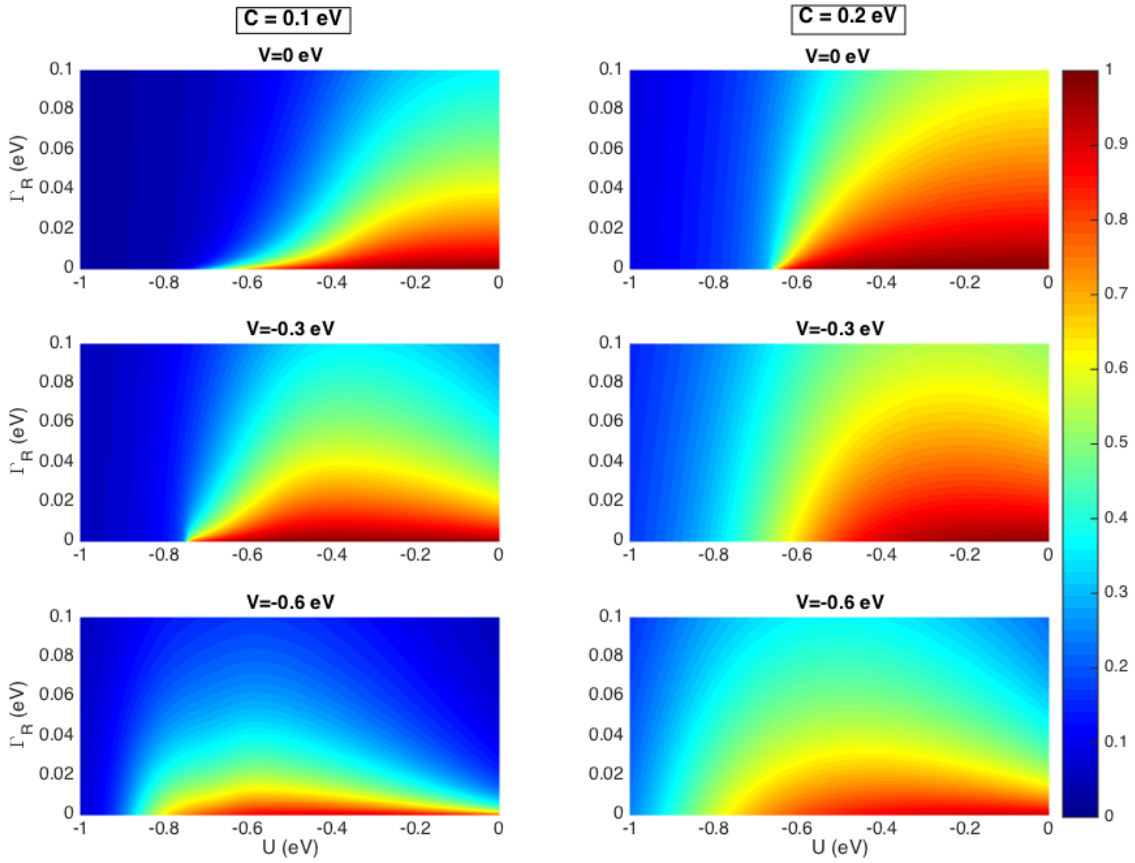

Figure 4-8: Charge separation yield as a function of short–range interaction energy (U) and recombination parameter (Γ_R). The various plots are obtained upon the variation of the electron–hole interaction and for different strengths of the coupling parameters. The coupling parameters in the panels of left and right columns are $C = 0.1\ eV$ and $C = 0.2\ eV$, respectively.

a consequence of electron–hole long–range interaction ($V \neq 0$), the maximum of the yield is at higher (more negative) values of U, i.e., in proximity of $U \approx V$.

Explicitly under the influence of strong interaction, the weight of localized states increases and consequently the possibility of recombination and annihilating the charge carriers enhances. For a given electron–hole interaction strength, the yield improves with increasing values of coupling parameter. Since the strong coupling extends the width of DOS line–shape and consequently improves the escaping rate, this behavior is understandable. Furthermore, the effect of non–radiative recombination is to diminish the yield and its impact is more important under the influence of strong long–range interaction condition.

4.1.3.3 Message To Take Home

We demonstrate that quantum scattering theory, in particular the Lippmann–Schwinger equation, provides a suitable framework to study the performance of molecular photocells. Using these tools, we found that long–range electron–hole interaction and non–radiative recombination reduce the photo-cell yield, especially under the weak coupling condition where the charge carriers cannot readily escape into the contacts.

4.2 Charge Injection In Polaronic Bands & Quantum Yield Of Excitonic Solar Cells

In the performance of excitonic solar cells, coupling to the phonon modes can play a major role as it may lead to the occurrence of polarons where a polaron is a moving charge surrounded by a cloud of phonons. To address how the electron–phonon coupling (in addition to the electron–hole interaction) can affect the charge separation process, here we propose a simple tight–binding based model. We analyse the spectrum of polaronic bands and focus on their effects on the charge separation yield which is defined as proportion of emitted electrons that arrive at the cathode electrode. We start the discussion by the model description.

4.2.1 Coupling To The Phonon Modes: Theoretical Model In The Small Polaron Limit

The charge carrier mobility can be influenced by the electron- and/or hole- vibration interaction. If the electron (hole)-phonon interaction is sufficiently strong a polaronic state can form and the charge carrier transport can be viewed as a polaron hopping from molecule to molecule. In the following, we present a mathematical model to investigate the influence polaron formation has on the charge separation process of excitonic solar cells. This model can be applied to any type of excitonic solar cells including the molecular photo-cells and the BHJ organic solar cells.

For clarity we consider from now on, the case of a BHJ OPV with an electron emitted at site $l = 0$ in a chain that represents the acceptor material. We construct a simple vibration chain model which is schematically illustrated in Fig. 4-9. In this model, the charge separation process follows an interesting scenario: after the exciton dissociation at the interface, the electron either recombines with the hole which is fixed at the interface or moves through a set of acceptor sites where it can be coupled to one single phonon mode. The physical interpretation of the model is that the charge transfer process is viewed as a hopping process when the electron interact

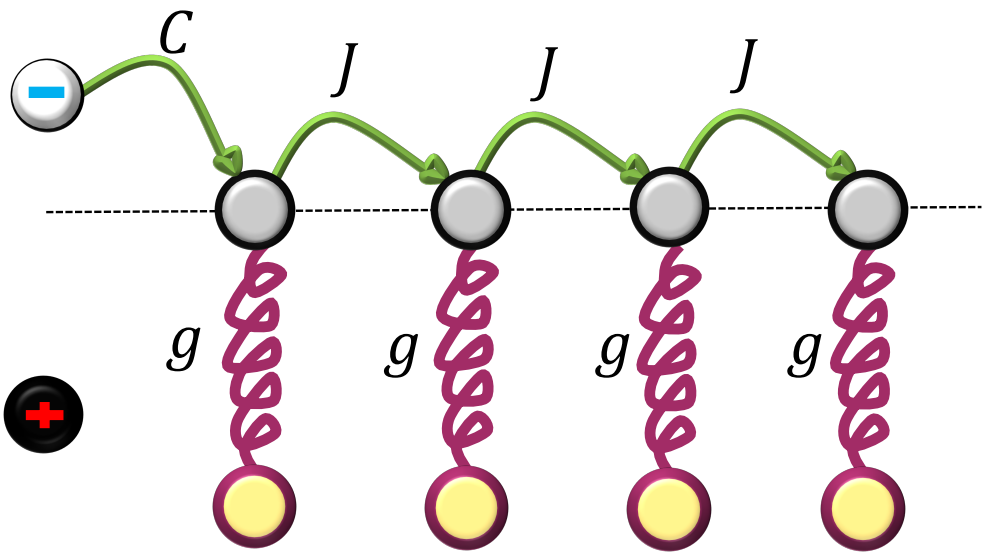

Figure 4-9: Schematic depiction of the chain model to describe the electron–vibration coupling which can occur on every single acceptor site when electron arrives at that site. C represents the coupling parameter between interface state and initial acceptor site. The coupling between adjacent sites on the acceptor chain is shown by J. g is the strength of coupling to the phonon chains.

sufficiently strongly with intramolecular vibrations.

The Hamiltonian of the considered system can be written based on the Holstein model [178]

$$H = \varepsilon_0\, c_0^\dagger c_0 + \sum_{l=1}^{N} \frac{V}{l}\, c_l^\dagger c_l + C\,(c_0^\dagger c_1 + c_1^\dagger c_0) + J \sum_{l=1}^{N-1} (c_l^\dagger c_{l+1} + c_{l+1}^\dagger c_l) + \hbar\omega_0 \sum_{l=1}^{N} a_l^\dagger a_l + g \sum_{l=1}^{N} c_l^\dagger c_l (a_l^\dagger + a_l) \tag{4.8}$$

where $a_l^\dagger(a_l)$ and $c_l^\dagger(c_l)$ are respectively the phonon and electron creation (destruction) operators on site l, $\hbar\omega_0$ is the energy of the relevant molecular vibration, g is the electron–phonon coupling constant, C is the coupling parameter between the initial site (site $l = 0$) and acceptor chain, ε_0 is the energy of the LUMO orbital of the electron at the interface of the BHJ, V sets the typical Coulomb potential binding the electron–hole pair, and J is the hopping amplitude within the chain. The unit of g, J, ε_0 and $\hbar\omega_0$ is eV. However, the unit of this parameters will be suppressed throughout

the discussion for greater clarity. In the following, we use the dimensionless Huang-Rhys parameter $\alpha^2 = (\frac{g}{\hbar\omega_0})^2$ to characterize the strength of the electron–phonon interaction [179, 180].

In the calculations, we consider only the nearest neighbor tight–binding interaction and study the model at zero temperature. This assumption is justified as the electronic and vibrational energies are much larger than $k_B T$. Furthermore, we examine the model in the small polaron limit which means that there are excited phonons only on the site where the electron is. The small polaron effect is present in a variety of materials, including many polymers (trans-polyacetylene, etc.) and most transition metals (MnO, NiO, etc) [181–183].

4.2.1.1 Local Green's Function & Spectrum Of Polaronic Bands

The local polaronic Green's function $G_{pol}(z)$ associated with the first site of the mentioned semi–infinite chain $l = 0$ or $|0\rangle$ can be expressed by

$$G_{pol}(z) = \frac{1}{z - \varepsilon_0 + i\frac{\Gamma_R}{2} - C^2\tilde{G}_1(z)} \tag{4.9}$$

where Γ_R is the recombination parameter which shows the possibility of electron–hole recombination when they are at the same place. $\tilde{G}_n(z)$ is the Green's function on site n when all sites between n and 0 are removed. The $\tilde{G}_n(z)$ obey a recurrence relation from which they are calculated

$$\tilde{G}_n(z) = \frac{1}{z - \frac{V}{n} - \Sigma_p(z) - J^2\tilde{G}_{n+1}(z)} \tag{4.10}$$

We will compute $G_{pol}(z)$ by considering intermediate Green's functions which correspond to the pure electron limit g=0 ($G_e(z)$) and the pure phonon limit $J = 0$ ($G_p(z)$), such that

$$G_e(z) = \frac{1}{z - \Sigma_e(z)} \quad \text{and} \quad G_p(z) = \frac{1}{z - \Sigma_p(z)} \tag{4.11}$$

where Σ_p represent the self–energy due to coupling between a site and the phonon-chain to which it is attached and Σ_e is the self–energy due to the coupling to the bare electron chain. For the pure phonon Green's function $G_p(z)$ where $(J = 0)$, the Hamilton of a given phonon chain H_{ph} can be expressed by

$$H_{ph} = \hbar\omega_0\, a^\dagger a + g\, c^\dagger c(a^\dagger + a) \tag{4.12}$$

This Hamiltonian operator is non–diagonal in the basis $|n\rangle$, but the following transformation turns it to a diagonalised Hamiltonian

$$\tilde{a} = \alpha + a \quad \text{and} \quad \tilde{a}^\dagger = \alpha + a^\dagger \tag{4.13}$$

These new operators $\tilde{a}$ and $\tilde{a}^\dagger$ obey the Bose Commutator relations and it can be easily shown by calculating the product of $\tilde{a}$ and $\tilde{a}^\dagger$ that the diagonalised Hamilton operator takes the form

$$H_{ph} = \hbar\omega_0\, c_0^\dagger c_0(\tilde{a}^\dagger\tilde{a} - \alpha^2) \tag{4.14}$$

where $\alpha = g/\hbar\omega_0$ is a dimensionless parameter which is given by the ratio of the coupling constant g and $\hbar\omega_0$ and therefore the model is controlled by only one parameter. Since

$$H_{ph}\,|\psi\rangle = E_n\,|\psi\rangle = \hbar\omega_0(n - \alpha^2)\,|\psi\rangle \tag{4.15}$$

we conclude that the eigen–energy is given by the energy spectrum of the harmonic oscillator lowered by $\alpha^2\hbar\omega_0$. Based on this explanations, Fig. 4-10 gives access to a comprehensive view of the model.

Equation (4.12) therefore describes an harmonic oscillator whose origin is shifted in x-direction by $\alpha\sqrt{2}$. The new eigen–states $|\tilde{n}\rangle$ are related by a basis transformation to the old eigenstate $|n\rangle$ corresponding to case $g = 0$. Here we just need to express the state $|0\rangle$ in the basis of the states $|\tilde{n}\rangle$. After Eq. (4.13) transformation, the state

$|0\rangle$ satisfy $(\tilde{a} - \alpha)\,|0\rangle = 0$ and this leads to

$$|0\rangle = \sum_n \frac{e^{-\alpha^2/2}(\alpha)^n}{\sqrt{n!}}\,|\tilde{n}\rangle \tag{4.16}$$

Using the normalization condition of the eigenstates $|\langle 0|n\rangle|^2$, we can finally derive the phonon Green's function $G_p(z)$ associated with the orbital $|0\rangle$

$$G_p(z) = \langle 0|G|0\rangle = \sum_n \frac{|\langle 0|\tilde{n}\rangle|^2}{z - \hbar\omega_0(n-\alpha^2)} = \sum_n \frac{\alpha^{2n}}{n!} e^{-\alpha^2} \frac{1}{z - \hbar\omega_0(n-\alpha^2)} \tag{4.17}$$

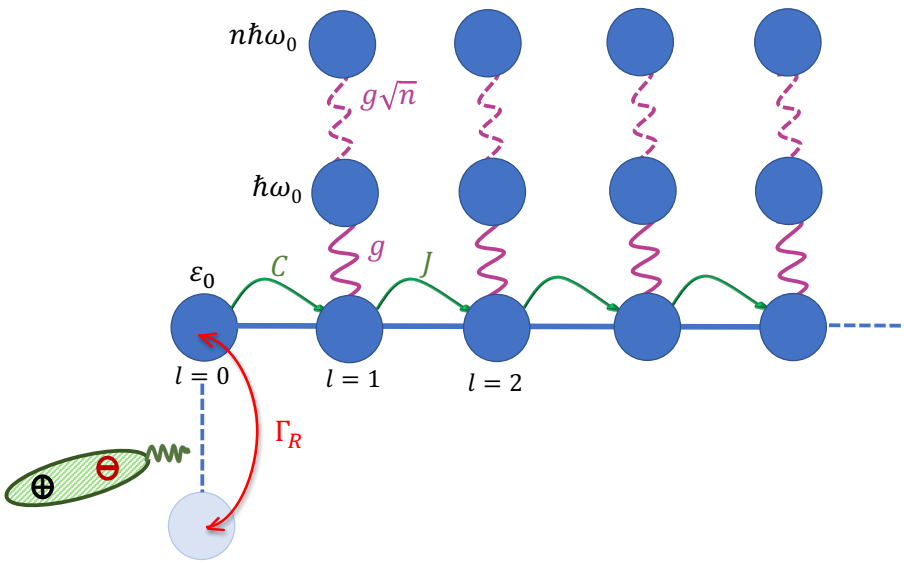

Figure 4-10: Schematic diagram of the electron–vibration chain model. The electron–vibration couplings occurs on every single site of the acceptor chain when electron arrives at that site. The onsite energy ϵ_0 is the energy of the LUMO orbital of the electron at the interface of the BHJ OPV. J and C are hopping integrals representing the coupling between adjacent electronic sites. The parameters $n\hbar\omega_0$ represent the onsite energy of the nth site of the phonon chain while $g\sqrt{n}$ is the hopping energy.

Here, we examine the behavior of phonon Green's G_p for different strength of electron coupling to the phonon chain (see Fig. 4-11). In the resulting spectra, there are series of equidistant poles which are centered at energies $\hbar\omega_0(n-\alpha^2)$ where n

represents the number of phonons. It should be noticed that an infinite number of peaks do exists but the spectral weight decreases with the number of peaks $1/n!$ and therefore all of them are not realizable.

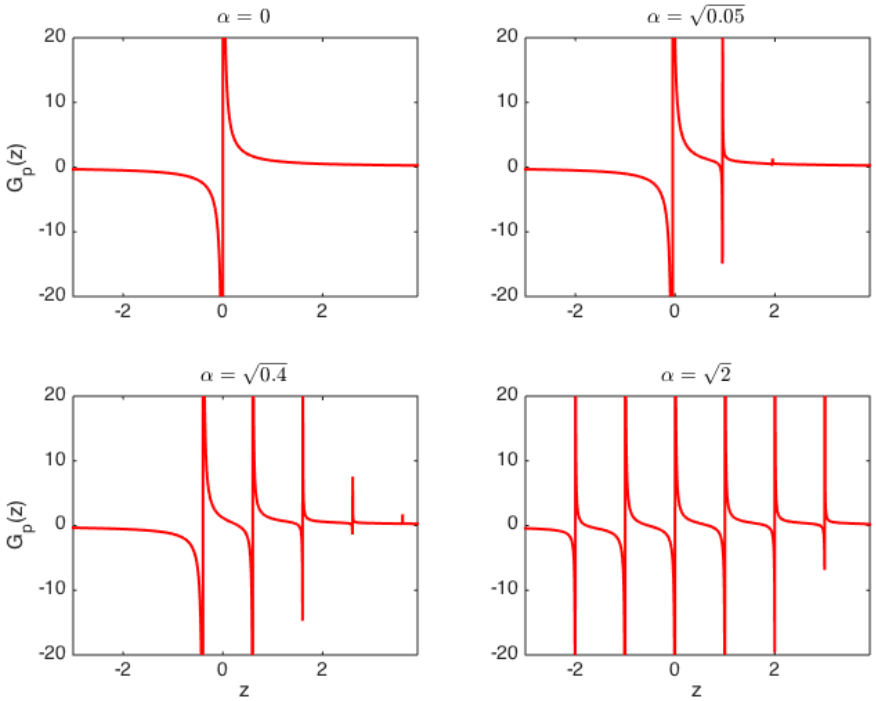

Figure 4-11: The phonon Green's function for different values of electron–phonon coupling parameter α. The figures are obtained for $\hbar\omega_0 = J = 1\ eV$.

We can also derive the pure hopping Green's function $G_e(z)$ (i.e., $g = 0$) based on the recursion method. Relying on the explanation given in the chapter two, the self–energy for a one dimensional semi–infinite chain associated with the site $|0\rangle$ can be expressed by a continuous fraction expansion

$$\Sigma_e(z) = \cfrac{J^2}{z - \cfrac{J^2}{z - \cfrac{J^2}{\cdots}}} \tag{4.18}$$

and from this self–energy we can compute the Green's function of a semi–infinite one

dimensional chain $G_e(z)$

$$G_e(z) = \frac{1}{z - \Sigma_e} \tag{4.19}$$

The nature of electron Green's function was discussed previously in chapter two. Combining results for the pure phonon and pure electron chains one deduces that for large n

$$\tilde{G}_n(z) = G_e(z - \Sigma_p(z)) \tag{4.20}$$

This is because beyond a sufficiently large n, each site has an onsite energy equal to zero and is attached to a pure phonon chain which effect is to give an additional self–energy $\Sigma_p(z)$. From this limit condition one can compute $G_{pol}(z)$ at all energies z and then all necessary quantities.

Now we are in the situation to investigate the influence of intramolecular vibrations on the electronic structure. We start by computing the local density of states far from the interface (so–called bulk part) for different values of electron–phonon coupling parameter α. This allows us to get a good physical image of the polaronic bands far from the interface. The parameter J is chosen to be 1 eV resulting in a energy continuum between -2 eV and $+2$ eV in the absence of electron–phonon coupling. The results are shown in Fig. 4-12.

The results show a series of bands with Van–Hove singularities at the edges. These are the polaronic bands. In the limit studied here there is essentially no scattering effect by the phonons and therefore the coupling to phonons has mainly the effect of renormalizing the bands. Obviously the bandwidth are decreased compared to the pure case (i.e., without electron–phonon coupling). The reduced bandwidth correspond to a reduced velocity or increased mass which is a well–known effect in the polaronic state.

Between the different bands the density of states for the polaronic model shows gaps originating from resonance energies caused by the coupling of the one–dimensional electronic chain to the phonon chain. Mathematically, these gaps occur when the phonon self–energy Σ_p diverges or equivalently when the polaron Green's function G_{pol} becomes zero. As a consequence, the real and imaginary part of the polaron

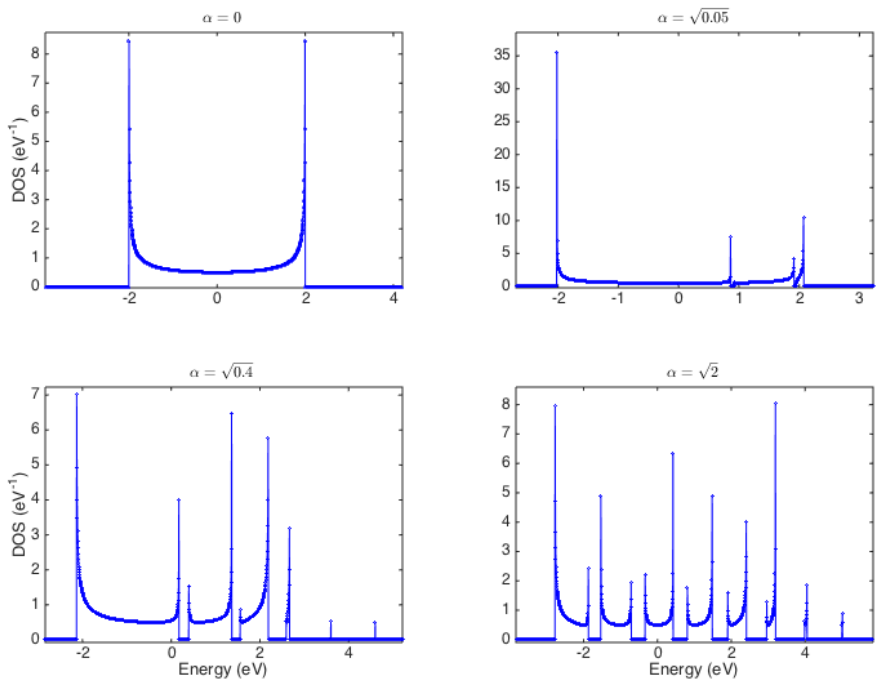

Figure 4-12: The local density of states in the bulk part for different electron–phonon coupling constant α. The figures are obtained for $\hbar\omega_0 = J = 1\ eV$.

Green's function become zero (Eq. (4.9)). The divergence of the self–energy of $\Sigma_p(z)$ can be understood from the fact that the pure phonon Green's function $G_p(z)$ always cancel between to poles as shown in Fig. 4-11.

We note also that there is an infinite number of polaronic bands which are centered around energies given by about $\hbar\omega_0(n-\alpha^2)$. However, the amplitude of the polaronic peaks decrease with $1/n!$ (n equals to the number of polaronic peaks) and therefore all of them cannot be seen in Fig. 4-12. The spectrum of the polaronic bands can be obtained easily from $\tilde{G}_n(z)$ at large n. Indeed the spectrum corresponds to energies for which $\tilde{G}_n(z) = G_e(z-\Sigma_p(z))$ has a non–zero imaginary part. This simply means that the effective energy $z-\Sigma_p(z)$ belongs to the spectrum of the pure electron chain which is in the interval $[-2J; 2J]$. For polaronic bands of high energy, the phonon Green's function $G_p(z)$ can be approximated only by one pole in the expression equation 4.17. One deduces that the bandwidth Δ_n is given approximately by

$$\Delta_n \simeq 4J\frac{\alpha^{2n}}{n!}e^{-\alpha^2} \tag{4.21}$$

4.2.2 The Impact Of Quantized Vibrations On The Charge Separation Yield

Now we intend to examine the charge separation yield in the presence of electron–hole and electron–phonon interactions. Let us recall that the yield is the proportion of the electrons that arrive at the cathode electrode, the other electrons being recombined at the interface with the hole.

We assume that the hole is localized on site $l = 0$. The effects of hole propagation can be described by extending Hamiltonian Eq. (4.8) and normally it is expected that the hole propagation decreases the effective Coulomb potential. To study the effects of lattice distortion, we consider a coupling between electron and single intramolecular vibration mode. Besides, a Coulomb interaction between the photo–generated electron–hole pair is considered but in principle other type of interaction potential should not significantly affect the results [184, 185]. Since both electronic and vibrational energy scales are much larger than $k_B T$, the investigation is done at zero temperature [186]. In the following we examine the charge separation yield in the presence of electron–phonon interaction in the two following cases:

I- short–range electron–hole interaction,

II- long–range electron–hole interaction.

4.2.2.1 Short–Range Electron–Hole Interaction

The initial state is comprised of an electron and hole on the LUMO and HOMO levels of the interface. We suppose hole is fixed on the initial site and electron can jump through the acceptor side. Referring to the short–range interaction condition, the electron and the hole can interact only when they are both at the site $l = 0$. Since the hole is fixed, the interaction of the elctron and the hole just amount to a change in the onsite energy of the electron when it is on site $l = 0$. Therefore, the interaction is integrated in the definition of the onsite energy ε_0, of the electron on site $l = 0$. The possibility of local charge recombination is also considered throughout the calculations. We set the hopping parameter $J = 1\,eV$, the donor to acceptor

tunneling rate $C = 0.5\,eV$ and the vibration energy $\hbar\omega_0 = 1$. We try to stay in the realistic experimental range, however as long as the calculation is done in the non–adiabatic regime ($\hbar\omega_0 \geq J$) [179, 180], the precise values are not so important. To explore the various aspects of the model, we vary the other three free parameters, i.e., the injection energy ε_0, the recombination parameter Γ_R, and the electron–phonon vibronic coupling α.

We start by considering the case without charge carriers recombination ($\Gamma_R = 0\ eV$), scanning for all possible values of the interface LUMO orbital energy ε_0 and varying the strength of the electron–phonon vibronic coupling α (See Fig. 4-13). As can be seen, in the non–interacting and non–recombining electron–hole case, the yield is one for $\alpha = 0$ within the acceptor bandwidth, i.e., $-2J \leq \varepsilon_0 \leq 2J$.

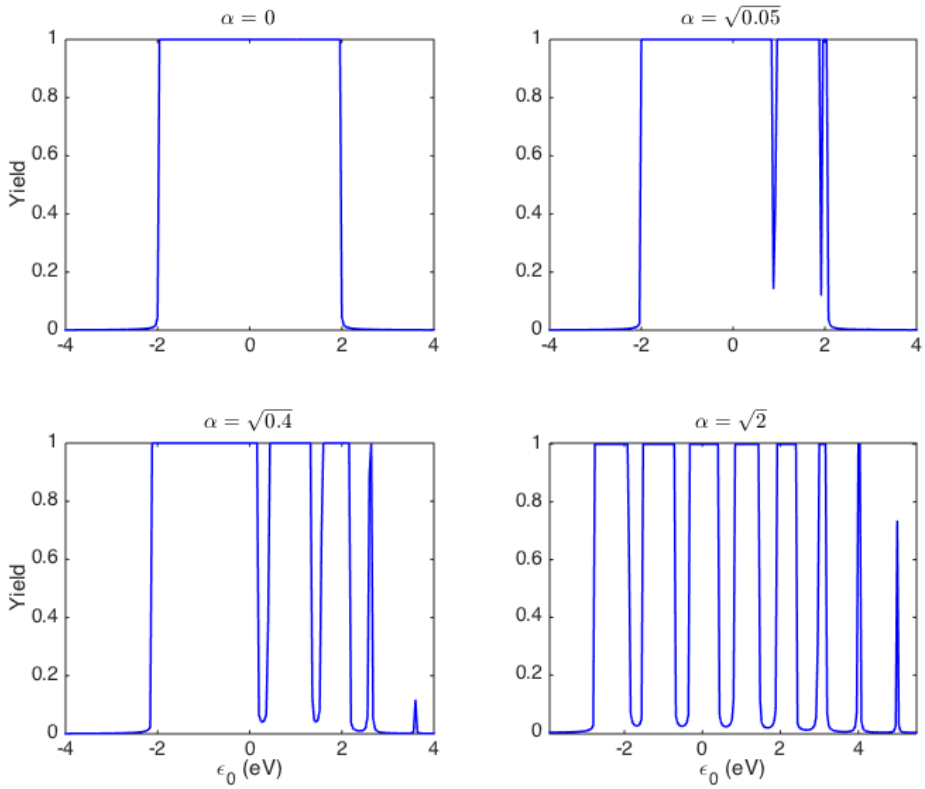

Figure 4-13: Yield as a function of incoming electron energy ε_0, for various values of the electron–phonon coupling constant α.

Upon increasing α, several sub–bands appear which is in conformity with the polaronic band structure of the acceptor side [187]. Interestingly, even for non–zero

α, there are some energy windows where the yield is nearly one.

The analysis of the electronic structure allows to understand the conditions for charge injection. Therefore, in order to interpret the yield, we examine the electronic structure in the bulk (far from the interface) and also close to the interface for different injection energies ε_0 and for an arbitrary α (Figs. 4-14 and 4-15).

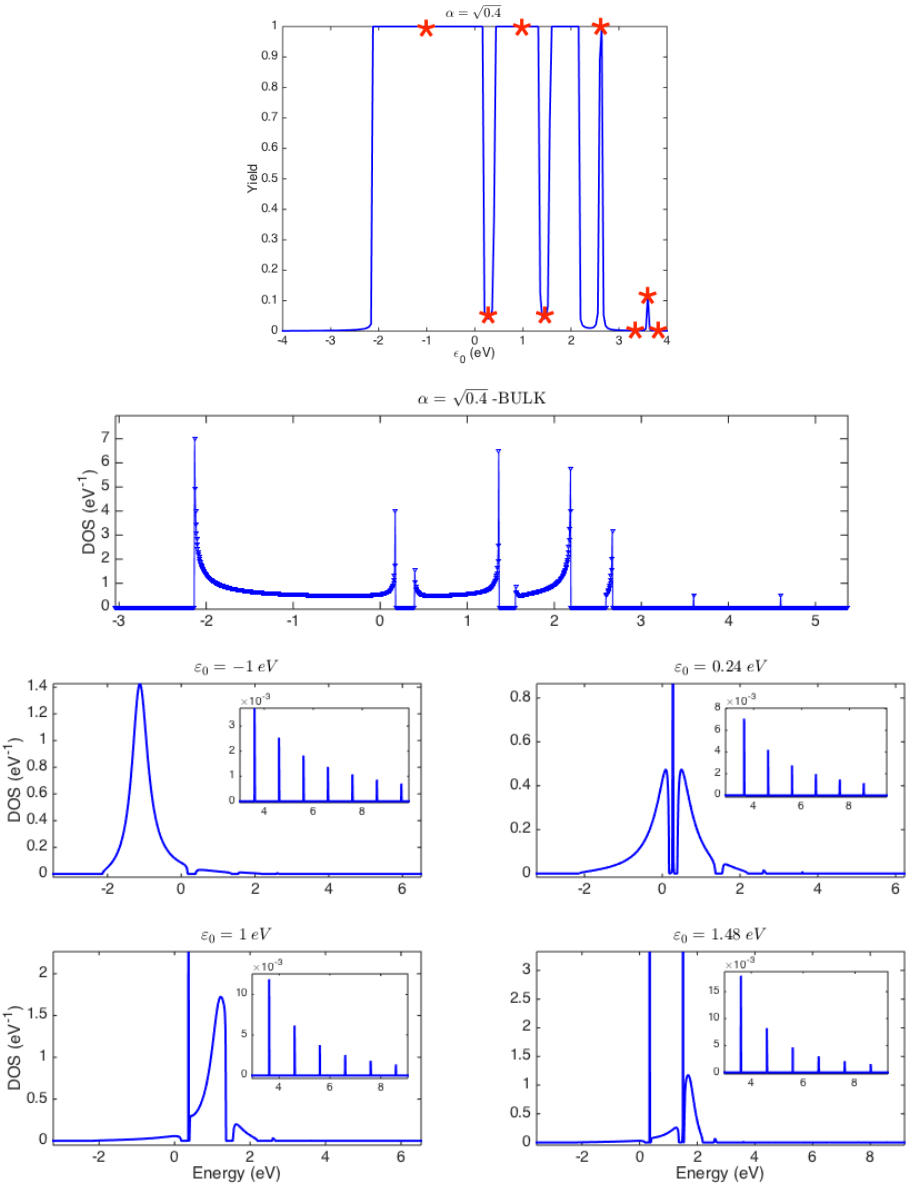

Figure 4-14: From top to the bottom: Charge separation yield, local density of states in the bulk part and close to the interface for different injection energies corresponding to the red marked points in the yield plot. The electron–phonon coupling constant is $\alpha = \sqrt{0.4}$.

The first panel of Fig. 4-14 repeats the yield plot with $\alpha = \sqrt{0.4}$ and shows a selected set of values of the interface LUMO orbital energy. The other panels represent the electronic structure. The electronic structure is examined in the bulk part (which is independent of the interface LUMO energy) and on site $l = 0$ for injection energies around the red marked points as well.

As shown in Fig. 4-14 and previously presented in Fig. 4-12, the electronic structure is composed of a series of bands, so called polaronic bands, which are separated by energy gaps. The electronic structure in the bulk part gives a view of all possible polaronic bands and the energy gap regimes.

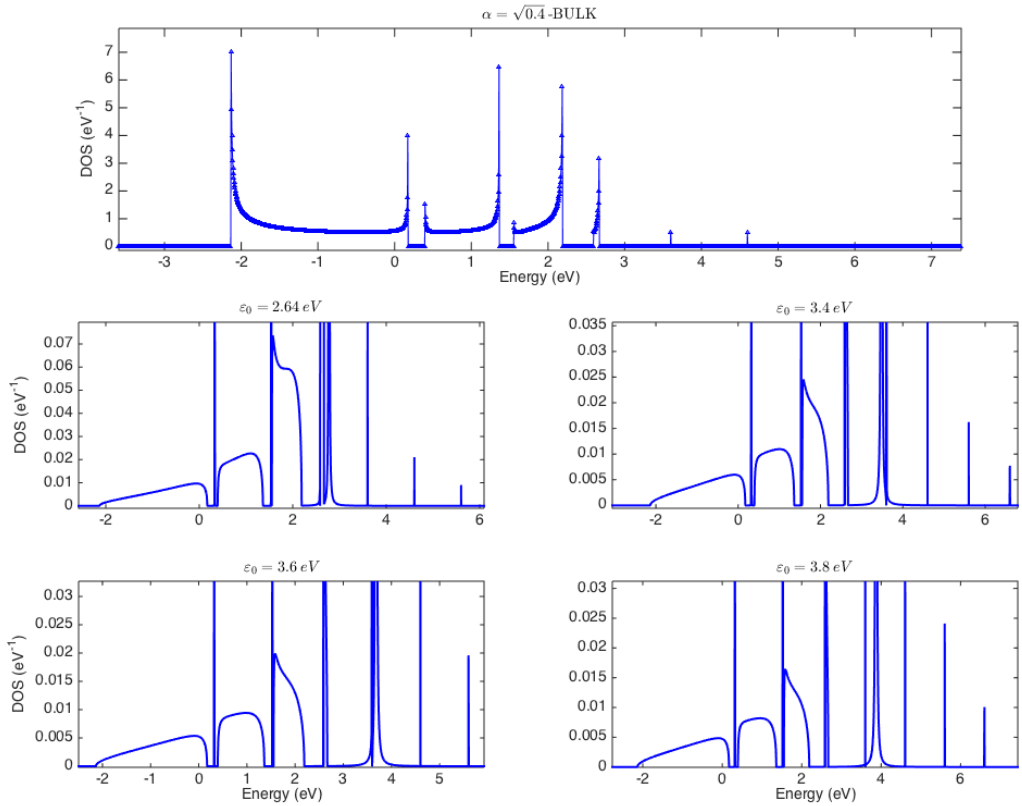

Figure 4-15: Continuation of Fig. 4-14. Local density of states close to the interface for different injection energies corresponding to the red marked points in the yield plot for different injection energies.

For a given injection energy ε_0, the electronic structure may contain the energy states on the allowed polaronic bands and also localized states in the energy gap (compared to the bulk DOS). The charge carriers lying in a polaronic band can evac-

uate and arrive at the electrodes. On the other hand, the charge carriers localized in the bound state in the gap recombine quickly and cannot lead to photovoltaic current which diminish the yield. Through this physical interpretation, yield values around the red marked points are in a good agreement with the corresponding electronic structure.

Here we draw the reader's attention to a delicate point: as can be seen, for injection energies well above the band of the bare electron chain ($2J$), the yield never reaches one. This behavior can be understood from our discussion in chapter three concerning the strong coupling limit. Indeed the effective coupling between site $l = 0$ and band of energy $E_n \simeq \hbar\omega_0(n - \alpha^2)$ is easily estimated to $C_{eff}(n) \simeq C\sqrt{\frac{\alpha^{2n}}{n!}e^{-\alpha^2}}$, whereas the bandwidth is given by Δ_n (Equation 4.21). Therefore at large band index n, i.e., in the regime of high orbital energy, the width of the polaronic band is so small that the coupling of the interface LUMO orbital to this band is stronger than the width of the band. Then as explained in chapter three, a localized state exists independently of the value of the initial orbital energy. Since there is always a localized polaronic state the bound charge ultimately recombines and therefore the yield is limited and cannot reach one (see Fig. 4-15).

Figure 4-16 represents the effects of recombination parameter Γ_R on charge separation yield. As previous figures, J and $\hbar\omega_0$ are taken equal to one. In a general statement, the effect of recombination is to reduce the yield and its impact is more evident in the large α case.

The influence that coupling parameter strength C has on charge separation yield is depicted in Fig. 4-17. Growing C values enhances the yield as long as the injection energy does not fall within the strong coupling limit. This is understandable since strong C facilitates the electron injection to the acceptor band. As the injection energy lies in the strong coupling limit, the possibility of bound states formation increases for larger C values which has a bad effect on yield.

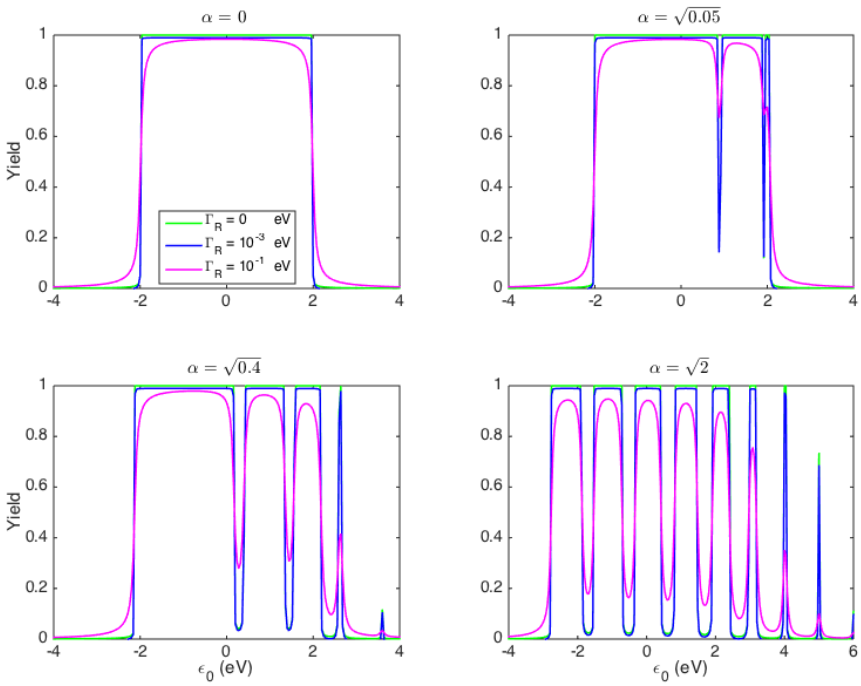

Figure 4-16: Yield as a function of incoming electron energy ε_0, for various values of the electron–phonon coupling constant α and electron–hole recombination parameter Γ_R.

4.2.3 Long–Range Electron–Hole Interaction

The effects of long–range electron–hole Coulomb interaction (with $V = -1\ eV$) is shown in Fig. 4-18. As can be seen, first, the yield keeps the periodic resonance structure as a consequence of polaronic band formation. Second, for all values of α, the combined effect of Coulomb interaction and polaronic dressing of the carriers leads to a strong overall suppression of the yield such that it never reaches one. Third, with increasing α, the yield shifts down even in the weak coupling limit, which is not observed in the absence of long–range Coulomb interaction.

To have clear understanding, again we refer to the spectral information. Figure 4-19 represents the yield and corresponding LDOS by considering electron–phonon coupling $\alpha = \sqrt{0.4}$.

The LDOS is represented in the bulk part (far from the interface) and also on site $l = 0$ for different injection energies corresponding to the red marks in the yield

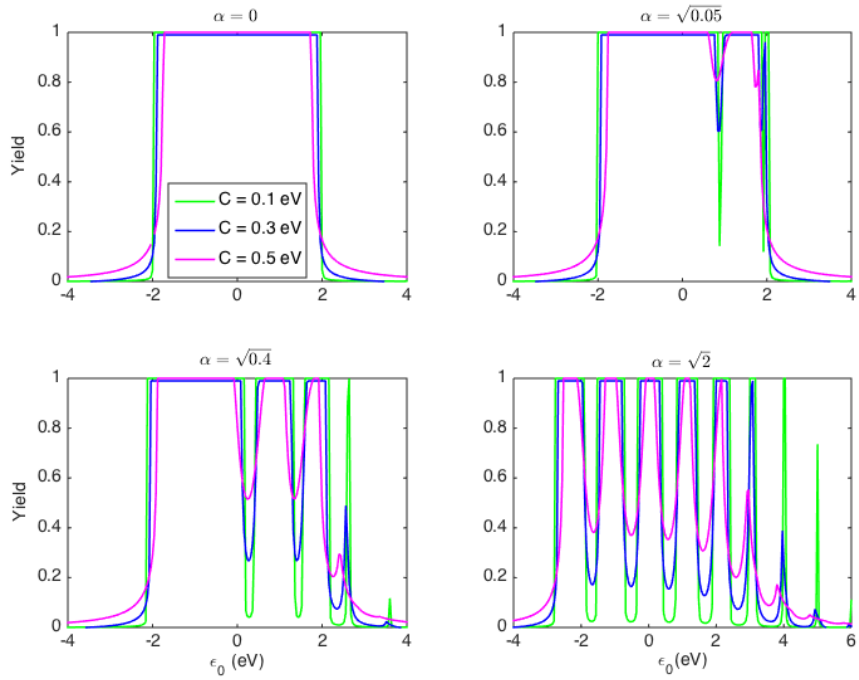

Figure 4-17: Yield as a function of incoming electron energy ε_0, for various values of the electron–phonon coupling constant α and coupling parameter C.

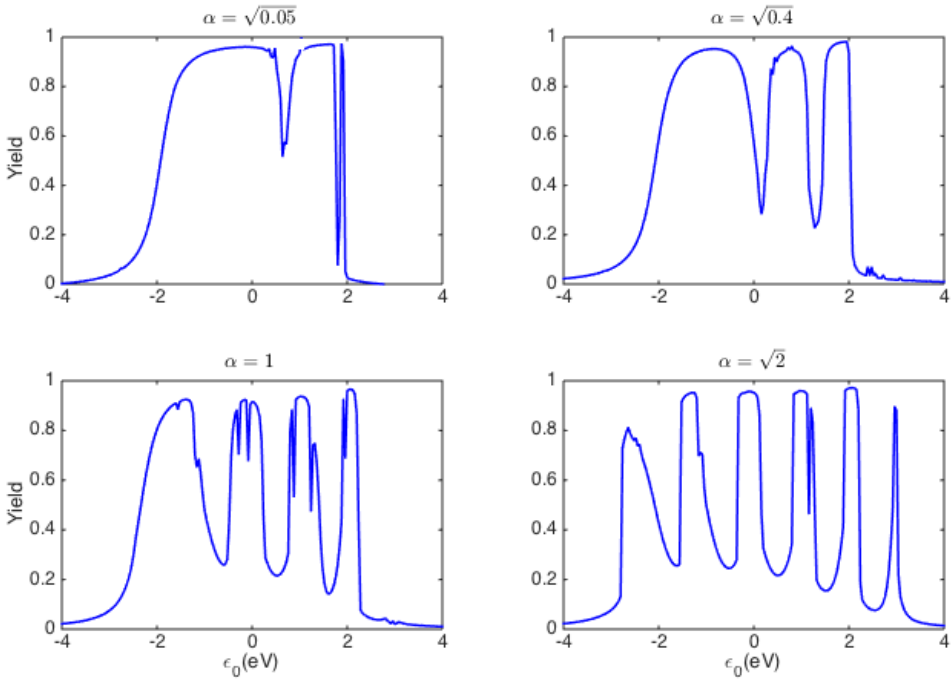

Figure 4-18: Yield as a function of incoming electron energy ε_0, for various values of the electron–phonon coupling constant α in the presence of long–range electron–hole binding $V = -1\ eV$.

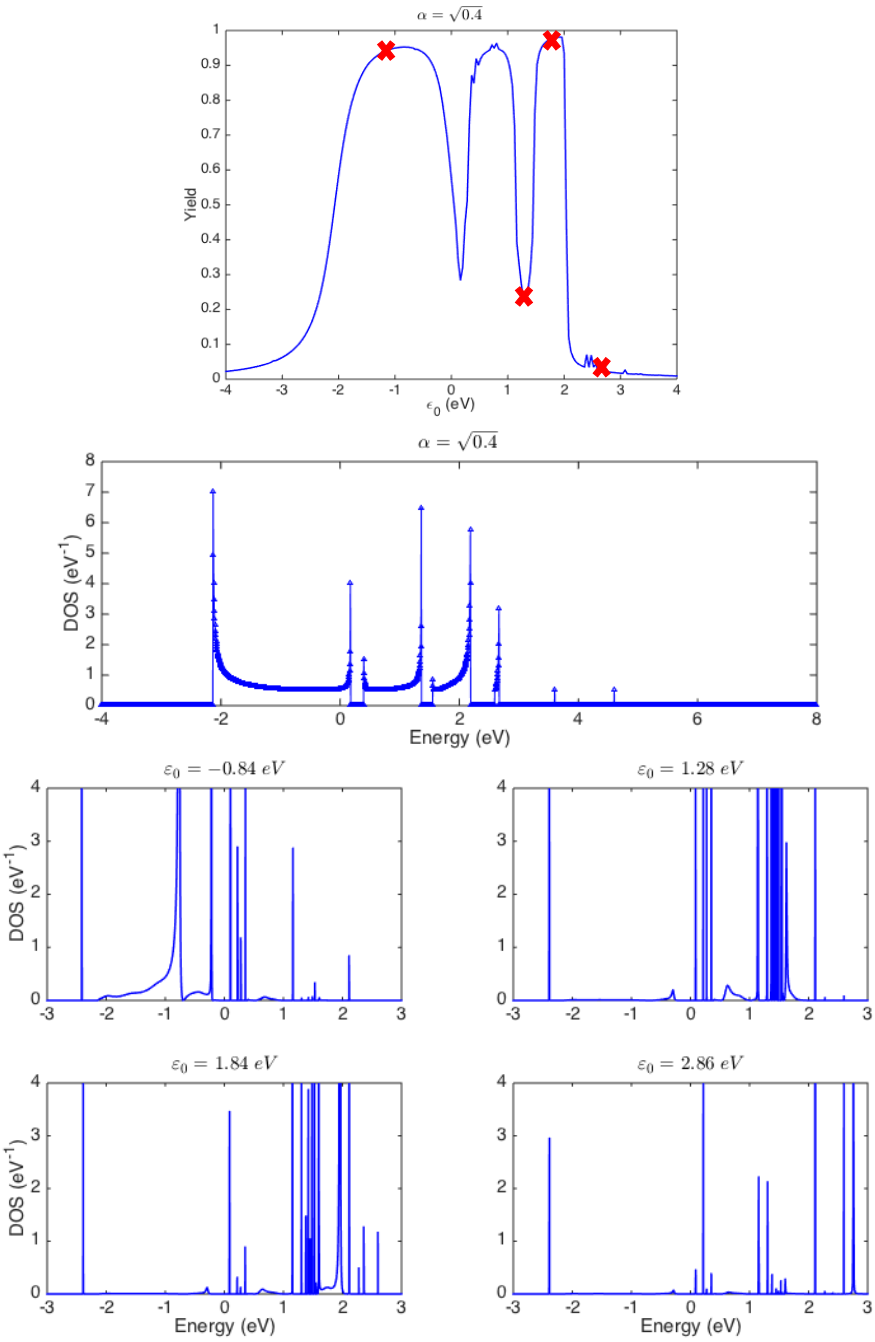

Figure 4-19: Yield and local density of states in the bulk part and close to the interface for different injection energies. The electron-phonon coupling constant is $\alpha = \sqrt{0.4}$ and the Coulomb interaction energy is $V = -1\ eV$.

plot. As can be seen the long–range Coulomb interaction leads to a more intricated spectrum with many localized and nearly localized states. This tendency to localizing the spectrum induces a lowering of the efficiency of the cell.

Figure 4-20 represents the effect of recombination parameter on the yield. As before, the effects of recombination (Γ_R) can be detected through the global reduction of yield (see Fig. 4-16). Although, its impact is more significant in the presence of long–range Coulomb interaction.

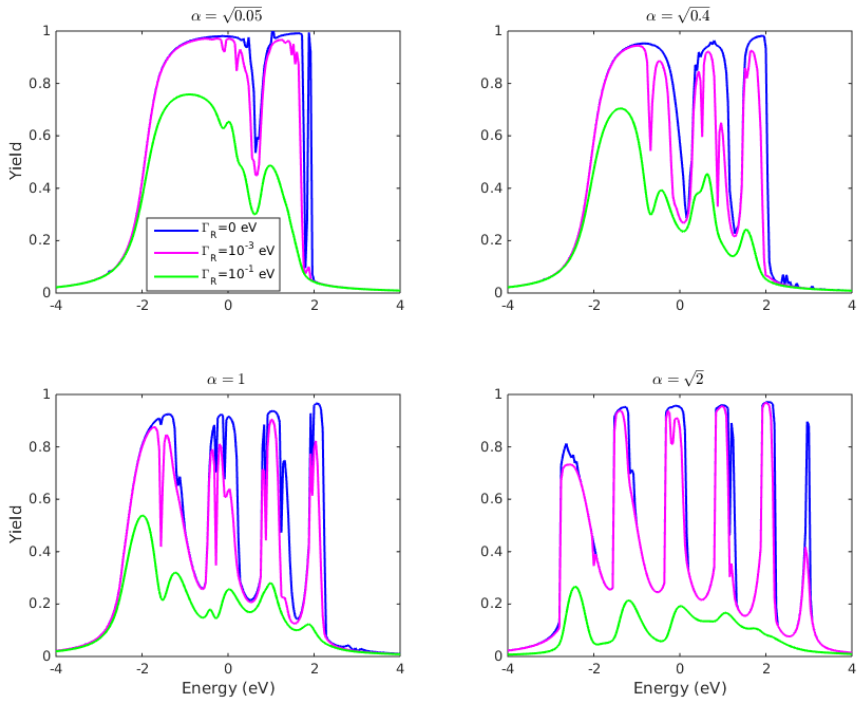

Figure 4-20: Yield as a function of incoming electron energy ε_0, in the presence of long–range electron–hole interaction $V = -1\ eV$, for various values of the electron–phonon coupling constant α and electron–hole recombination parameter Γ_R. The legend presented in the first panel is valid for all the other panels.

4.2.4 Message To Take Home

In conclusion, we provided microscopic evidence that the efficiency of charge transfer across an interface is subtly controlled by a coherent coupling of electron to high-energy quantized vibrational modes. In our study, the coupling to phonons creats polaronic bands that are separated in energy and therefore create a spectrum with many gaps. These numerous gaps tend to decrease the charge injection if the energy of the interface LUMO orbital falls near them through the existence of bound polaronic states localized at the interface. This leads to an oscillating behaviour of the yield

as a function of the interface LUMO orbital values. As expected increasing the recombination parameter tends to decrease the yield. The introduction of a long–range Couomb interaction between the injected electron and the fixed hole tends also to decrease the yield.

Chapter 5

Conclusions & Perspectives

The aim of this thesis was to acquire a deep understanding of the working mechanism of excitonic solar cells and to improve the device performance. Therefore, we developed a new quantum formalism based on the wave function of excitonic solar cells. The basic idea of this new methodology was demonstrated through the example of two–level excitonic solar cells. These two–level systems were studied in the permanent and transitory regimes of charges separation.

We demonstrated that this new methodology provides a quantitative picture of the fundamental processes underlying solar energy conversion, including photon absorption, exciton dissociation and charge separation as well as an understanding of their consequences on the cell performance. Interestingly, this theory could successfully analyse excitonic solar cell in the presence of strong Coulomb interaction between the electron and the hole.

Here we highlight some of the important achievements of this study:

(I) We showed that there is a competition between injection of charge carriers in the leads and recombination in the two–levels system. This competition depends sensitively on the parameters of the model such as the local electron–hole interaction, the recombination parameter, the coupling to the leads, and the band structure of the leads. When there are several evacuation channels for the charge carriers (electrons and/or holes), there is, in addition, a competition between injections in the different

channels.

(II) The quantum yield, i.e., the number of charge injected in the leads per photon absorbed, strongly depends on the local interaction energy U between the electron and the hole. There is a critical interaction energy $U_{Critical}$, which depends essentially on the band edges of the electron–hole excitations and the LUMO–HOMO energy offset on the initial site. We found that if $|U| < |U_{Critical}|$ the quantum yield can be high, provided the rate of recombination is small compared to the width of the exciton resonance. On the contrary when $|U| > |U_{Critical}|$ localized states of the electron–hole pair are created and hence the yield is strongly decreased even if the recombination parameter is small. Indeed in that case the electron and the hole cannot separate and after a sufficiently long time they necessarily recombine giving rise to no current in the lead.

(III) We investigated the effect of the hole propagation. Our results showed that by considering the hole as a fixed carrier, one underestimates $|U_{Critical}|$. Therefore, in the fixed–hole model, the yield of the cell can be underestimated, particularly for low recombination parameter. Hence, the mobility of the hole is an important parameter to improve the yield.

(IV) We found that the long–range electron–hole interaction and non–radiative recombination reduce the photo-cell yield, especially under the weak coupling condition where the charge carriers cannot readily escape into the contacts.

(V) Finally, we provided microscopic evidence that the efficiency of charge transfer across an interface is subtly controlled by an interplay of electrostatic confinement and coherent coupling of charge carrier(s) to high–energy quantized vibrational modes.

Several opportunities exist for the continuation of the work in this thesis to further deepen the understanding and development of excitonic solar cells:

(I) The model was applied to a two–level system; however, it has the capability of describing the performance of more complex systems. This method should help to understand the conditions needed for a high yield of an excitonic solar cell.

(II) For more precise study the data obtained from *ab-initio* calculation could be imported to the code.

(III) The model could be extended to study the effects of non–geminate recombinations, i.e., the case where at least one of the charge carriers is in its respective lead.

(IV) In this thesis we studied the coupling to phonon modes in the limit of narrow bandwidth. It is possible to go beyond this limit by using the Dynamical Mean-Field Theory (DMFT) of the polaron problem. Implementation of the DMFT in the context of solar cell is under current development. This will allow to describe in a more precise way the important role of coupling of charge carriers with optical phonon modes.

Appendix A

Tight–Binding Hamiltonian

A type of Hamilton that is frequently encountered to describe a lattice (or "grid" in the numerical sense) is the tight–binding Hamiltonian [188]. The term tight–binding is derived from the basis of atomic orbitals into which the electron wave function is decomposed. From the first developing of the tight–binding method by Bloch in 1928 [189], it is widely used as a standard method for electronic structure calculations by researchers in physics, chemistry, and material science [153, 190]. Relying on semi–empirical parameters, the tight–binding method usually provides a quick understanding the electronic behavior of a physical system. Tight–binding procedure is relatively straight–forward and popular because of its efficiency in large simulations [189, 191, 192].

Suppose $\vec{r}$ denotes a vector representing the spatial position of a certain lattice site. In two dimensions, this vector corresponds to a site $r = (m, n)$ where the m and n indices are in the $x-, y-$ directions. For a state that is centered at location r, $|r\rangle$, the following relations are valid:

$$Completeness : \sum_r |r\rangle\langle r| = 1, \tag{A.1}$$

$$Orthonormality : |r\rangle\langle r'| = \delta_{r,r'}. \tag{A.2}$$

The tight–binding Hamiltonian is introduced as

$$H = \sum_r \varepsilon_r \left|r\right\rangle\!\left\langle r\right| + \sum_{r,r'} t_{r,r'} \left|r\right\rangle\!\left\langle r'\right| \tag{A.3}$$

where ε_r is the onsite energy at r, and $t_{r,r'}$ is the hopping energy between r' and r. The most common assumption in the tight–binding model is that only nearest neighbor interactions are important. If Δ_r represents the vectors from r to all its nearest neighbor sites, then this assumption of nearest neighbor interactions means that Eq. A.3 may be written

$$H = \sum_r \varepsilon_r \left|r\right\rangle\!\left\langle r\right| + \sum_{r,\Delta_r} t_{r,\Delta_r} \left|r\right\rangle\!\left\langle r + \Delta_r\right|. \tag{A.4}$$

A convenient and commonly used way of writing a tight–binding Hamiltonian is to replace the dyadic products of states $|r\rangle$ by new operators using second quantization. One introduces creation operators, $a_r^\dagger$, and their adjoint annihilation operators, a_r, with each operator acting on grid point r. These operators corresponding to our tight–binding lattice obey the following fundamental bosonic commutator relations

$$[a_r, a_{r'}^\dagger] = \delta_{r,r'} \tag{A.5}$$

$$[a_r, a_{r'}] = [a_r^\dagger, a_{r'}^\dagger] = 0 \tag{A.6}$$

The Hamiltonian Eq. A.4 can be expressed in terms of these new operators. For simplicity, we assume a constant hopping potential t between nearest neighbor sites and obtain

$$H = \sum_r \varepsilon_r a_r^\dagger a_r + \sum_{r,\Delta_r} [t a_r^\dagger a_{r+\Delta_r} + (hermitian\ conjugate)]. \tag{A.7}$$

The Hamiltonian in this representation has diagonal contributions given by the on-site energy ε_r and the hopping contributions, which create and annihilate excitations on neighboring lattice sites and annihilate or create them respectively on site r.

To illustrate the matrix form of a tight–binding Hamiltonian, consider a one-dimensional chain of $N = 5$ lattice sites that exhibit nearest–neighbor hopping (Fig. A-1). The onsite energy of site n is denoted by ε_n, whereas the hopping energy between site $\varepsilon_{n'}$ and n is represented in general by $t_{n,n'}$.

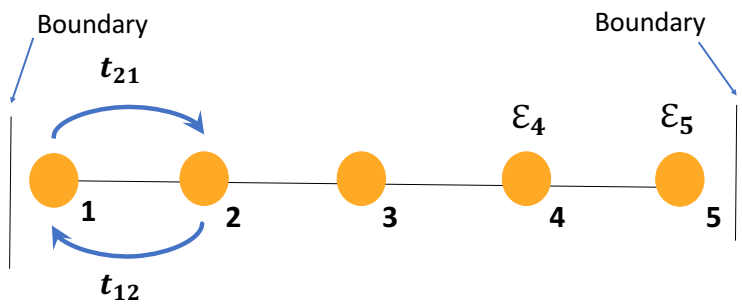

Figure A-1: Finite one–dimensional tight–binding chain of sites $n \in 1, ..., N = 5$.

Taking matrix elements $\langle n| H |n'\rangle$ where the indices n, n' run over all sites $1, ..., N$, the explicit form of the operator H corresponding to this one–dimensional problem is given by the N $\times$ N-matrix

$$H = \begin{bmatrix} \varepsilon_1 & t_{12} & 0 & 0 & 0 \\ t_{21} & \varepsilon_2 & t_{23} & 0 & 0 \\ 0 & t_{32} & \varepsilon_3 & t_{34} & 0 \\ 0 & 0 & t_{43} & \varepsilon_4 & t_{45} \\ 0 & 0 & 0 & t_{54} & \varepsilon_5 \end{bmatrix} \tag{A.8}$$

Appendix B

Projection Operators

In the linear algebra and functional analysis, a projection operator is the linear transformation from a vector space to itself. We consider two projection operators named P and $Q = 1 - P$ such that if P projects on a given space, then Q projects on the complementary and orthogonal subspace. The characteristic relations between P and Q are:

$$P = P^2 \tag{B.1}$$

$$Q = Q^2 \tag{B.2}$$

$$P = P^\dagger \tag{B.3}$$

$$Q = Q^\dagger \tag{B.4}$$

$$PQ = QP = 0 \tag{B.5}$$

$$P + Q = 1 \tag{B.6}$$

Starting form the Green's function

$$(z - H)G(z) = 1 \tag{B.7}$$

where $z = E + i\epsilon$ is a complex energy consisting of the real part E and ϵ, an infinitesimal positive imaginary part, we can multiply both sides of this equation on the right

by P and on the left either by P or by Q. Between $(z-H)$ and $G(z)$ one can insert the relation $P+Q=1$ and finally get the two following equations:

$$P(z-H)P(PG(z)P) - PHQ(QG(z)P) = P \tag{B.8}$$

$$-QHP(PG(z)P) + Q(z-H)Q(QG(z)P) = 0 \tag{B.9}$$

which are two equations between the two operators $PG(z)P$ and $QG(z)P$. By eliminating $QG(z)P$ from these two equations, one obtains:

$$PG(z)P = \frac{P}{z - PHP - PHQ\frac{Q}{z-QHQ}QHP} \tag{B.10}$$

Equation(2.40) has a simple physical meaning. PHP is a Hermitian operator ($(PHP)^\dagger = P^\dagger H^\dagger P^\dagger = PHP$) which indicates the restriction of Hamiltonian H to a space which contain the operator P. Furthermore, $PHQ\frac{Q}{z-QHQ}QHP$ is the self-energy due to the fact that the mentioned subspace is coupled to its complementary by Hamiltonian H.

B.1 Projection Operators On The Recursion Chain

On a recursion chain (see Fig. (B-1)), the projection operators can be defined as

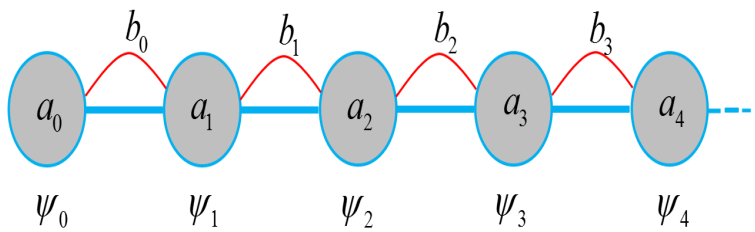

Figure B-1: A typical recursion chain. The parameters a_n represents the onsite energy of each state, while the parameters b_n are the hopping energies between two adjacent states. $|\Psi_n\rangle$ is the wave–function associated to the state n.

$$P = |\Psi_0\rangle\langle\Psi_0| \tag{B.11}$$

$$Q = \sum_{n=1}^{\infty} |\Psi_n\rangle\langle\Psi_n| \tag{B.12}$$

Therefore,

$$PG(z)P = |\Psi_0\rangle\langle\Psi_0|\, G(z)\, |\Psi_0\rangle\langle\Psi_0| = G_{00}(z)P \tag{B.13}$$

Thus based on the Eq. (B.10), we can write

$$G_{00}(z)P = \frac{P}{z - PHP - PHQ\frac{Q}{z-QHQ}QHP} \tag{B.14}$$

From the definition of recursion coefficients, one has

$$PHP = |\Psi_0\rangle\langle\Psi_0|\, H\, |\Psi_0\rangle\langle\Psi_0| = a_0 P \tag{B.15}$$

$$PHQ = \sum_{n=1}^{\infty} |\Psi_0\rangle\langle\Psi_0|\, H\, |\Psi_n\rangle\langle\Psi_n| = b_0\, |\Psi_0\rangle\langle\Psi_1| \tag{B.16}$$

$$QHP = b_0^*\, |\Psi_1\rangle\langle\Psi_0| = b_0\, |\Psi_1\rangle\langle\Psi_0| \tag{B.17}$$

The last two equations are obtained in the first neighbors approximation, i.e., there is coupling only between adjacent states. By substituting the Eqs. (B.15)-(B.17) in (B.14) one obtains

$$G_{00}(z) = \frac{1}{z - a_0 - b_0^2\, \langle\Psi_1|\frac{1}{z-QHQ}|\Psi_1\rangle} \tag{B.18}$$

By recurrence we get the general equality called the continuous fraction

$$G_{00}(z) = \cfrac{1}{z - a_0 - \cfrac{b_0^2}{z - a_1 - \cfrac{b_1^2}{z - a_2 - \ddots}}} \tag{B.19}$$

The calculation of recursion coefficients should be continued up to the convergence occurrence. Here, we suppose that the convergence occurs in the recursion step (N_{Rec}). Then, to terminate the continuous fraction we define the terminator $T(z)$ which includes the effects of the all the terms after the convergence occurrence step and it can be expressed as following

$$T(z) = \cfrac{1}{z - a_{N_{Rec}} - \cfrac{b_{N_{Rec}}^2}{z - a_{N_{Rec}} - \cfrac{b_{N_{Rec}}^2}{z - a_{N_{Rec}} - \ddots}}} \tag{B.20}$$

where the index "N_{Rec}" indicates all the recursion steps after the convergence occurrence step. The terminator $T(z)$ can be rewritten by a closed form including itself as follows

$$T(z) = \frac{1}{z - a_{N_{Rec}} - b_{N_{Rec}}^2 T(z)} \tag{B.21}$$

By solving Eq. (B.21) regarding $T(z)$, then we get a well known square root terminator

$$T(z) = \frac{z - a_{N_{Rec}} \pm \sqrt{(z - a_{N_{Rec}})^2 - 4b_{N_{Rec}}^2}}{4b_{N_{Rec}}^2} \tag{B.22}$$

Choosing the negative or positive sign in front of the square root depends on the

following condition

$$If\ \ z \to \infty\ \ Then\ \ T(z) \to 0 \tag{B.23}$$

which results in:

$$If\ \ |z| <\ 2b_{N_{Rec}}\ \ \ Then\ \ \ T(z) = \frac{z - a_{N_{Rec}} + i\sqrt{4b_{N_{Rec}}^2 - z^2}}{2b_{N_{Rec}}^2} \tag{B.24}$$

$$If\ \ |z| >\ 2b_{N_{Rec}}\ \ \ Then\ \ \ T(z) = \frac{z - a_{N_{Rec}} + \sqrt{z^2 - 4b_{N_{Rec}}^2}}{2b_{N_{Rec}}^2} \tag{B.25}$$

$$If\ \ |z| >\ 2b_{N_{Rec}}\ \ \ Then\ \ \ T(z) = \frac{z - a_{N_{Rec}} - \sqrt{z^2 - 4b_{N_{Rec}}^2}}{2b_{N_{Rec}}^2} \tag{B.26}$$

Bibliography

[1] P. Nejat, F. Jomehzadeh, M. M. Taheri, M. Gohari, and M. Z. A. Majid, "A global review of energy consumption, co_2 emissions and policy in the residential sector (with an overview of the top ten co_2 emitting countries)," *Renewable and Sustainable Energy Reviews*, vol. 43, pp. 843–862, 2015.

[2] D. Zielke, A. C. Hübler, U. Hahn, N. Brandt, M. Bartzsch, U. Fügmann, T. Fischer, J. Veres, and S. Ogier, "Polymer-based organic field-effect transistor using offset printed source/drain structures," *Applied Physics Letters*, vol. 87, no. 12, p. 123508, 2005.

[3] N. Panwar, S. Kaushik, and S. Kothari, "Role of renewable energy sources in environmental protection: a review," *Renewable and Sustainable Energy Reviews*, vol. 15, no. 3, pp. 1513–1524, 2011.

[4] K. Solangi, M. Islam, R. Saidur, N. Rahim, and H. Fayaz, "A review on global solar energy policy," *Renewable and sustainable energy reviews*, vol. 15, no. 4, pp. 2149–2163, 2011.

[5] S. Mekhilef, R. Saidur, and A. Safari, "A review on solar energy use in industries," *Renewable and Sustainable Energy Reviews*, vol. 15, no. 4, pp. 1777–1790, 2011.

[6] B. Ghobadian, G. Najafi, H. Rahimi, and T. Yusaf, "Future of renewable energies in iran," *Renewable and sustainable energy reviews*, vol. 13, no. 3, pp. 689–695, 2009.

[7] F. Dincer, "The analysis on photovoltaic electricity generation status, potential and policies of the leading countries in solar energy," *Renewable and Sustainable Energy Reviews*, vol. 15, no. 1, pp. 713–720, 2011.

[8] M. D. Archer and M. A. Green, *Clean electricity from photovoltaics*, vol. 4. World Scientific, 2014.

[9] A. Serchuk, "From space to earth: The story of solar electricity (review)," *Technology and Culture*, vol. 43, no. 2, pp. 460–461, 2002.

[10] P. E. Glaser, "Satellite solar power station," *Solar Energy*, vol. 12, no. 3, pp. 353–361, 1969.

[11] M. A. Green, "Solar cells: operating principles, technology, and system applications," 1982.

[12] X. D. Wang, E. Graugnard, J. S. King, Z. L. Wang, and C. J. Summers, "Large-scale fabrication of ordered nanobowl arrays," *Nano Letters*, vol. 4, no. 11, pp. 2223–2226, 2004.

[13] S. S. Hegedus and A. Luque, "Status, trends, challenges and the bright future of solar electricity from photovoltaics," *Handbook of photovoltaic science and engineering*, pp. 1–43, 2003.

[14] A. Goetzberger, J. Knobloch, and B. Voss, "Crystalline silicon solar cells," *editorial John Wiley & Sons Ltd*, vol. 1, 1998.

[15] M. A. Green, K. Emery, Y. Hishikawa, W. Warta, and E. D. Dunlop, "Solar cell efficiency tables (version 45)," *Progress in photovoltaics: research and applications*, vol. 23, no. 1, pp. 1–9, 2015.

[16] W. Shockley and H. J. Queisser, "Detailed balance limit of efficiency of p–n junction solar cells," *Journal of applied physics*, vol. 32, no. 3, pp. 510–519, 1961.

[17] X. Lin, R. Klenk, L. Wang, T. Köhler, J. Albert, S. Fiechter, A. Ennaoui, and M. C. Lux-Steiner, "11.3% efficiency cu (in, ga)(s, se) 2 thin film solar cells via drop-on-demand inkjet printing," *Energy & Environmental Science*, vol. 9, no. 6, pp. 2037–2043, 2016.

[18] M. C. Scharber, "On the efficiency limit of conjugated polymer: Fullerene–ĂŘbased bulk heterojunction solar cells," *Advanced Materials*, 2016.

[19] A. C. Mayer, S. R. Scully, B. E. Hardin, M. W. Rowell, and M. D. McGehee, "Polymer-based solar cells," *Materials today*, vol. 10, no. 11, pp. 28–33, 2007.

[20] N. Yeh and P. Yeh, "Organic solar cells: their developments and potentials," *Renewable and Sustainable Energy Reviews*, vol. 21, pp. 421–431, 2013.

[21] J. J. Choi, Y.-F. Lim, M. B. Santiago-Berrios, M. Oh, B.-R. Hyun, L. Sun, A. C. Bartnik, A. Goedhart, G. G. Malliaras, and H. D. Abruna, "Pbse nanocrystal excitonic solar cells," *Nano letters*, vol. 9, no. 11, pp. 3749–3755, 2009.

[22] S. E. Gledhill, B. Scott, and B. A. Gregg, "Organic and nano-structured composite photovoltaics: An overview," *Journal of Materials Research*, vol. 20, no. 12, pp. 3167–3179, 2005.

[23] B. A. Gregg and M. C. Hanna, "Comparing organic to inorganic photovoltaic cells: Theory, experiment, and simulation," *Journal of Applied Physics*, vol. 93, no. 6, pp. 3605–3614, 2003.

[24] B. A. Gregg, "Excitonic solar cells," *J. Phys. Chem. B*, vol. 107, no. 2, pp. 4688 –4698, 2003.

[25] S. M. Sze and K. K. Ng, *Physics of semiconductor devices.* John wiley & sons, 2006.

[26] S. R. Forrest and M. E. Thompson, "Introduction: organic electronics and optoelectronics," *Chemical Reviews*, vol. 107, no. 4, pp. 923–925, 2007.

[27] N. Kaur, M. Singh, D. Pathak, T. Wagner, and J. Nunzi, "Organic materials for photovoltaic applications: Review and mechanism," *Synthetic Metals*, vol. 190, pp. 20–26, 2014.

[28] T. Markvart and L. Castañer, "Principles of solar cell operation," *Practical Handbook of Photovoltaics: Fundamentals and Applications*, vol. 2, 2012.

[29] K.-M. Lee, C.-W. Hu, H.-W. Chen, and K.-C. Ho, "Incorporating carbon nanotube in a low-temperature fabrication process for dye-sensitized tio 2 solar cells," *Solar Energy Materials and Solar Cells*, vol. 92, no. 12, pp. 1628–1633, 2008.

[30] C. Yu, K. Choi, L. Yin, and J. C. Grunlan, "Light-weight flexible carbon nanotube based organic composites with large thermoelectric power factors," *Acs Nano*, vol. 5, no. 10, pp. 7885–7892, 2011.

[31] T. C. Bond and R. W. Bergstrom, "Light absorption by carbonaceous particles: An investigative review," *Aerosol science and technology*, vol. 40, no. 1, pp. 27–67, 2006.

[32] K. Kalyanasundaram, *Dye-sensitized solar cells.* EPFL press, 2010.

[33] W. C. Choy and W. A. A. Ho, *Organic solar cells*, vol. 2. Springer, 2013.

[34] V. Jain, B. K. Rajbongshi, A. T. Mallajosyula, G. Bhattacharjya, S. S. K. Iyer, and G. Ramanathan, "Photovoltaic effect in single-layer organic solar cell devices fabricated with two new imidazolin-5-one molecules," *Solar Energy Materials and Solar Cells*, vol. 92, no. 9, pp. 1043–1046, 2008.

[35] H. Gommans, D. Cheyns, T. Aernouts, C. Girotto, J. Poortmans, and P. Heremans, "Electro–ĂŘoptical study of subphthalocyanine in a bilayer organic solar cell," *Advanced functional materials*, vol. 17, no. 15, pp. 2653–2658, 2007.

[36] M. Liu, M. B. Johnston, and H. J. Snaith, "Efficient planar heterojunction perovskite solar cells by vapour deposition," *Nature*, vol. 501, no. 7467, pp. 395–398, 2013.

[37] S. H. Park, A. Roy, S. Beaupré, S. Cho, N. Coates, J. S. Moon, D. Moses, M. Leclerc, K. Lee, and A. J. Heeger, "Bulk heterojunction solar cells with internal quantum efficiency approaching 100%," *Nature photonics*, vol. 3, no. 5, pp. 297–302, 2009.

[38] J. Wu and Z. M. Wang, *Quantum dot solar cells.* Springer, 2014.

[39] F. E. Ala'a, J.-P. Sun, I. G. Hill, and G. C. Welch, "Recent advances of non-fullerene, small molecular acceptors for solution processed bulk heterojunction solar cells," *Journal of Materials Chemistry A*, vol. 2, no. 5, pp. 1201–1213, 2014.

[40] A. Mishra, M. K. Fischer, and P. Bäuerle, "Metal–free organic dyes for dye–sensitized solar cells: From structure: Property relationships to design rules," *Angewandte Chemie International Edition*, vol. 48, no. 14, pp. 2474–2499, 2009.

[41] H. Spanggaard and F. C. Krebs, "A brief history of the development of organic and polymeric photovoltaics," *Solar Energy Materials and Solar Cells*, vol. 83, no. 2, pp. 125–146, 2004.

[42] J. Bredas, R. Silbey, D. Boudreaux, and R. Chance, "Chain-length dependence of electronic and electrochemical properties of conjugated systems: polyacetylene, polyphenylene, polythiophene, and polypyrrole," *Journal of the American Chemical Society*, vol. 105, no. 22, pp. 6555–6559, 1983.

[43] S. Fratini, D. Mayou, and S. Ciuchi, "The transient localization scenario for charge transport in crystalline organic materials," *Advanced Functional Materials*, vol. 26, no. 14, pp. 2292–2315, 2016.

[44] S. Ciuchi, S. Fratini, and D. Mayou, "Transient localization in crystalline organic semiconductors," *Physical Review B*, vol. 83, no. 8, p. 081202, 2011.

[45] C. K. Chiang, C. Fincher Jr, Y. W. Park, A. J. Heeger, H. Shirakawa, E. J. Louis, S. C. Gau, and A. G. MacDiarmid, "Electrical conductivity in doped polyacetylene," *Physical Review Letters*, vol. 39, no. 17, p. 1098, 1977.

[46] C. W. Tang, "Two-layer organic photovoltaic cell," *Applied Physics Letters*, vol. 48, no. 2, pp. 183–185, 1986.

[47] N. Sariciftci, L. Smilowitz, A. J. Heeger, F. Wudl, *et al.*, "Photoinduced electron transfer from a conducting polymer to buckminsterfullerene," *Science*, vol. 258, no. 5087, pp. 1474–1476, 1992.

[48] G. Yu, J. Gao, J. C. Hummelen, F. Wudl, and A. J. Heeger, "Polymer photovoltiac cells: Enhanced efficiencies via a network of internal donor-acceptor heterojunctions," *Science*, vol. 270, no. 5243, pp. 1789–1791, 1995.

[49] A. McEvoy and M. Grätzel, "Sensitisation in photochemistry and photovoltaics," *Solar energy materials and solar cells*, vol. 32, no. 3, pp. 221–227, 1994.

[50] H. Gerischer and H. Tributsch, "Elektrochemische untersuchungen zur spektralen sensibilisierung von zno–ĂŘeinkristallen," *Berichte der Bunsengesellschaft für physikalische Chemie*, vol. 72, no. 3, pp. 437–445, 1968.

[51] G. Hodes, *Electrochemistry of nanomaterials.* John Wiley & Sons, 2008.

[52] H. Tsubomura, M. Matsumura, Y. Nomura, and T. Amamiya, "Dye sensitised zinc oxide: aqueous electrolyte: platinum photocell," *Nature*, vol. 261, no. 5559, pp. 402–403, 1976.

[53] M. P. Dare-Edwards, J. B. Goodenough, A. Hamnett, K. R. Seddon, and R. D. Wright, "Sensitisation of semiconducting electrodes with ruthenium-based dyes," *Faraday Discussions of the Chemical Society*, vol. 70, pp. 285–298, 1980.

[54] B. O'regan and M. Grfitzeli, "A low-cost, high-efficiency solar cell based on dye-sensitized," *nature*, vol. 353, no. 6346, pp. 737–740, 1991.

[55] M. K. Nazeeruddin, A. Kay, I. Rodicio, R. Humphry-Baker, E. Müller, P. Liska, N. Vlachopoulos, and M. Grätzel, "Conversion of light to electricity by cis-x2bis (2, 2'-bipyridyl-4, 4'-dicarboxylate) ruthenium (ii) charge-transfer sensitizers (x= cl-, br-, i-, cn-, and scn-) on nanocrystalline titanium dioxide electrodes," *Journal of the American Chemical Society*, vol. 115, no. 14, pp. 6382–6390, 1993.

[56] C. Lungenschmied, G. Dennler, H. Neugebauer, S. N. Sariciftci, M. Glatthaar, T. Meyer, and A. Meyer, "Flexible, long-lived, large-area, organic solar cells," *Solar Energy Materials and Solar Cells*, vol. 91, no. 5, pp. 379–384, 2007.

[57] D. Wöhrle and D. Meissner, "Organic solar cells," *Advanced Materials*, vol. 3, no. 3, pp. 129–138, 1991.

[58] A. Hagfeldt, "Brief overview of dye-sensitized solar cells," *Ambio*, vol. 41, no. 2, pp. 151–155, 2012.

[59] C. J. Brabec, "Organic photovoltaics: technology and market," *Solar energy materials and solar cells*, vol. 83, no. 2, pp. 273–292, 2004.

[60] N. S. Lewis, "Toward cost-effective solar energy use," *science*, vol. 315, no. 5813, pp. 798–801, 2007.

[61] M. Malekshahi Byranvand, A. Nemati Kharat, N. Taghavinia, and A. Dabirian, "Broadband and low-loss plasmonic light trapping in dye-sensitized solar cells using micrometer-scale rodlike and spherical core–shell plasmonic particles," *ACS applied materials & interfaces*, vol. 8, no. 25, pp. 16359–16367, 2016.

[62] C. M. Ip, A. Eleuteri, and A. Troisi, "Predicting with confidence the efficiency of new dyes in dye sensitized solar cells," *Physical Chemistry Chemical Physics*, vol. 16, no. 36, pp. 19106–19110, 2014.

[63] J. D. Roy-Mayhew and I. A. Aksay, "Graphene materials and their use in dye-sensitized solar cells," *Chemical reviews*, vol. 114, no. 12, pp. 6323–6348, 2014.

[64] G. Chidichimo and L. Filippelli, "Organic solar cells: problems and perspectives," *International Journal of Photoenergy*, vol. 2010, 2010.

[65] S. E. Shaheen, C. J. Brabec, N. S. Sariciftci, F. Padinger, T. Fromherz, and J. C. Hummelen, "2.5% efficient organic plastic solar cells," *Applied Physics Letters*, vol. 78, no. 6, pp. 841–843, 2001.

[66] S. Ito, T. N. Murakami, P. Comte, P. Liska, C. Grätzel, M. K. Nazeeruddin, and M. Grätzel, "Fabrication of thin film dye sensitized solar cells with solar to electric power conversion efficiency over 10%," *Thin solid films*, vol. 516, no. 14, pp. 4613–4619, 2008.

[67] N. S. Lewis and G. Crabtree, "Basic research needs for solar energy utilization: report of the basic energy sciences workshop on solar energy utilization, april 18-21, 2005," 2005.

[68] K. H. Lee, P. E. Schwenn, A. R. Smith, H. Cavaye, P. E. Shaw, M. James, K. B. Krueger, I. R. Gentle, P. Meredith, and P. L. Burn, "Morphology of all-solution-processed "bilayer" organic solar cells," *Advanced Materials*, vol. 23, no. 6, pp. 766–770, 2011.

[69] J. Nelson, "Polymer: fullerene bulk heterojunction solar cells," *Materials today*, vol. 14, no. 10, pp. 462–470, 2011.

[70] A. Yakimov and S. Forrest, "High photovoltage multiple-heterojunction organic solar cells incorporating interfacial metallic nanoclusters," *Applied Physics Letters*, vol. 80, no. 9, pp. 667–1669, 2002.

[71] G. Yu and A. J. Heeger, "Charge separation and photovoltaic conversion in polymer composites with internal donor/acceptor heterojunctions," *Journal of Applied Physics*, vol. 78, no. 7, pp. 4510–4515, 1995.

[72] M. T. Rispens, A. Meetsma, R. Rittberger, C. J. Brabec, N. S. Sariciftci, and J. C. Hummelen, "Influence of the solvent on the crystal structure of pcbm and the efficiency of mdmo-ppv: Pcbm 'plastic'solar cells," *Chemical Communications*, no. 17, pp. 2116–2118, 2003.

[73] Y. Ruiz-Morales, "Homo-lumo gap as an index of molecular size and structure for polycyclic aromatic hydrocarbons (pahs) and asphaltenes: A theoretical study. i," *The Journal of Physical Chemistry A*, vol. 106, no. 46, pp. 11283–11308, 2002.

[74] J.-L. Brédas, J. P. Calbert, D. da Silva Filho, and J. Cornil, "Organic semiconductors: A theoretical characterization of the basic parameters governing charge transport," *Proceedings of the National Academy of Sciences*, vol. 99, no. 9, pp. 5804–5809, 2002.

[75] J. Min, *Solution-Processed Small Molecule Bulk Heterojunction Organic Solar Cells: Molecular, Morphological, Interfacial and Device Engineering.* PhD thesis, der Friedrich-Alexander-Universität, 2015.

[76] C. Deibel and V. Dyakonov, "Polymer–fullerene bulk heterojunction solar cells," *Reports on Progress in Physics*, vol. 73, no. 9, p. 096401, 2010.

[77] S. Martin, D. Bradley, P. Lane, H. Mellor, and P. Burn, "Linear and nonlinear optical properties of the conjugated polymers ppv and meh-ppv," *Physical Review B*, vol. 59, no. 23, p. 15133, 1999.

[78] H. Hoppe, N. Arnold, N. Sariciftci, and D. Meissner, "Modeling the optical absorption within conjugated polymer/fullerene-based bulk-heterojunction organic solar cells," *Solar energy materials and solar cells*, vol. 80, no. 1, pp. 105–113, 2003.

[79] E. Lioudakis, A. Othonos, I. Alexandrou, and Y. Hayashi, "Optical properties of conjugated poly (3-hexylthiophene)/[6, 6]-phenylc61-butyric acid methyl ester composites," *Journal of Applied Physics*, vol. 102, no. 8, p. 083104, 2007.

[80] M. C. Scharber, D. Mühlbacher, M. Koppe, P. Denk, C. Waldauf, A. J. Heeger, and C. J. Brabec, "Design rules for donors in bulk-heterojunction solar cells—towards 10% energy-conversion efficiency," *Advanced materials*, vol. 18, no. 6, pp. 789–794, 2006.

[81] Y. Liang, D. Feng, Y. Wu, S.-T. Tsai, G. Li, C. Ray, and L. Yu, "Highly efficient solar cell polymers developed via fine-tuning of structural and electronic properties," *Journal of the American Chemical Society*, vol. 131, no. 22, pp. 7792–7799, 2009.

[82] D. Moses, A. Dogariu, and A. J. Heeger, "Ultrafast detection of charged photocarriers in conjugated polymers," *Physical Review B*, vol. 61, no. 14, p. 9373, 2000.

[83] R. Kersting, U. Lemmer, M. Deussen, H. Bakker, R. Mahrt, H. Kurz, V. I. Arkhipov, H. Bässler, and E. Göbel, "Ultrafast field-induced dissociation of excitons in conjugated polymers," *Physical review letters*, vol. 73, no. 10, p. 1440, 1994.

[84] J.-L. Brédas, J. Cornil, and A. J. Heeger, "The exciton binding energy in luminescent conjugated polymers," *Advanced Materials*, vol. 8, no. 5, pp. 447–452, 1996.

[85] D. Hertel and H. Bässler, "Photoconduction in amorphous organic solids," *ChemPhysChem*, vol. 9, no. 5, pp. 666–688, 2008.

[86] C. L. Braun, "Electric field assisted dissociation of charge transfer states as a mechanism of photocarrier production," *The Journal of chemical physics*, vol. 80, no. 9, pp. 4157–4161, 1984.

[87] P. Peumans and S. R. Forrest, "Separation of geminate charge-pairs at donor–acceptor interfaces in disordered solids," *Chemical Physics Letters*, vol. 398, no. 1, pp. 27–31, 2004.

[88] C. Deibel, T. Strobel, and V. Dyakonov, "Origin of the efficient polaron-pair dissociation in polymer-fullerene blends," *Physical review letters*, vol. 103, no. 3, p. 036402, 2009.

[89] D. Caruso and A. Troisi, "Long-range exciton dissociation in organic solar cells," *Proceedings of the National Academy of Sciences*, vol. 109, no. 34, pp. 13498–13502, 2012.

[90] P. Peumans, A. Yakimov, and S. R. Forrest, "Small molecular weight organic thin-film photodetectors and solar cells," *Journal of Applied Physics*, vol. 93, no. 7, pp. 3693–3723, 2003.

[91] S. Günes, H. Neugebauer, and N. S. Sariciftci, "Conjugated polymer-based organic solar cells," *Chemical reviews*, vol. 107, no. 4, pp. 1324–1338, 2007.

[92] C. Lee, G. Yu, D. Moses, and A. Heeger, "Picosecond transient photoconductivity in poly (p-phenylenevinylene)," *Physical Review B*, vol. 49, no. 4, p. 2396, 1994.

[93] M. Theander, A. Yartsev, D. Zigmantas, V. Sundström, W. Mammo, M. Andersson, and O. Inganäs, "Photoluminescence quenching at a p o l y t h i o p h e n e/c 60 heterojunction," *Physical Review B*, vol. 61, no. 19, p. 12957, 2000.

[94] D. Markov, C. Tanase, P. Blom, and J. Wildeman, "Simultaneous enhancement of charge transport and exciton diffusion in poly (p-phenylene vinylene) derivatives," *Physical Review B*, vol. 72, no. 4, p. 045217, 2005.

[95] C. Deibel, T. Strobel, and V. Dyakonov, "Role of the charge transfer state in organic donor–acceptor solar cells," *Advanced materials*, vol. 22, no. 37, pp. 4097–4111, 2010.

[96] T. M. Clarke and J. R. Durrant, "Charge photogeneration in organic solar cells," *Chemical reviews*, vol. 110, no. 11, pp. 6736–6767, 2010.

[97] T. M. Clarke and J. R. Durrant, "Charge photogeneration in organic solar cells," *Chemical reviews*, vol. 110, no. 11, pp. 6736–6767, 2010.

[98] L. Onsager, "Initial recombination of ions," *Physical Review*, vol. 54, no. 8, p. 554, 1938.

[99] S. Cook, R. Katoh, and A. Furube, "Ultrafast studies of charge generation in pcbm: P3ht blend films following excitation of the fullerene pcbm," *The Journal of Physical Chemistry C*, vol. 113, no. 6, pp. 2547–2552, 2009.

[100] V. Coropceanu, J. Cornil, D. A. da Silva Filho, Y. Olivier, R. Silbey, and J.-L. Brédas, "Charge transport in organic semiconductors," *Chemical reviews*, vol. 107, no. 4, pp. 926–952, 2007.

[101] Z. Shuai, L. Wang, and C. Song, *Theory of charge transport in carbon electronic materials*. Springer Science & Business Media, 2012.

[102] M. M. Wienk, J. M. Kroon, W. J. Verhees, J. Knol, J. C. Hummelen, P. A. van Hal, and R. A. Janssen, "Efficient methano [70] fullerene/mdmo-ppv bulk heterojunction photovoltaic cells," *Angewandte Chemie*, vol. 115, no. 29, pp. 3493–3497, 2003.

[103] Y. M. Yang, W. Chen, L. Dou, W.-H. Chang, H.-S. Duan, B. Bob, G. Li, and Y. Yang, "High-performance multiple-donor bulk heterojunction solar cells," *Nature Photonics*, vol. 9, no. 3, pp. 190–198, 2015.

[104] L. M. Peter, "Dye-sensitized nanocrystalline solar cells," *Physical Chemistry Chemical Physics*, vol. 9, no. 21, pp. 2630–2642, 2007.

[105] J. Bisquert, D. Cahen, G. Hodes, S. Rühle, and A. Zaban, "Physical chemical principles of photovoltaic conversion with nanoparticulate, mesoporous dye-sensitized solar cells," *The Journal of Physical Chemistry B*, vol. 108, no. 24, pp. 8106–8118, 2004.

[106] A. Hagfeldt and M. Grätzel, "Molecular photovoltaics," *Accounts of Chemical Research*, vol. 33, no. 5, pp. 269–277, 2000.

[107] M. Grätzel, "Photoelectrochemical cells," *Nature*, vol. 414, no. 6861, pp. 338–344, 2001.

[108] A. Yella, H.-W. Lee, H. N. Tsao, C. Yi, A. K. Chandiran, M. K. Nazeeruddin, E. W.-G. Diau, C.-Y. Yeh, S. M. Zakeeruddin, and M. Grätzel, "Porphyrin-sensitized solar cells with cobalt (ii/iii)–based redox electrolyte exceed 12 percent efficiency," *science*, vol. 334, no. 6056, pp. 629–634, 2011.

[109] Y. Chiba, A. Islam, Y. Watanabe, R. Komiya, N. Koide, and L. Han, "Dye-sensitized solar cells with conversion efficiency of 11.1%," *Japanese Journal of Applied Physics*, vol. 45, no. 7L, p. L638, 2006.

[110] L. Schmidt–Mende, U. Bach, R. Humphry–Baker, T. Horiuchi, H. Miura, S. Ito, S. Uchida, and M. Grätzel, "Organic dye for highly efficient solid–state dye–sensitized solar cells," *Advanced Materials*, vol. 17, no. 7, pp. 813–815, 2005.

[111] Q. Wang, S. Ito, M. Grätzel, F. Fabregat-Santiago, I. Mora-Seró, J. Bisquert, T. Bessho, and H. Imai, "Characteristics of high efficiency dye-sensitized solar cells," *The Journal of Physical Chemistry B*, vol. 110, no. 50, pp. 25210–25221, 2006.

[112] Z. Yu, S. You, C. Wang, C. Bu, S. Bai, Z. Zhou, Q. Tai, W. Liu, S. Guo, and X.-z. Zhao, "Efficient dye-sensitized solar cells employing highly environmentally-friendly ubiquinone 10 based i 2-free electrolyte inspired by photosynthesis," *Journal of Materials Chemistry A*, vol. 2, no. 24, pp. 9007–9010, 2014.

[113] Q. Miao, M. Wu, W. Guo, and T. Ma, "Studies of high-efficient and low-cost dye-sensitized solar cells," *Frontiers of Optoelectronics in China*, vol. 4, no. 1, pp. 103–107, 2011.

[114] H. Shibl, H. Hafez, R. Rifai, and M. A. Mottaleb, "Environmental friendly, low cost quasi solid state dye sensitized solar cell: polymer electrolyte introduction," *Journal of Inorganic and Organometallic Polymers and Materials*, vol. 23, no. 4, pp. 944–949, 2013.

[115] W. Ghann, H. Kang, T. Sheikh, S. Yadav, T. Chavez-Gil, F. Nesbitt, and J. Uddin, "Fabrication, optimization and characterization of natural dye sensitized solar cell," *Scientific Reports*, vol. 7, 2017.

[116] B. E. Hardin, H. J. Snaith, and M. D. McGehee, "The renaissance of dye-sensitized solar cells," *Nature Photonics*, vol. 6, no. 3, pp. 162–169, 2012.

[117] W. J. Lee, E. Ramasamy, D. Y. Lee, and J. S. Song, "Efficient dye-sensitized solar cells with catalytic multiwall carbon nanotube counter electrodes," *ACS applied materials & interfaces*, vol. 1, no. 6, pp. 1145–1149, 2009.

[118] T.-L. Hsieh, H.-W. Chen, C.-W. Kung, C.-C. Wang, R. Vittal, and K.-C. Ho, "A highly efficient dye-sensitized solar cell with a platinum nanoflowers counter electrode," *Journal of Materials Chemistry*, vol. 22, no. 12, pp. 5550–5559, 2012.

[119] T. Bessho, S. M. Zakeeruddin, C.-Y. Yeh, E. W.-G. Diau, and M. Grätzel, "Highly efficient mesoscopic dye-sensitized solar cells based on donor–acceptor-substituted porphyrins," *Angewandte Chemie*, vol. 122, no. 37, pp. 6796–6799, 2010.

[120] J. A. Chang, J. H. Rhee, S. H. Im, Y. H. Lee, H.-j. Kim, S. I. Seok, M. K. Nazeeruddin, and M. Gratzel, "High-performance nanostructured inorganic–ĹŠorganic heterojunction solar cells," *Nano letters*, vol. 10, no. 7, pp. 2609–2612, 2010.

[121] G. Calogero, A. Sinopoli, I. Citro, G. Di Marco, V. Petrov, A. M. Diniz, A. J. Parola, and F. Pina, "Synthetic analogues of anthocyanins as sensitizers for dye-sensitized solar cells," *Photochemical & Photobiological Sciences*, vol. 12, no. 5, pp. 883–894, 2013.

[122] L. Peter, "Transport, trapping and interfacial transfer of electrons in dye-sensitized nanocrystalline solar cells," *Journal of Electroanalytical Chemistry*, vol. 599, no. 2, pp. 233–240, 2007.

[123] D. Kuang, S. Ito, B. Wenger, C. Klein, J.-E. Moser, R. Humphry-Baker, S. M. Zakeeruddin, and M. Grätzel, "High molar extinction coefficient heteroleptic ruthenium complexes for thin film dye-sensitized solar cells," *Journal of the American Chemical Society*, vol. 128, no. 12, pp. 4146–4154, 2006.

[124] F. Fabregat-Santiago, J. Bisquert, G. Garcia-Belmonte, G. Boschloo, and A. Hagfeldt, "Influence of electrolyte in transport and recombination in dye-sensitized solar cells studied by impedance spectroscopy," *Solar Energy Materials and Solar Cells*, vol. 87, no. 1, pp. 117–131, 2005.

[125] E. Palomares, J. N. Clifford, S. A. Haque, T. Lutz, and J. R. Durrant, "Control of charge recombination dynamics in dye sensitized solar cells by the use of conformally deposited metal oxide blocking layers," *Journal of the American Chemical Society*, vol. 125, no. 2, pp. 475–482, 2003.

[126] N. Robertson, "Optimizing dyes for dye-sensitized solar cells," *Angewandte Chemie International Edition*, vol. 45, no. 15, pp. 2338–2345, 2006.

[127] K. Zhu, T. B. Vinzant, N. R. Neale, and A. J. Frank, "Removing structural disorder from oriented tio2 nanotube arrays: reducing the dimensionality of transport and recombination in dye-sensitized solar cells," *Nano Letters*, vol. 7, no. 12, pp. 3739–3746, 2007.

[128] X. Zhang, F. Liu, Q.-L. Huang, G. Zhou, and Z.-S. Wang, "Dye-sensitized w-doped tio2 solar cells with a tunable conduction band and suppressed charge recombination," *The Journal of Physical Chemistry C*, vol. 115, no. 25, pp. 12665–12671, 2011.

[129] N. Kopidakis, N. R. Neale, and A. J. Frank, "Effect of an adsorbent on recombination and band-edge movement in dye-sensitized tio2 solar cells: evidence for surface passivation," *The Journal of Physical Chemistry B*, vol. 110, no. 25, pp. 12485–12489, 2006.

[130] S. Ajisaka, B. Žunkovič, and Y. Dubi, "The molecular photo-cell: Quantum transport and energy conversion at strong non-equilibrium," *Scientific reports*, vol. 5, p. 8312, 2015.

[131] M. Einax, M. Dierl, and A. Nitzan, "Heterojunction organic photovoltaic cells as molecular heat engines: A simple model for the performance analysis," *The Journal of Physical Chemistry C*, vol. 115, no. 43, pp. 21396–21401, 2011.

[132] M. Einax, M. Dierl, P. R. Schiff, and A. Nitzan, "Multiple state representation scheme for organic bulk heterojunction solar cells: A novel analysis perspective," *EPL (Europhysics Letters)*, vol. 104, no. 4, p. 40002, 2013.

[133] Y. Yamada, Y. Yamaji, and M. Imada, "Exciton lifetime paradoxically enhanced by dissipation and decoherence: Toward efficient energy conversion of a solar cell," *Physical review letters*, vol. 115, no. 19, p. 197701, 2015.

[134] A. V. Semichaevsky and H. T. Johnson, "Carrier transport in a quantum dot solar cell using semiclassical and quantum mechanical models," *Solar Energy Materials and Solar Cells*, vol. 108, pp. 189–199, 2013.

[135] U. Aeberhard, "Simulation of ultrathin solar cells beyond the limits of the semiclassical bulk picture," *IEEE Journal of Photovoltaics*, vol. 6, no. 3, pp. 654–660, 2016.

[136] A. J. White, U. Peskin, and M. Galperin, "Coherence in charge and energy transfer in molecular junctions," *Physical Review B*, vol. 88, no. 20, p. 205424, 2013.

[137] Y. Gao and M. Galperin, "Optical spectroscopy of molecular junctions: Nonequilibrium green's functions perspective," *The Journal of chemical physics*, vol. 144, no. 17, p. 174113, 2016.

[138] A. J. White, M. A. Ochoa, and M. Galperin, "Nonequilibrium atomic limit for transport and optical response of molecular junctions," *The Journal of Physical Chemistry C*, vol. 118, no. 21, pp. 11159–11173, 2014.

[139] S. Lacic and O. Inganäs, "Modeling electrical transport in blend heterojunction organic solar cells," *Journal of applied physics*, vol. 97, no. 12, p. 124901, 2005.

[140] Q. Wang, J.-E. Moser, and M. Grätzel, "Electrochemical impedance spectroscopic analysis of dye-sensitized solar cells," *The Journal of Physical Chemistry B*, vol. 109, no. 31, pp. 14945–14953, 2005.

[141] D. W. Sievers, V. Shrotriya, and Y. Yang, "Modeling optical effects and thickness dependent current in polymer bulk-heterojunction solar cells," *Journal of applied physics*, vol. 100, no. 11, p. 114509, 2006.

[142] P. K. Watkins, A. B. Walker, and G. L. Verschoor, "Dynamical monte carlo modelling of organic solar cells: the dependence of internal quantum efficiency on morphology," *Nano letters*, vol. 5, no. 9, pp. 1814–1818, 2005.

[143] G. Li, A. Nitzan, and M. A. Ratner, "Yield of exciton dissociation in a donor–acceptor photovoltaic junction," *Physical Chemistry Chemical Physics*, vol. 14, no. 41, pp. 14270–14276, 2012.

[144] O. V. Kozlov, F. de Haan, R. A. Kerner, B. P. Rand, D. Cheyns, and M. S. Pshenichnikov, "Real-time tracking of singlet exciton diffusion in organic semiconductors," *Physical review letters*, vol. 116, no. 5, p. 057402, 2016.

[145] X. Blase, C. Attaccalite, and V. Olevano, "First-principles gw calculations for fullerenes, porphyrins, phtalocyanine, and other molecules of interest for organic photovoltaic applications," *Physical Review B*, vol. 83, no. 11, p. 115103, 2011.

[146] C. Faber, P. Boulanger, C. Attaccalite, I. Duchemin, and X. Blase, "Excited states properties of organic molecules: from density functional theory to the gw and bethe–salpeter green's function formalisms," *Philosophical Transactions of the Royal Society of London A: Mathematical, Physical and Engineering Sciences*, vol. 372, no. 2011, p. 20130271, 2014.

[147] J. R. Taylor, *Scattering theory: the quantum theory of nonrelativistic collisions*. Courier Corporation, 2012.

[148] J. J. Sakurai, S.-F. Tuan, and E. D. Commins, *Modern quantum mechanics, revised edition*, vol. 3. AAPT, 1995.

[149] R. H. Landau, *Quantum mechanics II: a second course in quantum theory*. John Wiley & Sons, 2008.

[150] P. Weinberger, *Electron scattering theory for ordered and disordered matter*. Clarendon Press Oxford, 1990.

[151] S. Datta, *Electronic transport in mesoscopic systems*. Cambridge university press, 1997.

[152] E. N. Economou, *Green's functions in quantum physics*, vol. 3. Springer, 1983.

[153] P. Vogl, H. P. Hjalmarson, and J. D. Dow, "A semi-empirical tight-binding theory of the electronic structure of semiconductors–Ăă," *Journal of Physics and Chemistry of Solids*, vol. 44, no. 5, pp. 365–378, 1983.

[154] H. A. Van Der Vorst, "Krylov subspace iteration," *Computing in science & engineering*, vol. 2, no. 1, pp. 32–37, 2000.

[155] M. K. Schneider and A. S. Willsky, "Krylov subspace estimation," *SIAM Journal on Scientific Computing*, vol. 22, no. 5, pp. 1840–1864, 2001.

[156] D. Weaire and E. O'Reilly, "A comparison of the recursion method and the equation-of-motion method for the calculation of densities of states," *Journal of Physics C: Solid State Physics*, vol. 18, no. 7, p. 1401, 1985.

[157] V. Viswanath and G. Müller, *The Recursion Method: Application to Many Body Dynamics*, vol. 23. Springer Science & Business Media, 1994.

[158] T. Hoshi and T. Fujiwara, "Large-scale electronic structure theory for simulating nanostructure processes," *Journal of Physics: Condensed Matter*, vol. 18, no. 48, p. 10787, 2006.

[159] C. Lanczos, *An iteration method for the solution of the eigenvalue problem of linear differential and integral operators*. United States Governm. Press Office Los Angeles, CA, 1950.

[160] D. M. Woodruff, S. M. Anlage, and D. Smith, "Density-of-states calculations within the recursion method," *Physical Review B*, vol. 36, no. 3, p. 1725, 1987.

[161] F. Triozon, J. Vidal, R. Mosseri, and D. Mayou, "Quantum dynamics in two- and three-dimensional quasiperiodic tilings," *Physical Review B*, vol. 65, no. 22, p. 220202, 2002.

[162] D. Mayou, "Calculation of the conductivity in the short-mean-free-path regime," *EPL (Europhysics Letters)*, vol. 6, no. 6, p. 549, 1988.

[163] S. Roche and D. Mayou, "Formalism for the computation of the rkky interaction in aperiodic systems," *Physical Review B*, vol. 60, no. 1, p. 322, 1999.

[164] D. Mayou and S. Khanna, "A real-space approach to electronic transport," *Journal de Physique I*, vol. 5, no. 9, pp. 1199–1211, 1995.

[165] P. Darancet, V. Olevano, and D. Mayou, "Quantum transport through resistive nanocontacts: Effective one-dimensional theory and conductance formulas for nonballistic leads," *Physical Review B*, vol. 81, no. 15, p. 155422, 2010.

[166] M. Galperin and A. Nitzan, "Current-induced light emission and light-induced current in molecular-tunneling junctions," *Physical review letters*, vol. 95, no. 20, p. 206802, 2005.

[167] T. Nemati Aram, A. Asgari, and D. Mayou, "Charge separation in organic solar cells: Effects of coulomb interaction, recombination and hole propagation," *EPL (Europhysics Letters)*, vol. 115, no. 1, p. 18003, 2016.

[168] T. Nemati Aram, P. Anghel-Vasilescu, A. Asgari, M. Ernzerhof, and D. Mayou, "Modeling of molecular photocells: Application to two-level photovoltaic system with electron-hole interaction," *The Journal of Chemical Physics*, vol. 145, no. 12, p. 124116, 2016.

[169] T. Nemati Aram, M. Ernzerhof, A. Asgari, and D. Mayou, "The impact of long-range electron-hole interaction on the charge separation yield of molecular photocells," *The Journal of Chemical Physics*, vol. 146, no. 3, p. 034103, 2017.

[170] X.-Y. Zhu, Q. Yang, and M. Muntwiler, "Charge-transfer excitons at organic semiconductor surfaces and interfaces," *Accounts of chemical research*, vol. 42, no. 11, pp. 1779–1787, 2009.

[171] G. Li, B. Movaghar, A. Nitzan, and M. A. Ratner, "Polaron formation: Ehrenfest dynamics vs. exact results," *The Journal of chemical physics*, vol. 138, no. 4, p. 044112, 2013.

[172] S. Bera, N. Gheeraert, S. Fratini, S. Ciuchi, and S. Florens, "Impact of quantized vibrations on the efficiency of interfacial charge separation in photovoltaic devices," *Physical Review B*, vol. 91, no. 4, p. 041107, 2015.

[173] J. Weickert, R. B. Dunbar, H. C. Hesse, W. Wiedemann, and L. Schmidt–ĂŘMende, "Nanostructured organic and hybrid solar cells," *Advanced Materials*, vol. 23, no. 16, pp. 1810–1828, 2011.

[174] M. Mandoc, F. Kooistra, J. Hummelen, B. De Boer, and P. Blom, "Effect of traps on the performance of bulk heterojunction organic solar cells," *Applied Physics Letters*, vol. 91, no. 26, p. 263505, 2007.

[175] M. Mandoc, L. Koster, and P. Blom, "Optimum charge carrier mobility in organic solar cells," *Applied physics letters*, vol. 90, no. 13, p. 133504, 2007.

[176] H. A. Bethe and E. E. Salpeter, *Quantum mechanics of one-and two-electron atoms*. Springer Science & Business Media, 2012.

[177] C. Groves, "Developing understanding of organic photovoltaic devices: kinetic monte carlo models of geminate and non-geminate recombination, charge transport and charge extraction," *Energy & Environmental Science*, vol. 6, no. 11, pp. 3202–3217, 2013.

[178] G. Wellein and H. Fehske, "Polaron band formation in the holstein model," *Physical Review B*, vol. 56, no. 8, p. 4513, 1997.

[179] D. Feinberg, S. Ciuchi, and F. de Pasquale, "Squeezing phenomena in interacting electron-phonon systems," *International Journal of Modern Physics B*, vol. 4, no. 07n08, pp. 1317–1367, 1990.

[180] M. Capone, S. Ciuchi, and C. Grimaldi, "The small-polaron crossover: comparison between exact results and vertex correction approximation," *EPL (Europhysics Letters)*, vol. 42, no. 5, p. 523, 1998.

[181] T. A. Skotheim and J. Reynolds, *Handbook of Conducting Polymers, 2 Volume Set*. CRC press, 2007.

[182] W. R. Salaneck, R. H. Friend, and J. L. Brédas, "Electronic structure of conjugated polymers: Consequences of electron–lattice coupling," *Physics Reports*, vol. 319, no. 6, pp. 231–251, 1999.

[183] R. P. Fornari, P. W. Blom, and A. Troisi, "How many parameters actually affect the mobility of conjugated polymers?," *Physical Review Letters*, vol. 118, no. 8, p. 086601, 2017.

[184] I. Duchemin and X. Blase, "Resonant hot charge-transfer excitations in fullerene-porphyrin complexes: Many-body bethe-salpeter study," *Physical Review B*, vol. 87, no. 24, p. 245412, 2013.

[185] H. Tamura and I. Burghardt, "Potential barrier and excess energy for electron–hole separation from the charge-transfer exciton at donor–acceptor heterojunctions of organic solar cells," *The Journal of Physical Chemistry C*, vol. 117, no. 29, pp. 15020–15025, 2013.

[186] S. Fratini and S. Ciuchi, "Dynamical mean-field theory of transport of small polarons," *Physical review letters*, vol. 91, no. 25, p. 256403, 2003.

[187] S. Ciuchi, F. De Pasquale, S. Fratini, and D. Feinberg, "Dynamical mean-field theory of the small polaron," *Physical Review B*, vol. 56, no. 8, p. 4494, 1997.

[188] D. K. Ferry, S. M. Goodnick, and J. Bird, *Transport in nanostructures*. Cambridge University Press, 2009.

[189] R. M. Martin, *Electronic structure: basic theory and practical methods*. Cambridge university press, 2004.

[190] L. Goodwin, A. Skinner, and D. Pettifor, "Generating transferable tight-binding parameters: application to silicon," *EPL (Europhysics Letters)*, vol. 9, no. 7, p. 701, 1989.

[191] S. Goedecker and L. Colombo, "Efficient linear scaling algorithm for tight-binding molecular dynamics," *Physical review letters*, vol. 73, no. 1, p. 122, 1994.

[192] W. Zhang, W.-C. Lu, H.-X. Zhang, K. Ho, and C. Wang, "Tight-binding calculation studies of vacancy and adatom defects in graphene," *Journal of Physics: Condensed Matter*, vol. 28, no. 11, p. 115001, 2016.

Persian Resume

چکیده فارسی رساله

مدلبندی غیرتعادلی سلول‌های خورشیدی: آثار کوانتومی در مقیاس نانو

۱ هدف رساله

حیات انسان وابسته به انرژی است. جمعیت جهان به سرعت در حال رشد است و بنابراین تقاضا برای منابع مختلف انرژی به طور چشمگیری افزایش یافته است. مردم نیازمند منابع انرژی در دسترس، قابل اعتماد، ارزان و تمیز هستند. از زمان انقلاب صنعتی، عمده انرژی جهان از سوخت‌های فسیلی از جمله زغال سنگ، نفت و گاز طبیعی تأمین شده است. با این حال، این منابع انرژی محدود هستند و علی رغم اثرات چشمگیر آنها بر پیشرفت تکنولوژی، به همراه معایبی از جمله خطرات زیست محیطی، گران‌قیمت بودن، باران اسیدی، اثرات مخرب بر سلامت انسان و عدم تجدیدپذیری هستند. بنابراین، ادامه‌ی تکیه بر آنها ممکن است پیامدهای زیست محیطی و اجتماعی ناگواری را به همراه داشته باشد.

این وضعیت دانشمندان از سراسر جهان را برای توسعه منابع انرژی جایگزین و ایجاد یک مرحله گذار در تولید انرژی واداشته است. خوشبختانه، توجه بسیاری به انرژی‌های تجدید پذیر، پایدار، ارزان و پاک شده است و انتظار می‌رود که آن‌ها بتوانند تقاضای تحولات مدرن را برآورده کند.

انرژی‌های تجدیدپذیر از جمله انرژی باد، انرژی خورشیدی، هیدرو الکتریک و... مزایای قابل توجهی برای شرایط آب و هوایی و همچنین اقتصاد فراهم می‌کنند. با این وجود، آنها در بخش محدودی از تولید انرژی سهیم هستند. در میان آنها انرژی خورشیدی منبع بسیار جذابی است زیرا در دسترس، فراوان و بدون کربن دی اکسید است. چنانچه گزارش‌ها نشان می‌دهند انرژی که مناطق کویری تنها در عرض ۶ ساعت از خورشید دریافت می‌کنند بیش از مصرف سالیانه انرژی در جهان است. ارزیابی‌ها حاکی از این واقعیت هستند که جهان استفاده مؤثر از انرژی خورشیدی را آغاز کرده است.

یکی از چالش‌های مهم جهانی در حوزه انرژی، توسعه تکنولوژی ارزان قیمت، پایدار و کارآمد برای بکارگیری مؤثر نور خورشید و تبدیل آن به الکتریسیته می‌باشد. در این راستا، تکنولوژی فوتوولتاییک بسیار مورد توجه محققان و صنعتگران قرار گرفته است به طوری‌که نسل‌های مختلفی از سلول‌های خورشیدی

توسعه یافته‌اند. در یک بیان کلی، انواع مختلف سلول‌های خورشیدی را می توان به دو گروه کلی دسته بندی کرد: سلول‌های خورشیدی سنتی (مبتنی بر مواد غیرآلی) و سلول‌های خورشیدی اکسایتونی.

مکانیسم عملکرد مختلف این دو دسته سلول منجر به تفاوت‌های اساسی در رفتار فوتوولتاییکی آنها می گردد. بر اساس مواد استفاده شده در ساختار آن‌ها، سلول‌های خورشیدی اکسایتونی را می توان به دو گروه سلول‌های خورشیدی رنگینه حساس و سلول‌های خورشیدی آلی توسعه یافته در شکل تک لایه و دو لایه شامل ساختار دووجهی و هتروجانکشن طبقه‌بندی نمود. در حالیکه در طی چندین سال اخیر، درک عملکرد سلول‌های خورشیدی اکسایتونی مورد توجه جامعه علمی بوده است هنوز نیاز مبرمی برای گسترش تئوری‌هایی که درک نقش اندرکنش و بازترکیب الکترون_حفره را تسهیل کنند، وجود دارند.

لزوما، باید تصویری کمّی از فرایندهای اساسی تبدیل انرژی خورشیدی، از جمله جذب فوتون، انتشار اکسایتون، تفکیک و جدایی اکسایتون و همچنین درک پیامدهای آن‌ها بر عملکرد دستگاه وجود داشته باشد. تئوری‌های نیمه‌کلاسیکی ابزار ناکارامدی برای بررسی پدیده‌های کوانتومی در سلول‌های نانوساختاری هستند و از سوی دیگر به سبب جاذبه کولنی بین حاملین بار، استفاده از تئوری تابع گرین غیرتعادلی پیچیدگی‌های زیادی را به همراه دارد. بنابراین به منظور فراهم آوردن چهارچوب جامعی از درک فرآیندهایی که در عملکرد سلول‌های خورشیدی اکسایتونی به وقوع می‌پیوندند، در این پایان‌نامه ما یک تئوری جدیدی را ارائه می‌دهیم که بر پایه نظریه پراکندگی کوانتومی و معادله لیپمن_شوینگر است. ما روی جنبه‌هایی تمرکز می‌کنیم که در گذشته کمتر مورد توجه قرار گرفته‌اند از جمله: آثار برهمکنش کولنی کوتاه_برد و بلند_برد الکترون_حفره، بازترکیب الکترون_حفره، وجود کانال‌های اضافی خروج بار، اندرکنش الکترون_فونون و تشکیل باندهای پلارونی.

از ویژگی‌های بسیار جالب این متدولوژی جدید آنست که تولید و تفکیک اکسایتون‌ها در فضای انرژی مورد بررسی قرار می‌گیرد و بنابراین دسترسی به اطلاعات طیفی وجود دارد که می‌تواند به عنوان چهارچوبی برای درک عملکرد سلول مورد استفاده قرار گیرد. ایده اصلی این تئوری در قالب مثال‌هایی از سلول‌های خورشیدی دو ترازی نشان داده شده است. در اینجا، سلول‌های خورشیدی دو ترازی در رژیم‌های تزریق بار دائم و گذرا مورد بررسی قرار گرفته‌اند. فوتوسل‌های مولکولی که در آنجا فرآیند تبدیل انرژی در یک مولکول دهنده_پذیرنده متصل به الکترودها روی می‌دهد به عنوان نماینده سلول‌های خورشیدی اکسایتونی در ناحیه تزریق بار دائم در نظر گرفته شده است. مثال سلول‌های خورشیدی فعال در ناحیه تزریق بار گذرا، سلول‌های خورشیدی آلی با ساختار توده‌ای هتروجانکشن است که در آنجا مواد دهنده و پذیرنده ادغام شده‌اند و به عنوان رایج‌ترین نوع سلول‌های خورشیدی آلی شناخته شده است. در این سلول‌ها، اکسایتون

تولید شده در طی جذب فوتون در قسمت ماده پدیرنده، ابتدا باید به فصل مشترک دهنده_پذیرنده برسد. از این لحظه وارد رژیم گذرا می‌شود که در آنجا بارها جدا می‌شوند و به لیدهای متناظر تزریق می‌گردند.

ما نشان می‌دهیم که فرآیند جدایش حاملین بار پروسه‌ای پیچیده است که توسط پارامترهای مختلفی از جمله شدت برهمکنش الکترون_حفره، کوپلینگ الکترون_فونون و همچنین آهنگ بازترکیب متأثر می‌گردد. علاوه بر این، تحت تأثیر پارامترهای سلول، برهمکنش الکترون_حفره می‌تواند به صورت نرمال منجر به کاهش و به صورت غیرنرمال منجر به افزایش بازده سلول گردد. این مدل پیشنهادی درک عملکرد سلول‌های خورشیدی را تسهیل می‌سازد و می‌تواند برای بهینه کردن عملکرد سلول‌ها مورد استفاده قرار گیرد.

۲ روش‌های تئوری

بخش عمده دانش ما در مورد فیزیک میکروسکوپی از آزمایش‌های پراکندگی نشأت می‌گیرد که در آنجا برهمکنش بین ذرات اتمی یا زیر_اتمی می‌تواند مورد مطالعه قرار گیرد. در تئوری پراکندگی، یک ذره فرودی در حالت Ψ_0 با پتانسیل V پراکنده می‌شود و منجر به حالت پراکنده شده Ψ_S می‌گردد. فرض برآنست که حالت فرودی Ψ_0 ویژه حالت هامیلتونی H_0 با ویژه مقدار E است. به زبان ریاضی:

$$(E - H_0)\,|\Psi_0\rangle = 0 \tag{۱}$$

H_0 هامیلتونی ذره آزاد است،

$$H_0 = \frac{P^2}{2M} \tag{۲}$$

بنابراین هدف تئوری پراکندگی حل مسأله ویژه مقداری زیر می‌باشد:

$$(E - H_0 - V)\,|\Psi\rangle = 0 \tag{۳}$$

که در آنجا Ψ ویژه حالت هامیلتونی کل $H = H_0 + V$ با انرژی E می‌باشد . نکته جالب توجه آنست که به ازای هر انرژی E، Ψ_0 و متعاقباً Ψ مختلف وجود دارد.

۱.۲ معادله لیپمن ـ شوینگر

ارتباط بین حالت‌های فرودی و پراکنده شده با معادله لیپمن ـ شوینگر مشخص می‌شود. ما با تعریف حالت پراکنده شده Ψ_S توسط رابطه زیر شروع می‌کنیم:

$$|\Psi_S\rangle = |\Psi\rangle - |\Psi_0\rangle \tag{۴}$$

معادله شرودینگر (۳) را می‌توان به صورت زیر بازنویسی کرد:

$$(E - H_0)\,|\Psi\rangle = V\,|\Psi\rangle \tag{۵}$$

با جایگزینی $\Psi = \Psi_S + \Psi_0$ در معادله (۵) و استفاده از (۱) داریم:

$$(E - H_0)\,|\Psi_S\rangle = V\,|\Psi\rangle \tag{۶}$$

اعمال $(E - H_0)^{-1}$ به هر دو طرف رابطه منجر به عبارت زیر می‌شود:

$$\Psi_S = (E - H_0)^{-1} V\,|\Psi\rangle \tag{۷}$$

که آن با اضافه کردن Ψ_0 به هر دو طرف به معادله زیر تبدیل می‌شود:

$$|\Psi\rangle = |\Psi_0\rangle + (E - H_0)^{-1} V\,|\Psi\rangle \tag{۸}$$

این به عنوان معادله لیپمن ـ شوینگر شناخته شده است.

۲.۲ روش تابع گرین

بسیاری از کمیت‌های جالب در تئوری پراکندگی می‌توانند بر پایه تابع گرین بیان شوند. در اینجا، ما تابع گرین را به مسأله پراکندگی اعمال می‌کنیم.

$$G_0(z) = (z - H_0)^{-1} \tag{۹}$$

که آن تابع گرین برای ذره آزاد با هامیلتونی H_0 می‌باشد و

$$G(z) = (z - H)^{-1} \tag{۱۰}$$

تابع گرین اختلالی است. z یک عدد مختلط است.
با این تعاریف، معادله شرودینگر را می‌توان به صورت زیر نوشت:

$$|\Psi\rangle = |\Psi_0\rangle + G_0 V |\Psi\rangle \tag{۱۱}$$

که در آنجا $z = E + i\epsilon$ و ϵ یک عدد مثبت بی‌نهایت کوچک است.

۳.۲ سری برن

معادله لیپمن ـ شوینگر یک معادله دقیق برای مسأله پراکندگی است و باید حل شود. در یک بیان کلی، هیچ راه ساده‌ای برای یافتن جواب‌های دقیق معادله لیپمن ـ شوینگر وجود ندارد. یک راه ممکن، حل این معادله با تئوری اختلال است، یعنی بسط سری توانی در پتانسیل V به نحوی که در غیاب پتانسیل $\Psi = \Psi_0$.

$$|\Psi\rangle = |\Psi_0\rangle + G_0 V |\Psi_0\rangle + G_0 V G_0 V |\Psi_0\rangle + G_0 V G_0 V G_0 V |\Psi_0\rangle + ... \tag{۱۲}$$

بنابراین پایین‌ترین مرتبه تصحیحات را می‌توان به صورت زیر نوشت:

$$|\Psi\rangle = |\Psi_0\rangle + G_0 V |\Psi_0\rangle + O(V^2) \tag{۱۳}$$

که در آنجا از تصحیحات $O(V^2)$ صرفنظر شده است.
این تقریب مرتبه اول برن نامیده می‌شود. این تقریب تنها برای شرایطی که پراکندگی ضعیف است، صادق می‌باشد.

۴.۲ سیستم‌های فوتوولتائیک دو ترازی

ایده اصلی این متدولوژی جدید توسط مثال‌هایی از سیستم‌های فوتوولتائیک دوترازی در حضور برهمکنش و بازترکیب غیر تابشی الکترون‌ـ‌حفره توصیف شده است. سیستم دوترازی با HOMO (بالاترین اوربیتال مولکولی اشغال شده) و LUMO (پایین‌ترین اوربیتال مولکولی اشغال نشده) مشخص شده و در دو رژیم تزریق بار دائم و گذرا مطالعه می‌شود.

در اینجا، برای ادوات فوتوولتائیک در رژیم تزریق بار دائم، ما فوتوسلهای مولکولی را در نظر می‌گیریم که در آنجا فرآیند تبدیل انرژی در یک تک مولکول دهنده‌ـ‌پذیرنده که متصل به لیدهای انتقال بار است، اتفاق می‌افتد. در ابتدا، کل سیستم در حالت پایه با باند رسانش کاملاً خالی و باند ظرفیت کاملاً پر است. در نتیجه‌ی جذب فوتون توسط مولکول، یک الکترون و یک حفره به ترتیب در LUMO و HOMO قرار می‌گیرند. هر دو حامل بار با یک پتانسیل کولنی با هم برهمکنش می‌کنند و نهایتاً یا در داخل مولکول بازترکیب می‌شوند و یا به کانال‌های متناظر منتقل می‌شوند و منجر به جریان فوتوولتائیک می‌شوند (شکل ۱).

علاوه بر این، همانطور که در بالا اشاره شد، این فرمالیسم را می‌توان به سیستم‌های فوتوولتائیک که در ناحیه تزریق بار گذرا کار می‌کنند نیز اعمال کرد. مثال ادوات فوتوولتائیک در این رژیم، سلول‌های آلی توده‌ای با ساختار هتروجانکشن هستند. کل سیستم شامل دو لید نیمه بی‌نهایت از مواد پذیرنده و دهنده است. برای هر دو لید، حالت اولیه را در فصل مشترک در نظر می‌گیریم. همه مولکول‌های دهنده و پذیرنده با یک تک انرژی در نظر گرفته شده‌اند که به ترتیب متناظر با HOMO و LUMO می‌باشند.

در ساختار توده‌ای هتروجانکشن، در نتیجه جذب فوتون، یک اکسایتون در سمت ماده دهنده در یک زمان منفی تشکیل می‌شود و سپس به سمت فصل مشترک (سیستم دوترازی) انتشار می‌یابد. این اکسایتون در زمان $t = 0$ به فصل مشترک می‌رسد و هدف ما آنست که کل بار تزریق شده به هر کانتکت را به سبب تفکیک اکسایتون در زمان‌های بزرگتر ارزیابی کنیم.

در این مطالعه، اختلاف انرژی بین ترازهای LUMO و HOMO در مولکول جاذب (رژیم دائم) یا در فصل مشترک (رژیم گذرا) برابر با Δ فرض شده است. عناصر ماتریس کوپلینگ بین حالت‌های مولکول یا فصل مشترک و کانال‌های انتقال دهنده بار با C نشان داده شده‌اند. این عناصر در داخل کانال‌ها یکنواخت فرض شده و با J مشخص شده‌اند. انرژی الکترون در سایت (x) و حفره در سایت (y) به ترتیب برابر با $\varepsilon_e(x)$ و $\varepsilon_h(y)$ فرض شده است. علاوه بر این، برهمکنش کولنی بین آنها $I(x, y)$ به

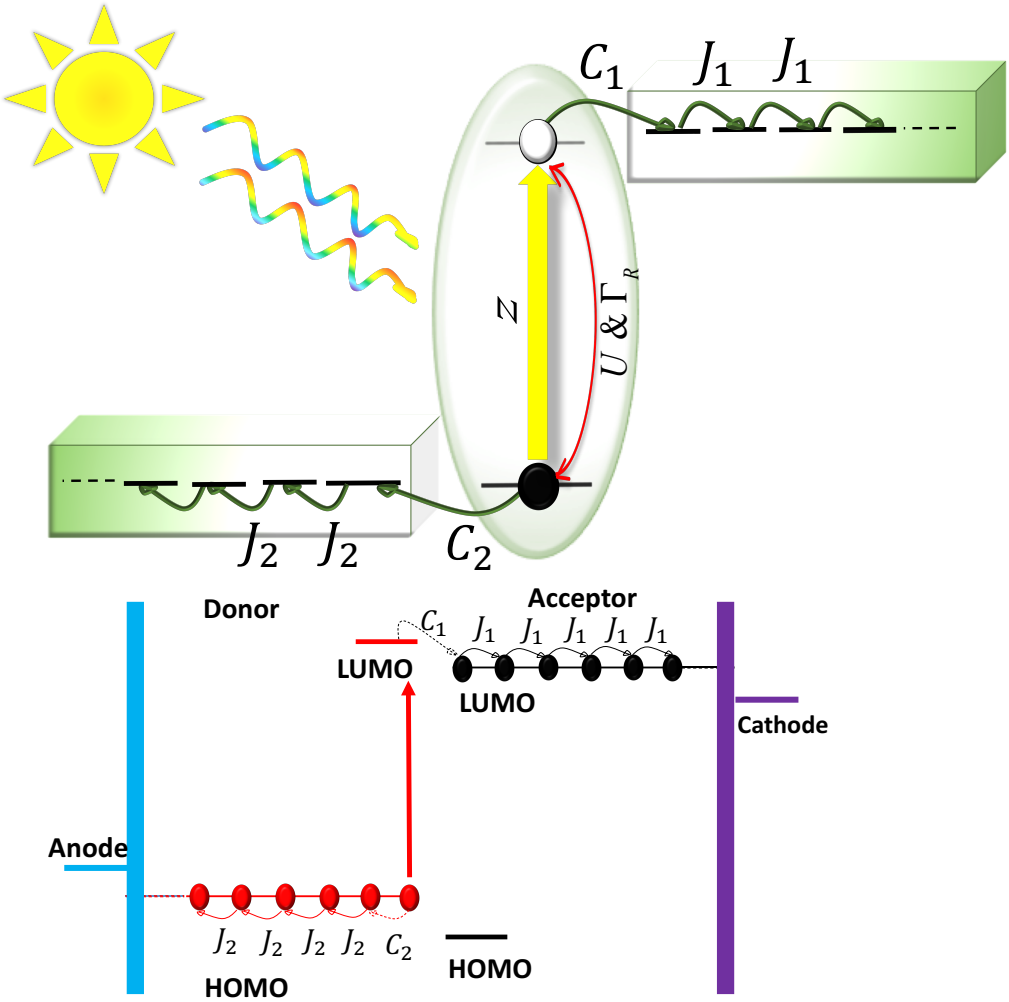

شکل ۱: مدل سلول‌های فوتوولتائیک دوترازی. پنل بالا یک فوتوسل مولکولی را نشان می‌دهد که در آن‌جا یک مولکول جاذب به لیدهای انتقال بار متصل است و ساختار تحت تابش نور قرار دارد. پنل پایین مدلی از یک سلول آلی توده‌ای با ساختار هتروجانکشن را نشان می‌دهد. در هر دو ساختار C و J پارامترهای کوپلینگ هستند. U و Γ_R پارامترهای اندرکنش و بازترکیب الکترون–حفره هستند و z انرژی فوتون جذب شده است.

صورت زیر مدل‌بندی شده است:

$$I(x,y) = \begin{cases} U, & \text{if} \quad x = 0 \quad and \quad y = 0, \\ \frac{V}{(x+y)}, & \text{if} \quad x \neq 0 \quad or \quad y \neq 0. \end{cases} \tag{۱۴}$$

از آنجایی که $I(x,y)$ یک پتانسیل کولنی از نوع جاذبه است، U و V مقادیر منفی دارند. در معادله بالا، U شدت برهمکنش کوتاه‌ـ برد الکترون‌ـ حفره (حالتی که هر دو حامل بار در یک مکان مشترک قرار دارند) را نشان می‌دهد. از سوی دیگر، V شدت برهمکنش بلندـ برد الکترون‌ـ حفره (حالتی که در آن حداقل یکی از حاملین بار در لید متناظر است) را مشخص می‌کند.

۵.۲ فضای هیلبرت جفت الکترون‌ـ حفره

فضای هیلبرت ساختارهای دوترازی ذکر شده، را می‌توان یک شبکه مربعی در نظر گرفت. برای ادوات فوتوولتائیک در رژیم تزریق بار دائم، x (y) مکان الکترون (حفره) را در لید متناظر نشان می‌دهد به طوریکه ($x=0,\ y=0$) موقعیت جفت الکترون‌ـ حفره را در مولکول یعنی حالت برانگیخته را نشان می‌دهد و سایت‌های $x>0$ ($y>0$) نشان دهنده‌ی موقعیت الکترون (حفره) در لید متناظر می‌باشد. به طور مشابه، برای ادوات فوتوولتائیک در ناحیه گذرا، x (y) موقعیت الکترون (حفره) در فصل مشترک دهنده‌ـ پذیرنده و یا در لیدهای متناظر است.

۶.۲ هامیلتونی جفت الکترون‌ـ حفره

هامیلتونی سیستم را با می‌توان با روش تنگ بست که شامل جمله اضافی برهمکنش جفت الکترون‌ـ حفره نیز هست به صورت زیر در نظر گرفت:

$$H=\sum_i \varepsilon_i \left|i\right\rangle\left\langle i\right| + \sum_{i,j} J_{i,j} \left|i\right\rangle\left\langle j\right| \tag{۱۵}$$

در اینجا، جمله اول نشان دهنده‌ی انرژی هر سایت شبکه مربعی است که به صورت مجموع ان سایت انرژی الکترون، حفره و همچنین انرژی برهمکنش بین آن‌ها تعریف شده است:

$$\varepsilon(x,y)=\varepsilon(x)+\varepsilon(y)+I(x,y) \tag{۱۶}$$

احتمال بازترکیب جفت الکترون‌ـ حفره تولید شده به واسطه جذب فوتون در داخل مولکول جاذب یا در فصل مشترک ماده دهنده‌ـ پذیرنده با افزودن یک بخش موهومی $-i\Gamma_R/2$ به ان سایت انرژی سایت $(0,0)$ در نظر گرفته شده است که در آنجا Γ_R نشان دهنده‌ی آهنگ برهمکنش است.

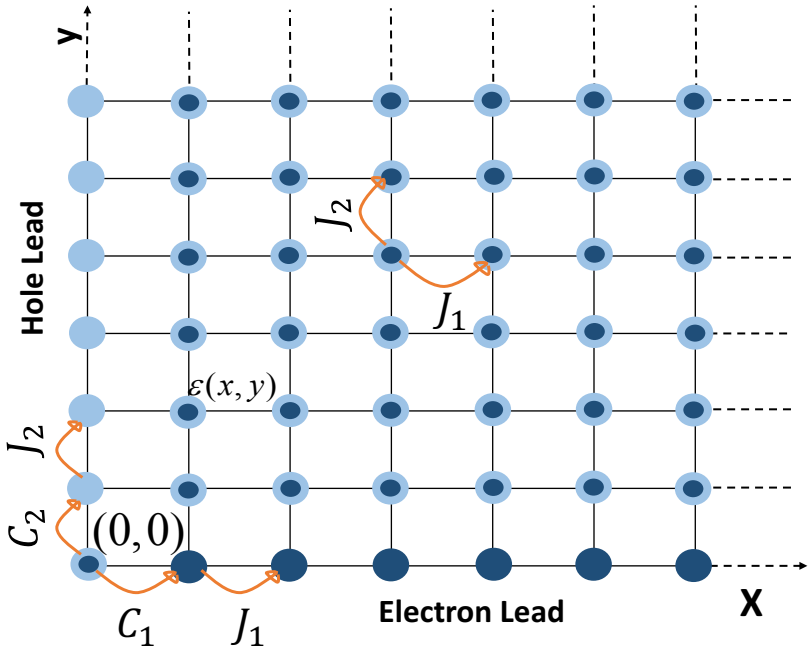

شکل ۲: فضای هیلبرت جفت الکترون_حفره با در نظر گرفتن تنها یک لید انتقال بار برای هر یک از حاملین. مختصات x و y نشان دهنده موقعیت الکترون و حفره در لیدهای متناظرشان است. $\varepsilon(x,y)$ ان_سایت انرژی هر یک از سایت‌های شبکه مربعی و C و J پارامترهای کوپلینگ هستند.

۷.۲ چگالی حالت‌ها

در اغلب مباحث مطرح شده در این رساله، ما به دنبال محاسبه چگالی حالتهای موضعی (LDOS) برای یک اوربیتال Φ_0 از روش هامیلتونی تنگ_بست هستیم. LDOS به منظور درک آثار سایر قسمت‌های یک جامد بر روی یک ناحیه موضعی مشخص، مثلاً یک اتم، به کار برده می‌شود. برای سیستمی توصیف شده با هامیلتونی H و توابع ویژه نرمالیزه شده Ψ_m و ویژه مقادیر E_m، تعریف ریاضی LDOS به صورت زیر می‌باشد:

$$n_0(E) = \sum_m |\langle \Phi_0 | \Psi_m \rangle|^2 \delta(E - E_m) \qquad (۱۷)$$

به طوریکه چگالی حالت‌های کل، مجموعی از چگالی حالت‌های اندازه‌گیری شده بر روی یک مجموعه کاملی از حالت‌های اورتونرمال $|\Phi_m\rangle$ می‌باشد.

رابطه (۱۷) یک تعریف نسبتاً کلی از چگالی حالت‌های موضعی است. به هر حال، این تعریف می‌تواند به اپراتور گرین $G(z) = (z - H)^{-1}$ مرتبط شود و از اینرو، ما در اینجا قصد محاسبه LDOS مرتبط با اوربیتال Φ_0 را داریم. ما تنها نیاز به عنصر $G_{00}(z)$ داریم. عناصر قطری ماتریس تابع گرین به صورت زیر تعریف شده است:

$$G_{00}(E + i\epsilon) = \langle\Phi_0|\frac{1}{E + i\epsilon - H}|\Phi_0\rangle \tag{۱۸}$$

که در آنجا ϵ یک عدد مثبت بی‌نهایت کوچک است. با وارد ساختن اپراتور واحد $\sum_m |\Psi_m\rangle\langle\Psi_m|$ به این معادله و استفاده از $H|\Psi_m\rangle = E_m|\Psi_m\rangle$، داریم:

$$G_{00}(E + i\epsilon) = \sum_m |\langle\Phi_0|\Psi_m\rangle|^2 \frac{E - E_m - i\epsilon}{(E - E_m)^2 + \epsilon^2} \tag{۱۹}$$

در اینجا بخش حقیقی قطب‌ها را نشان می‌دهد که متناظر با ویژه مقادیر گسسته H هستند و بخش موهومی منجر به تکینگی‌هایی از نوع دلتا می‌گردد.

$$\lim_{\epsilon\to 0} \frac{1}{\pi} \frac{\epsilon}{(E - E_m)^2 + \epsilon^2} = \delta(E - E_m) \tag{۲۰}$$

شکل (۳) رفتار بخش حقیقی و موهومی تابع گرین را در نزدیکی یک قطب نشان می‌دهد.

روابطی که در بالا بیان شدند تئوری استاندارد طیفی را مشخص می‌سازند:

$$n_0(E) = \sum_m |\langle\Phi_0|\Psi_m\rangle|^2 \lim_{\epsilon\to 0} \frac{1}{\pi} \frac{\epsilon}{(E - E_m)^2 + \epsilon^2} \tag{۲۱}$$

$$\to n_0(E) = -\frac{1}{\pi} \lim_{\epsilon\to 0} \operatorname{Im} G_{00}(E + i\epsilon) \tag{۲۲}$$

بنابراین، بخش موهومی تابع گرین $G_{00}(z)$ شدت هر ویژه مقدار بر یک اوربیتال نوعی Φ_0 مشخص می‌سازد و می‌توان آن را با استفاده از روش کسر مداوم محاسبه کرد (فصل دوم رساله). شایان ذکر است که در این فرمالیسم، چگالی حالت‌ها نشان دهنده‌ی تمامی حالت‌های انرژی ممکن برای جفت الکترون‌ـ

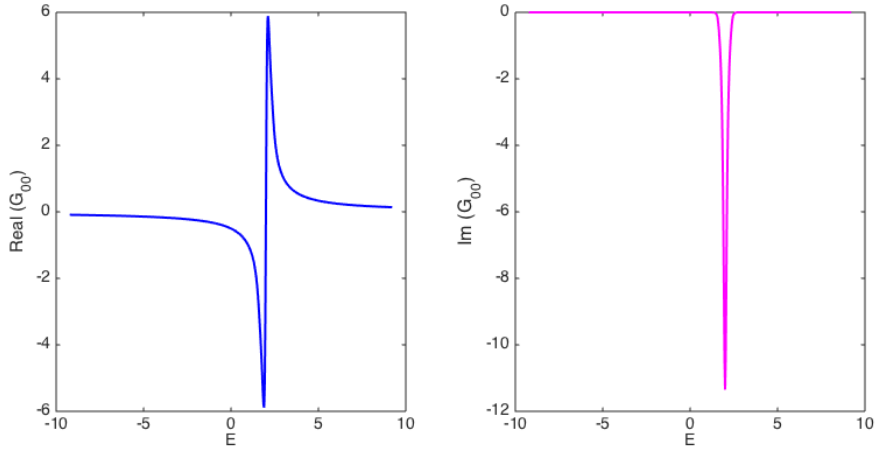

شکل ۳: بخش‌های حقیقی و موهومی تابع گرین $G_{00}(E)$.

حفره می‌باشد.

با داشتن هامیلتونی مؤثر و استفاده از نظریه پراکندگی کوانتومی، می‌توان تابع موج پراکنده شده و به تبع آن، شار فوتون‌های فرودی جذب شده، شار جریان و شار بازترکیب را محاسبه نمود. با داشتن این اطلاعات می‌توان به محاسبه بازده جدایش بار پرداخت تا تصویر روشنی از عملکرد سلول در دست داشته باشیم.

۳ نتایج

۱.۳ نتایج ارئه شده در فصل سوم

با تکیه بر مدل تئوری که در این رساله توسعه یافته است، می‌توان به بررسی عملکرد سلول‌های خورشیدی نانوساختاری از جمله فوتوسل‌های مولکولی و سلول‌های خورشیدی آلی توده‌ای با ساختار هتروجانکشن تحت شرایط کوپلینگ متقارن و نامتقارن و همچنین در حضور کانال‌های ناخواسته‌ی انتقال بار پرداخت. این مباحث به تفصیل در فصل سوم رساله مورد بررسی قرار گرفته‌اند. آنالیزها بر پایه‌ی طیف انرژی جفت الکترون–حفره هستند و نتایج ما گویای آن هستند که بازده به شدت تحت تأثیر انرژی برهمکنشی الکترون و حفره است. یک انرژی بحرانی $U_{Critical}$ وجود دارد که اساساً وابسته به لبه باند برانگیزش‌های الکترون–حفره و اختلاف انرژی بین HOMO–LUMO است. ما نشان داده‌ایم که اگر $|U| < |U_{Critical}|$،

سلول بسیار کارامدتر از حالتی است که $|U| > |U_{Critical}|$ که در آن‌جا حالت‌های مقید ایجاد می‌شوند و باعث کاهش بازده می‌گردند. نتایج ما همچنین نشان می‌دهد که تحرک‌پذیری حفره پارامتر مهمی برای بهبود بازده جدایش بار است.

این مطالعه همچنین به بررسی رقابت بین تزریق حاملین بار به لیدها و بازترکیب می‌پردازد. نتایج نشان می‌دهند که این رقابت به شدت وابسته به پارامترهای سلول ازجمله شدت برهمکنش الکترون‌ـحفره، پارامتر بازترکیب، کوپلینگ به لیدها و ساختار باند لیدهاست. هنگامی که بیش از یک لید انتقال بار برای یکی یا هر دو حاملین بار مهیاست، رقابتی بین تزریق در لیدها نیز وجود دارد. در این شرایط، پهنای باند پیوستارهای انرژی و همچنین پارامتر کوپلینگ به لیدها عوامل تعیین کننده‌ای هستند.

۲.۳ نتایج ارئه شده در فصل چهارم رساله

در فصل چهارم رساله، ما به بررسی عملکرد سلول در حضور برهمکنش‌های بلندـبرد پرداخته‌ایم. در آن‌جا دو شرایط کلی در نظر گرفته شده است: ۱ ـ برهمکنش کولنی بلندـبرد الکترون‌ـحفره که اشاره به شرایطی دارد که در آن‌جا حداقل یکی از حاملین بار در لید متناظرش است. ۲ ـ برهمکنش بین الکترون و فونون در ماده پذیرنده. نتایج ما نشان می‌دهند که در حضور برهمکنش کولنی بلندـبرد الکترون‌ـحفره یک سری از پیک‌های اکسایتونی در لبه پایین پیوستار انرژی ظاهر می‌شوند و وزن این پیک‌ها تأثیر مهمی بر بازده جدایش بار و عملکرد سلول دارد. همچنین برهمکنش الکترون‌ـحفره منجر به شکل‌گیری باندهای پلارونی می‌گردد و به‌ازای انرژی‌های تزریق الکترون مختلف، سلول می‌تواند کارامد یا ناکارامد باشد.

۴ پیشنهادها برای ادامه کار

چندین پیشنهاد مختلف برای ادامه کار این رساله و عمیق‌تر کردن درک ما از نحوه عملکرد سلول‌های خورشیدی اکسایتونی وجود دارد:

(I) مدل در این‌جا به یک سیستم فوتوولتائیک دوترازی اعمال شد ولی قابلیت آن را دارد که ساختارهای بسیار پیچیده‌تر را مورد ارزیابی قرار دهد و شرایط لازم برای افزایش بازده را مشخص سازد.

(II) برای مطالعه دقیقتر، پارامترها باید با استفاده از محاسبات *ab-initio* بدست آیند و آنگاه آن‌ها را در کد جایگزین نمود.

(III) مدل را می‌توان تعمیم داد تا آثار بازترکیب‌های غیرموضعی را در نظر گرفت.

(IV) در فصل چهارم رساله، در مساله کوپلینگ الکترون_فونون، حد پلارون کوچک در نظر گرفته شده است. با استفاده از Dynamical Mean-Field Theory (DMFT) می‌توان فراتر از این حد رفت. این روش اجازه خواهد داد که مساله برهمکنش الکترون_فونون را با دقت بیشتری ارزیابی نماییم.

French Resume

Introduction

L'existence humaine demande un apport en énergie. La population mondiale augmente rapidement et ainsi la demande en énergie et en différentes sources d'énergie augmente aussi dramatiquement. Ainsi l'humanité a besoin d'une énergie qui soit disponible, fiable, propre et bon marché.

Depuis la révolution industrielle la grande majorité de l'énergie utilisée provient de l'énergie fossile ce qui comprend principalement le charbon, le pétrole et le gaz. Toutefois en dépit de leur effet majeur sur les progrès technologiques elles souffrent d'un ensemble de défauts importants. Ainsi ces sources d'énergie fossiles entraînent des effets dangereux sur l'environnement tels que les pluies acides et les effets sur la santé humaine. De plus les ressources sont limitées et leurs prix augmentent. Ainsi s'appuyer uniquement sur ces ressources aura des conséquences néfastes environnementales et sociétales.

Cette situation impose aux scientifiques du monde entier de développer des sources d'énergie alternatives, pour démarrer une transition des moyens de production d'énergie. Plus largement ce mouvement s'intègre dans une transition énergétique et une transition écologique. Toutefois il existe déjà des sources d'énergies qui soient propres, renouvelables et qui à terme peuvent aussi devenir peu chères.

Ces énergies qui incluent notamment l'éolien, le solaire, l'énergie géothermique, l'hydroélectricité et la biomasse peuvent apporter un bénéfice considérable pour les problèmes écologique et climatique. A terme ils joueront un rôle économique de plus en plus important, même si actuellement ils contribuent pour une part limitée à la production d'énergie.

Parmi ces ressources le solaire est une énergie attractive car il est disponible partout sur la planète et ne produit pas de CO2. Ainsi en seulement 6 heures les déserts de la planète reçoivent plus d'énergie solaire que la consommation humaine sur une année. En supposant l'utilisation de seulement 1% des surfaces désertiques de la planète le potentiel de production d'énergie électrique serait suffisant pour subvenir aux besoins énergétiques de l'humanité. Clairement le potentiel de l'énergie solaire électrique est très élevé et de ce fait le photovoltaïque connaît un développement important.

En dehors de l'introduction de la conclusion et d' appendices techniques la thèse est essentiellement organisée en quatre chapitres.

Le chapitre 1 rappelle le développement historique du photovoltaïque et les principes de fonctionnement de différents types de cellules.

Le chapitre 2 présente un nouveau formalisme pour le traitement quantique des cellules solaires. Ce formalisme qui est basé sur l'équation de Lippmann-Schwinger permet de traiter la cellule en train de fonctionner et donne accès aux courants de charges et aux taux de recombinaison des électrons et de trous en fonction des paramètres fondamentaux de la cellule étudiée. Ce formalisme est mis en œuvre dans les chapitres 3 et 4 sur des systèmes à deux niveaux qui sont sous éclairements permanents (cellules de Gräetzel) ou qui décrivent des phénomènes transitoires (hétéro-jonctions en volume).

Le chapitre 3 décrit l'opération de cellules excitoniques en présence d'interaction électron-trou à courte portée, c'est à dire uniquement lorsque l'électron et le trou sont tout les deux localisés sur le même site. (molécule absorbant la lumière pour les cellules à colorant et interface donneur-accepteur dans le cas des hétéro-jonctions en volume). Il décrit un système à deux niveaux couplés à un ou plusieurs canaux d'évacuation pour les électrons et les trous.

Le chapitre 4 décrit l'opération de cellules excitoniques en présence d'interactions à plus longue portée. Il s'agit par exemple d'une interaction Coulombienne à longue portée entre l'électron et le trou lorsqu'ils ne sont pas sur le même site. Il s'agit aussi d'une interaction entre l'électron et des modes de vibrations des molécules sur lesquelles l'électron se déplace dans le côté accepteur.

Chapitre 1

Ce chapitre présente une introduction à la thèse et au contexte historique du photovoltaïque. Une présentation succinte des principes de fonctionnement des cellules solaires y est aussi développée.

Les systèmes photovoltaïques ont commencé à se développer avec l'avènement des semi-conducteurs dans les années 1950 à Bell Labs. Les chercheurs de la Compagnie Bell ont développé des cellules dont l'efficacité atteignait 6%.

Des années 1950 aux années 1970 les recherches sur le photovoltaïque visaient des applications au spatial. Toutefois après la crise du pétrole dans les années 1970 le photovoltaïque a commencé à être envisagé comme une source d'énergie alternative sérieuse. Depuis lors les recherches pour développer cette technologie se sont élargies.

On peut distinguer trois grandes générations de cellules même si cette classification n'est toujours parfaitement universelle.

Première génération : c'est la technologie à base de silicium cristallin. Elle représente encore plus de 80% de la production industrielle mondiale. Ces cellules de première génération sont relativement chères et atteignent des rendements énergétiques de l'ordre de 25 %. Ce rendement est réduit dans les produits commerciaux et ne peut en tout cas pas dépasser la limite de Schokley-Queisser qui est d'environ 33% pour une cellule à une seule jonction.

Seconde génération : les films minces sont présents dans 1à à 15 % des cellules produites. Ils ont un rendement plus faible que le silicium cristallin qui est d'environ 10-15 %. Cette efficacité diminue avec le vieillissement. On a ainsi des films basé sur du Silicium amorphe, du CdTe (Cadmium Tellure) ou du CIS et du CIGS (Cuivre Indium Disélénure et Cuivre Indium Gallium Disélénure)

Troisième génération : Il s'agit d'une génération qui utilise les semi-conducteurs organiques. Il s'agit de combiner les avantages de la première de la deuxième génération et d'obtenir des systèmes ayant un bon rendement et un coût peu élevé. Ces cellules de troisième génération sont des cellules excitoniques. Ceci signifie que pour ces cellules l'absorption du photon donne une paire électron-trou dans un espace restreint soit parce que l'électron et le trou sont liés énergétiquement soit parce qu'ils sont produits dans une zone de petite taille nanométrique.

Les cellules excitoniques offrent la possibilité de faibles coûts et donne des systèmes souples dont les usages sont renouvelés (nomades par exemple) par rapport aux panneaux solaires usuels qui sont à la fois rigides et lourds. A l'heure actuelle ces systèmes ne satisfont pas au critères d'utilisations souhaités notamment concernant la stabilité à long terme qui est possible avec les premières et deuxièmes générations.

Il n'est pas possible de dresser un paysage des systèmes photovoltaïque sans mentionner aussi les nouvelles perovskites hybrides. Ces systèmes sont à l'heure actuelle porteurs de grands espoirs de par leurs performances excellentes (comparable au silicium cristallin) et leur coût très bas. Toutefois quelques sérieuses difficultés restent à surmonter concernant leur stabilité et la présence de plomb.

L'objectif principal de cette thèse est d'améliorer la connaissance et la modélisation des cellules de troisième génération. Ainsi dans les cellules organiques dites à hétéro-jonction en volume la lumière est absorbée dans une zone de molécules de type donneur et crée une paire électron-trou liée appelée exciton. Cet exciton diffuse ensuite jusqu'à l'interface avec la zone occupée par des molécules de type accepteur. A l'interface se produit la séparation entre l'électron et le trou qui est une étape complexe mais essentielle pour l'efficacité de la cellule. Cette étape est un des aspects étudiés dans cette thèse.

D'autre type de cellules de troisième génération sont les cellules dites à colorant (ou cellules de Grätzel). La aussi les mécanismes fondamentaux sont encore mal décrits dans le détail. Dans une telle cellule une molécule (de colorant) absorbe un photon et libère un électron côté accepteur et un trou côté donneur. Le processus de séparation de charge est aussi étudié dans cette thèse. Un des résultats de cette thèse est d'ailleurs de montrer la proximité des processus de séparations de charges (au moins à un premier niveau de description) entre ces cellules à colorants et les hétéro-jonction en volume mentionnées ci-dessus.

Chapitre 2

Formalisme et méthodes numériques

Dans ce chapitre on expose le nouveau formalisme quantique hors équilibre qui permet d'analyser les modèles dans cette thèse. Ce nouveau formalisme quantique est bien adapté au problème d'une cellule photovoltaïque et devrait s'appliquer à de nombreuses situations. Ici l'idée de base est exposée et ensuite elle est développée et appliquée au cas d'un système à deux niveaux qui est le modèle le plus simple d'une cellule solaire quantique.

Le formalisme présenté ici repose sur la théorie de la diffusion quantique et notamment sur l'équation de Lippmann-Schwinger. L'idée est de considérer un flux de photon incident sur le système matériel est de décrire les excitations du système crées par l'absorption des photons. Dans la limite ou le flux lumineux n'est pas trop intense on peut se contenter d'une approximation perturbative (approximation de Born) pour traiter l'effet du flux incident. Ceci suppose que une paire électron-trou créée par l'absorption d'un photon évolue dans un champ moyen, qui est décrit par un hamiltonien de la paire. Ce hamiltonien peut inclure des effets de charges d'espace lié à la présence d'un flux constant de charges créées et injectées mais ce Hamlitonien ne décrit que une paire d'électron-trou. Aller au delà et considérer des paires de paires mène tout de suite à un espace des états possibles beaucoup plus grand et donc à une complexité beaucoup plus grande.

Dans ce formalisme l'équation de Lippmann-Schwinger fourni l'expression d'une fonction d'onde de diffusion. Cette fonction d'onde décrit le flux des paires électrons-trous et peut être vue aussi comme la fonction d'onde qui décrit la cellule en train de fonctionner.

A partir de cette fonction d'onde on peut calculer les principaux flux qui sont : le flux de photon absorbés, le flux de paires recombinées, le flux d'électrons et de trous injectés dans les différents canaux etc.. On peut aussi en principe calculer la population des différents états électroniques et donc le potentiel créé par la distribution des charges créées par l'absorption des photons. Ce calcul auto-cohérent est en principe obtenu par la solution de l'équation de Poisson et devrait permettre un calcul auto-cohérent du hamiltonien dans lequel les paires évoluent. Nous n'avons toutefois pas développé ce genre de calcul ici et nous n'avons considéré que les flux et analysé le fonctionnement de la cellule à partir de ces flux.

Dans toute la thèse nous présentons le hamiltonien des électrons des trous en interaction dans une approche de type liaisons fortes, i.e. pour un modèle d'états discrets. Formellement nous écrivons donc un hamiltonien de liaisons fortes qui décrit l'énergétique de la fonction d'onde de la paire électron-trou une fois

qu'elle est créée par l'absorption du photon. Si l'électron et le trou se déplace sur des chaînes alors la paire électron-trou « vit » sur le produit de deux chaînes c'est à dire sur un réseau à deux dimensions que l'on peut représenter par un réseau carré. Ainsi la dynamique d'une particule sur un réseau carré dont on connaît le hamiltonien donne une première approche du problème photovoltaïque.

La fonction d'onde de Lippmann Schwinger dans l'approximation de Born s'écrit essentiellement comme la résolvante du Hamiltonien de la paire appliqué à l'état initial de la paire juste après l'absorption du photon (i.e. l'électron dans l'orbitale LUMO et le trou dans l'orbitale HOMO). Cette expression de la fonction d'onde permet certains développements analytiques. Ainsi nous avons pu généraliser des résultats sur le courant et le rendement quantique démontrés dans le cas sans interaction au cas ou l'électron et le trou interagissent.

Dans le cas général l'approche devient numérique. La méthode dite de récursion (qui est liée à la méthode de Lanczos) permet une détermination numérique efficace de la fonction d'onde de la cellule et par la même des courants de charges et des flux d'absorption de photon ou de recombinaison.

Le formalisme permet aussi de montrer le lien exact entre le problème en régime transitoire et le problème en régime permanent. La photocellule moléculaire est notre exemple de système en régime permanent et l'interface d'une hétéro-jonction dans les cellules organiques est notre exemple de système en régime transitoire. Si l'on s'intéresse à un éclairement dont la puissance est indépendante de la fréquence alors le rendement quantique pour le régime transitoire et pour le régime permanent ont la même expression mathématique. C'est ce qui nous permet dans cette thèse d'étudier en parallèle les deux situations. Notons que cette analogie exacte pour le rendement quantique n'a pas jusque là été notée dans la littérature. Pourtant elle apporte un élément important car l'analyse du régime permanent est techniquement plus simple qu'une analyse basée sur l'évolution temporelle. Ceci permet une analyse numérique beaucoup plus précise et ceci donne aussi une compréhension physique meilleure du cas transitoire.

Le formalisme mis en place dans ce chapitre ainsi que la méthode de récursion ont permis de réaliser les études présentées dans les chapitres 3 et 4.

Chapitre 3

Système à deux niveaux avec interaction locale

En utilisant le formalisme développé au chapitre 2 nous étudions les effets d'une interaction locale entre l'électron et le trou, et ses conséquences sur le rendement quantique de la cellule dans les régimes permanents et transitoires. Comme indiqué ci-dessus la photocellule moléculaire est notre exemple de système en régime permanent et l'interface d'une hétéro-jonction dans les cellules organiques est notre exemple de système en régime transitoire.

L'interaction locale signifie que l'électron et le trou n'interagissent que lorsqu'ils sont tous les deux dans la molécule. Orbitale LUMO pour l'électron et orbitale HOMO pour le trou. Dans le cas d'une hétéro-jonction l'interaction locale signifie que l'électron et le trou n'interagissent que lorsqu'ils sont tous les deux à l'interface entre les zones D et A (Donneur et Accepteur). Nous modélisons et analysons l'absorption du photon, la création de l'exciton et sa dissociation ou recombinaison. Ceci nous donne accès au rendement qauntique de la cellule en fonction des paramètres du hamiltonien qui décrit la paire électron-trou. Nous considérons trois types de configurations :

(I) Cas mono-canal : dans ce cas il y a juste un canal d'évacuation pour chaque charge (électron et trou). Nous étudions différentes conditions de couplage asymétrique ou symétrique entre les orbitales HOMO et LUMO avec leurs canaux respectifs. Nous avons montré que le formalisme développé au chapitre 2 permet d'analyser finement ces différentes situations à la fois numériquement et qualitativement en terme de compréhension des phénomènes.

Nos résultats montrent que le rendement quantique dépend de l'interaction locale entre l'électron et le trou. Si ce couplage est suffisamment fort il se crée un état lié excitonique dans lequel la paire électron trou est majoritairement injectée. Une fois la paire injectée dans cet état lié la séparation de charge ne peut plus s'opérer et un taux de recombinaison même minime mène ultimement à la recombinaison de la paire électron trou. Dans ces conditions le rendement quantique devient mauvais. L'étude de couplage asymétrique ou symétrique montre que a mobilité du trou qui est souvent négligée dans la littérature est un élément favorable pour un meilleur rendement quantique.

(II) Cas multi-canaux : dans ce cas il y a plusieurs canaux d'évacuation pour au moins un des porteurs de charge. Nous considérons le cas ou seuls les trous sont évacués dans le matériau II alors que les électrons mais aussi les trous peuvent être évacués dans le matériau I. Dans ce

cas la largeur des continuums EC1 et EC 2 joue un rôle important. EC1 représente le continuum d'excitations ou un électron est injecté dans le matériau I et un trou dans le matériau II. C'est l'injection des paires électrons trous dans ce continuum qui est le processus souhaité pour un bon fonctionnement de la cellule. EC 2 représente le continuum d'excitations ou un électron est injecté dans le matériau I et un trou dans le même matériau I. L'injection des paires électrons trous dans ce continuum conduit à une détérioration des performances de la cellule.

Lorsqu'il y a plusieurs canaux d'évacuation des charges il existe une compétition entre l'injection des paires électrons trous dans les « bons » et les « mauvais » canaux. Nous avons montré que le principe de conservation de l'énergie qui implique que la paire injectée possède l'énergie du photon absorbé peut dans certains cas permettre l'injection dans un seul des deux canaux. Dans ce cas le rendement de la cellules dépend prioritairement des spectres des continuums EC1 et EC2.

(III) Couplage non résonant aux canaux : dans les deux cas précédents le couplage de chaque orbitale (HOMO et LUMO ou D et A) avec les canaux est résonant. Ceci signifie que l'énergie des orbitales du système à deux niveau est identique à celle des orbitales qui constituent les canaux d'évacuation. De plus les couplage entre ces orbitales et les canaux est plus faible que le terme de saut entre orbitales des canaux. Dans cette troisième partie on étudie pour le cas mono-canal les conséquences d'un écart à ces conditions. Nous étudions notamment le cas d'un écart LUMO-LUMO tel qu'il est discuté dans la littérature pour l'injection des charges côté accepteur dans les cellules organiques. Si cet écart est négatif (énergie de l'orbitale interface plus faible que celle des molécule côté accepteur alors l'interaction électron-trou tend à détériorer encore plus le rendement quantique. Dans le cas inverse l'interaction électron-trou peut jouer un rôle favorable et restaurer un meilleur rendement quantique.

Cet écart positif est habituellement considéré dans la littérature comme une condition favorable pour un bon rendement de la cellule. Cependant dans notre modèle même si la conclusion est analogue les raisons en sont différentes. En effet nous ne discutons ici que de processus cohérents ou il n'y a pas d'échange d'énergie avec d'autres degrés de liberté alors que dans la littérature il est supposé souvent que l'échange d'énergie avec le bain de phonons est rapide et déterminant pour la séparation de charges.

Chapitre 4

Système à deux niveaux avec interaction non locale

Ce chapitre explore les effets d'interaction non locale sur la performance photovoltaïque de cellules dans le régime permanent (photo-cellule moléculaire) ou dans le régime transitoire (hétéro-jonction en volume dans les cellules organiques). Ceci signifie que, contrairement au chapitre 3, il y a une interaction même si les porteurs de charges ne sont pas tous les deux dans la molécule (régime permanent) ou à l'interface donneur-accepteur (régime transitoire).

Un cas important d'interaction non-locale est l'interaction Coulombienne entre l'électron et le trou photogénérés. Ceci signifie que l'électron et le trou intéragissent même s'ils ne sont pas dans la molécule. Ici bien-sûr l'interaction n'est pas l'interaction Coulombienne « nue » mais une interaction écrantée par l'environnement, c'est à dire toutes les charges mobiles dans le matériau. L'effet de cette interaction écrantée est bien représenté par une constante diélectrique effective, qui est usuellement de l'ordre de quelques unités dans les semi-conducteurs. Nous montrons que le formalisme développé au chapitre 2 s'applique bien aussi à ce type de situation et permet une analyse en parallèle des régimes permanent et transitoire qui n'avait pas été faite dans la littérature. Nous trouvons que l'interaction attractive à longue distance entre l'électron et le trou réduit le rendement de la cellule, particulièrement dans le cas ou le couplage avec les canaux d'évacuation des porteurs de charge est faible.

Un autre cas d'interaction non locale est le couplage entre les électrons (ou les trous) avec les phonons lorsque les porteurs de charges se déplacent dans leurs canaux respectifs jusqu'aux électrodes. Nous étudions ce cas avec un modèle de type Holstein pour l'interaction électron-phonon. Ce modèle décrit essentiellement l'interaction avec les modes de vibrations acoustiques. Nous montrons que l'efficacité de la séparation des charges dépend subtilement du couplage cohérent aux modes de vibration optiques. Dans notre étude le couplage aux modes de phonons peut créer des bandes polaroniques étroites et aussi un spectre qui présente des nombreuses bandes interdites. Ces bandes polaroniques étroites sont peu favorables au transport des charges et en présence de processus de recombinaison l'électron et le trou peuvent se recombiner avant d'être évacués. On peut retrouver aussi la formation d'états liés à l'interface qui sont équivalents aux étas excitoniques présentés dans le chapitre 3. Ceci mène à un comportement oscillant du rendement quantique en fonction de la valeur de l'énergie de l'orbitale LUMO d'ou partent les électrons. En règle générale l'augmentation du taux de la recombinaison diminue le rendement quantique. Nous trouvons aussi que en règle générale l'interaction Coulombienne attractive entre l'électron mobile et le trou fixe (pour ce modèle) tend à diminuer le rendement.

Conclusions et perspectives

Le but de cette thèse était d'acquérir une compréhension des principes de fonctionnement de cellules solaires excitoniques et à terme de permettre une amélioration des performances d'une cellule. Nous avons développé un nouveau formalisme quantique basé sur la notion de fonction d'onde d'une cellule excitonique en fonctionnement. L'idée de base de ce formalisme a été illustrée sur l'exemple de cellules solaires à deux niveaux. Les systèmes à deux niveaux ont été étudiés soit en régime permanent soit en régime transitoire de séparation de charges.

Nous avons démontré que cette nouvelle méthodologie fourni une image quantitative des phénomènes fondamentaux sous-jacents à la conversion énergétique : absorption du photon, dissociation de l'exciton et séparation de charge ou recombinaison, et conséquences sur les performances de la cellule. Ce formalisme permet notamment de traiter le cas d'une interaction Coulombienne forte entre l'électron et le trou alors que ce problème est difficile à traiter par les autres approches quantiques hors équilibre.

Quelques résultats importants de la thèse sont listés ci-dessous :

(I) Nous avons montré qu'il y a une compétition entre l'injection de charge dans les canaux et la recombinaison électron-trou. Cette compétition dépend sensiblement des paramètres du modèle tel que l'interaction Coulombienne électron-trou, le temps de recombinaison, le couplage aux canaux d'évacuation des charges et la structure de bande de ces canaux. Lorsqu'il y a plusieurs canaux d'évacuation pour un type de charge (électron ou trou) il y a en plus une compétition entre l'injection dans les différents canaux.

(II) Le rendement quantique, c'est à dire le nombre de charge injectées par photon absorbé dépend fortement de l'interaction Coulombienne locale entre l'électron et le trou. Il y a une valeur critique au delà de laquelle le rendement quantique chute très rapidement. Cette valeur dépend en premier lieu des bords de bandes des canaux d'évacuations des électrons et des trous et des énergies des orbitales HOMO et LUMO. Lorsque la valeur critique de l'attraction électron-trou est dépassée un état lié excitonqiue se forme dans le quel la paire électron-trou est presque entièrement injectée. La paire électron trou est alors piégée et finit toujours par se recombiner, même si le taux de recombinaison est faible. Ceci entraîne alors une réduction drastique du rendement quantique.

(III) Nous avons étudié le rôle de la propagation du trou qui est négligé dans la plupart des modèles dans la littérature. Nos résultats montrent si le trou est considéré comme fixe on tend à sur estimer la formation d'état excitonique lié. De ce fait on sous estime la performance de la cellule. Ainsi la mobilité du trou et un élément favorable pour améliorer les performances de la cellule excitonique.

(IV) Nous trouvons que l'interaction à longue distance entre l'électron et le trou et la recombinaison non radiative réduisent les performances de la cellule. En particulier lorsque le couplage aux canaux d'évacuation est faible.

(V) Finalement nous avons apporté des évidences sur le fait que le transfert aux travers des interfaces dans les cellules à hétéro-jonctions en volume est subtilement contrôlé par le couplage des électrons avec des modes de vibrations optiques côté accepteur.

Cette thèse ouvre aussi de nouvelles perspectives pour améliorer notre compréhension et description quantitative des cellules excitoniques.

(I) Le formalisme a été appliqué à un système à deux niveaux cependant il peut être appliqué à des systèmes plus complexes, comprenant davantage de niveaux et ainsi aller vers une description plus réaliste de certains colorants ou accéder à une description de points quantiques.

(II) Pour une description plus précise les données de base utilisées dans ces modèles pourraient être tirées de calcul *ab-initio.*

(III) Le modèle pourrait être utilisé pour décrire aussi une recombinaison non-géminale, c'est à dire entre un électron et un trou qui ne sont pas issus de l'absorption du même photon.

(IV) Dans cette thèse nous avons étudiés le couplage avec des modes de phonons dans la limite de faible largeur de bande. Il est possible de dépasser cette limite en utilisant la théorie du champ moyen dynamique telle qu'elle a déjà été appliquée au problème du polaron. L'implémentation de cette approche est actuellement en cours. Cela permettra de décrire d'une façon plus précise le rôle important du couplage entre les porteurs de charges et les modes de vibration optiques.